Transport and Retention of Particulate Organic Matter in Riverbed Sediments: Laboratory Experiments and Modelling

by

Riley Hanson Mills

A thesis

presented to the University of Waterloo

in fulfilment of the

thesis requirement for the degree of

Master of Science

in

Earth Sciences (Water)

Waterloo, Ontario, Canada, 2022

Author’s Declaration

This thesis consists of material all of which I authored or co-authored: see *Statement of Contributions* included in the thesis. This is a true copy of the thesis, including any required final revisions, as accepted by my examiners. I understand that my thesis may be made electronically available to the public.

Statement of Contributions

I am the sole author of this thesis. I designed the laboratory experiments under the guidance of my co-supervisors (Dr. Fereidoun Rezanezhad and Dr. Philippe Van Cappellen) with input from two of my supervisory committee members (Dr. Matthew Ginder-Vogel and Dr. Eric Roden). All transport experiments presented in this thesis were conducted by me. Some of the post-experiment analyses of the samples that I collected and prepared during my experiments were completed by others: Marianne Vandergriendt performed ion chromatography analysis for determination of bromide concentrations, Dr. Shuhuan Li performed elemental analysis of *Chlorella* powder, and a team of Research Assistants (listed in *Acknowledgements*) performed dissolved carbon analyses. The experimental flow-through reactor apparatus described in this thesis was constructed by staff in the Science Technical Services 'Machine Shop' at the University of Waterloo (listed in *Acknowledgements*). Yuba Bhusal assisted with testing of the design for transport experiments. Sam Smith assisted with testing of the design for settling experiments and conducted the final settling experiment independently. My research was funded by the United States Department of Energy, and Global Water Futures.

I wrote the MATLAB scripts for the numerical reactive transport model presented in this thesis. I used numerical methods that I learned from the *EARTH 652: Reactive Transport Modelling* course taught by my co-supervisors. Dr. Matthew Ginder-Vogel, Dr. Eric Roden, and my co-supervisors all provided valuable discussions and literature recommendations to guide me in further developing this model to include retention processes.

I adapted the introductory chapter of this thesis (Chapter 1) from my course paper that I wrote independently for *GEOG 656: Eutrophication* (taught by Dr. Helen Jarvie), in which my assignment was to write a review paper related to both my thesis project and the course.

Abstract

Infiltration of river water into riverbeds can deliver particulate organic matter (POM: the remains of plants, algae, and other life), which has an important role for transforming nutrients in watersheds. Once POM is degraded to dissolved organic matter (DOM), it can provide a source of carbon, electron donors, and nutrients for microorganisms to use in redox reactions that drive nutrient cycles. Remobilized POM, DOM, and oxidation products may be returned to rivers during flow reversals. Over the length of a river, these small-scale riverbed processes can have a cumulative impact on river biogeochemistry, so understanding POM transport and retention processes in riverbeds could help improve large-scale nutrient cycling models.

Previous research has shown that in regulated river reaches, river stage fluctuations caused by upstream dams can increase the magnitude of hydrologic fluxes into riverbeds and the frequency of flux reversals. To investigate how the magnitude of vertical hydrologic fluxes into riverbeds influences the vertical transport and retention of POM, this study aimed to identify and quantify vertical transport and retention processes for POM in riverbeds under different flow rates using flow-through reactor (FTR) experiments. It was expected that increasing the flow rate increases the POM mass retained by filtration (not only per unit time, but per unit volume of flux).

In FTRs (10 cm length), algae powder (*Chlorella*, an analog for POM) was applied as a paste to the upper surface of 8 cm of saturated silica sand. The experiment was repeated at downward vertical flow rates of 10-, 15-, and 30- mL h^{-1} (specific discharge of 0.2-, 0.3-, and 0.6- m d^{-1}), selected to represent the range of hydrologic fluxes into riverbeds that occur in regulated river reaches (based on available literature). To plot breakthrough curves (BTCs), *Chlorella* concentrations in outflow were determined by measuring absorbance (at 660 nm wavelength). To plot retention profiles (RPs), the mass of *Chlorella* retained on sand in 1 cm depth intervals was determined using the loss-on-ignition method.

A numerical transport model of the experiments was constructed in MATLAB. Velocity enhancement (early arrival) of suspended *Chlorella* (relative to non-reactive tracer tests) was interpreted to be the result of gravitational settling of the particles, so transport of *Chlorella* was modelled by advection, hydrodynamic dispersion, and gravitational settling. Retention of *Chlorella* was modelled by filtration. Experimental data were used to estimate model parameters (porosity and dispersivity for sand; settling rate, input concentration, and filtration coefficient for *Chlorella*), which allowed the model to produce BTCs and RPs that matched the experimental results.

Pulses of dissolved organic carbon (DOC) associated with breakthrough of *Chlorella* demonstrated the potential for POM to provide a source of DOM in riverbeds. The percentage of applied *Chlorella* that entered the sand (per unit volume of flux) was found to increase with increased flow rate, which suggests that increasing the vertical hydrologic flux into riverbeds could increase the mass of POM transferred (per unit volume of flux) from rivers (or riverbed surfaces) into riverbeds. To account for the different durations and masses entered in each experiment, the calculated mass of *Chlorella* retained was expressed as a percentage of the calculated total mass entered (during the entire experiment) per unit volume eluted.

At each selected flow rate, experimental results and model simulations both support the hypothesis that in addition to the mass retained per unit time increasing with flow rate (since mass is introduced at a faster rate), the mass retained (as % of mass entered) per unit volume of flux also increases. Additionally, the velocity enhancement of suspended *Chlorella* particles during downward vertical flow conditions suggests that under repeated vertical flow reversals in riverbeds, there could be net infiltration and downward transport of POM. Therefore, in river reaches where dam operations increase the magnitude of riverbed exchange fluxes and the frequency of reversals in flux direction, the mass of POM delivered to microbial communities in riverbeds may also be increased.

Acknowledgements

I thank my co-supervisors (Dr. Fereidoun Rezanezhad and Dr. Philippe Van Cappellen) for providing me with an opportunity to work independently on a thesis project that connected the aspects of Earth Science that fascinate me most (surface-water/groundwater interactions, nutrient cycles), and for carving out valuable time to listen to my (long-winded, often confused) weekly updates. Their guidance was immensely helpful, keeping me aimed in a productive direction. I also thank them for the many previous opportunities they provided me with in the Ecohydrology Research Group (ERG), which prepared me to pursue an MSc degree.

I extend thanks to my external committee members: Dr. Matthew Ginder-Vogel and Dr. Eric Roden. Despite being limited to remote communications, they made me feel welcomed in our project meetings. I express special thanks to Dr. Ginder-Vogel for staying connected outside of official committee meetings, and to Dr. Roden for extended conversations during 'virtual' poster sessions (the only interactive part of my first science conference). I am grateful for the support of my internal committee members as well. I thank Dr. Thai Phan for filling this role during the first half of my MSc program, and I thank Dr. Tonya DelSontro for joining my committee for the second half. They have both raised challenging questions in my committee meetings, which I appreciated.

I also extend thanks to Marianne Vandergriendt, Dr. Shuhuan Li, and Stephanie Slowinski for providing training and support in the ERG lab (both during my MSc, and in years prior). It was a pleasure to work with all of you. I thank the Research Assistants and Technicians in ERG for their support in the lab: Yuba Bhusal, Konrad Krogstad, Danielle Green, Christina Lam, Richard Pham, Tara Ferguson, and Sam Smith. I thank Dr. Eric Prouzet and Dr. Martin Ross for training and use of their FLOWCAM and particle size analyzer instruments, respectively. I thank the Science Technical Services staff (Harmen Vander Heide, Andrew Dube, Hiruy Haile) for constructing flow-through reactors to meet my design requests.

I appreciated the ongoing encouragement and friendship of my fellow MSc students in ERG: Ari Lisogorsky and Jane Ye. Jane's positivity is contagious, and Ari's energy seems to have no limits (if only that were contagious, too!). I thank all ERG members (past and present), for forming a community that I have had the privilege of being part of, and for their exemplary research. I wish to specifically thank Dr. Clement Alibert for informal and constructive conversations regarding the shared challenges of our research.

I also thank the Graduate Coordinator for the Department of Earth and Environmental Sciences (Susan Fisher) and the Project Coordinators of the ERG and Global Water Futures (Linden Fairbairn, Mickey Nielsen, Bhaleka Persaud, and Anita Ghosh), for their administrative work, which I depended on as a graduate student.

In addition to all those listed above who had an important role in my research experience, I wish to thank everyone who had an important role in the other aspects of my graduate studies. I thank Dr. Colby Steelman and Dr. Randy Stotler for supervising me as a teaching assistant for *Fields Methods in Hydrology*. I was thrilled to be involved in my favourite undergraduate course, which first inspired my interest in surface-water/groundwater interactions. I also thank all my instructors and classmates from my graduate courses, each of which addressed specific topics and skills that I genuinely desired to learn. My MSc program was certainly worthwhile to me. Outside of academics, I thank everyone who coached me or trained with me as part of the Warriors Varsity Cross Country Team and the Warriors Triathlon Club. Having communities in which I could share my passion for endurance sports and push my limits has been a pillar for my mental health.

Finally, I thank my supportive friends and family, especially my parents: Mom (Jenn), Dad (Al), Step-Dad (John), and Step-Mom (Dawn). Each of them has always let me know, in their own unique way, that they believed I could succeed - even when I felt certain I could not.

Table of Contents

List of Figures

List of Tables

List of Abbreviations

ABD	Area-Based Diameter
ADE	Advection-Dispersion Equation
Br^-	Bromide Ion
BTC	Breakthrough Curve
C	Carbon
CHNS	Carbon, Hydrogen, Nitrogen, Sulfur
CO_2	Carbon Dioxide
CTAB	Cetyltrimethylammonium Bromide
D[4,3]	Volume Moment Mean Diameter
DIC	Dissolved Inorganic Carbon
DOC	Dissolved Organic Carbon
DOM	Dissolved Organic Matter
FTR	Flow-Through Reactor
IC	Ion Chromatography
KBr	Potassium Bromide
LOI	Loss-On-Ignition
MDL	Method Detection Limit
OC	Organic Carbon
OCUL	Ontario Council of University Libraries
OM	Organic Matter
POC	Particulate Organic Carbon
POM	Particulate Organic Matter
PTFE	Polytetrafluoroethylene
RP	Retention Profile
SOP	Standard Operating Procedure

List of Symbols

Symbols are listed in the order they appear in the thesis.

Symbol	Name	[units]
C	concentration of solute or suspended particles (Br^- concentration in model)	Br^- model: [mmol cm^{-3}]
t	time	[s]
D	hydrodynamic dispersion coefficient	[cm^2 s^{-1}]
x	distance in flow direction (depth from sand surface in flow-through reactor)	[cm]
v	average linear pore water velocity	[cm s^{-1}]
Q	volumetric discharge (flow rate)	[cm^3 s^{-1}]
A	cross-sectional area perpendicular to flow direction (cross-sectional area within flow-through reactor)	[cm^2]
ϕ	porosity	[-]
q	specific discharge ($q = Q/A$, $v = q/\phi$)	[cm^3 cm^{-2} s^{-1}] = [cm s^{-1}]
λ	filtration coefficient	[cm^{-1}]
d_m	median grain size (diameter) of porous collector medium	[cm]
α	collision efficiency	[-]
η	collector efficiency	[-]
η_D	diffusion component of collector efficiency	[-]
η_I	interception component of collector efficiency	[-]
η_G	sedimentation component of collector efficiency	[-]
k_B	Boltzmann constant	[g cm^2 s^{-2} K^{-1}]
T	absolute temperature	[K]
μ	dynamic viscosity of water	[g cm^{-1} s^{-1}]
ρ_w	density of water	[g cm^{-3}]
d_p	diameter of suspended particles	[cm]
ρ_p	density of suspended particles	[g cm^{-3}]
g	constant for gravitational acceleration	[cm s^{-2}]
C_0	input concentration of solute or suspended particles (Br^- input concentration in model)	Br^- model: [mmol cm^{-3}]
C_{max}	breakthrough concentration of suspended particles	mass/volume, *e,g.*, [mg cm^{-3}]
L	length of column packed with porous media	[cm]
M_{D_i}	initial oven-dry sample mass	[g]
M_{D_a}	oven-dry mass of ash (material remaining post-ignition)	[g]
R_{Chl}	ash content of *Chlorella* (fraction of M_{D_i} recovered as M_{D_a} in *Chlorella* samples)	[-]
M_c	combusted sample mass	[g]
$M_{c_{fraction}}$	fraction of M_{D_i} (of sand sample) lost during ignition	[-]
$M_{c_{sand}}$	mass of sand combusted	[g]
$M_{c_{Chl}}$	mass of *Chlorella* combusted	[g]

M_{Chl}	total mass of *Chlorella* in sample	[g]
$R_{Chl_{avg}}$	mean ash content (R_{Chl}) from the three *Chlorella* blanks	[-]
M_{sand}	total mass of sand in sample	[g]
$C_{Chl/sand}$	concentration of *Chlorella* in sample (expressed as a mass ratio, mg *Chlorella* per g sand)	[mg g^{-1}]
$C_{POC/sand}$	concentration of POC in sample (expressed as a mass ratio, mg POC per g sand)	[mg g^{-1}]
α_L	dispersivity of sand medium	[cm]
D^*	effective molecular diffusion coefficient (for Br^- in model)	[cm^2 s^{-1}]
D_m	molecular diffusion coefficient (for Br^- in model)	[cm^2 s^{-1}]
Δt	timestep size in numerical transport model	[s]
Δx	spatial cell size in numerical transport model	[cm]
n	superscript indicating current timestep	[-]
$n+1$	superscript indicating next timestep	[-]
$n-1$	superscript indicating previous timestep	[-]
i	superscript indicating spatial cell	[-]
$i+1$	superscript indicating next spatial cell	[-]
$i-1$	superscript indicating previous spatial cell	[-]
s, p	dimensionless grouped constants for Br^- model	[-]
C_c	concentration of suspended *Chlorella* particles	[mg cm^{-3}] = [g L^{-1}]
D_c	hydrodynamic dispersion coefficient (for suspended *Chlorella* particles)	[cm^2 s^{-1}]
v_s	gravitational settling rate of *Chlorella* particles in sand	[cm s^{-1}]
D_c^*	effective diffusion coefficient for *Chlorella* particles	[cm^2 s^{-1}]
C_{c_0}	input concentration of suspended *Chlorella* particles	[mg cm^{-3}] = [g L^{-1}]
$C_{c_{max}}$	breakthrough concentration of suspended *Chlorella* particles	[mg cm^{-3}] = [g L^{-1}]
l	depth of FTR outlet below upper boundary of sand (8 cm)	[cm]
s_c, p_c, w_c	dimensionless grouped constants for *Chlorella* model	[-]
$F_{c_{in}}$	*Chlorella* flux entering spatial cell in the sand medium	[mg cm^{-2} s^{-1}]
$F_{c_{out}}$	*Chlorella* flux exiting spatial cell in the sand medium	[mg cm^{-2} s^{-1}]
$M_{c_{filtered}}$	mass of *Chlorella* filtered in spatial cell during timestep	[mg]
PV_{cell}	pore volume of a single spatial cell in sand medium	[cm^3]
V_{cell}	total volume of a single spatial cell in sand medium	[cm^3]
C_{cr}	concentration of *Chlorella* retained on sand (mg *Chlorella* per cm^3 of pore space)	[mg cm^{-3}]
ρ_s	particle density of sand	[g cm^{-3}]
ρ_b	bulk density of sand	[g cm^{-3}]
M_{cell}	mass of sand in each spatial cell in the sand medium	[g]
a	coefficient in exponential curve representing *Chlorella* RP	[mg g^{-1}]
b	coefficient in exponential curve representing *Chlorella* RP	[cm^{-1}]

Chapter 1: Introduction

1.1: Organic Matter

Organic matter (OM) refers to a wide variety of carbon-based molecules (Williams & Frausto da Silva, 2005) in non-living material within soils and aquatic environments (Swift, 1996; Lehmann & Kleber, 2015). OM has an important role in nutrient cycling because it can provide a source of carbon and electron donors for microbes to use in reduction and oxidation reactions that transform nutrient elements (Boano *et al.*, 2014; Lehmann & Kleber, 2015). Reduction of various electron acceptors in the typical 'redox ladder' of microbial energy-yielding reactions is usually paired to oxidation of OM, and these reactions are drivers of biogeochemical nutrient cycles (LaRowe & Van Cappellen, 2011). OM may also function as a source or carrier of nutrient elements in aquatic environments.

OM in aquatic environments can be divided into two broad classes: dissolved organic matter (DOM) and particulate organic matter (POM). The particle size that distinguishes between these two classes is not defined consistently (Ortega-Retuerta *et al.*, 2009; Spencer *et al.*, 2009; Zhang *et al.*, 2009; Nimptsch *et al.*, 2014), but a common distinction is that organic particles >0.45 µm are considered POM (Thurman, 1985; Nimptsch *et al.*, 2014; Brailsford *et al.*, 2017). This thesis is focused on POM.

1.1.1: Organic Matter in Rivers

OM can be delivered to rivers (allochthonous OM) or produced within them (autochthonous OM). In large rivers, OM often originates from plant remains delivered by soil erosion (rather than being produced within the rivers themselves) because large rivers can carry loads of suspended sediment that are sufficient to block the sunlight that is required for production of OM by photosynthesizing organisms (Benner, 2002). Suspended sediment in rivers can be trapped by dams, so there is potential for reduced suspended sediment and increased light penetration downstream from dams to allow autochthonous POM to be

produced by photosynthesis within the water column (by planktonic algae) or on riverbeds (by periphyton).

1.1.2: Biogeochemical Importance of Organic Matter in Riverbeds

When river water flows into riverbeds, it can deliver OM. POM (such as algal cells) transferred from rivers into riverbeds may be retained and degrade into DOM that can be used in microbial reactions. Products of the reactions may flow back into rivers. Over long river reaches, these small-scale processes within riverbeds may have large cumulative impacts.

'Hyporheic zones' (sometimes collectively referred to as 'the hyporheic zone') are areas where river water flows into riverbeds and then back up into rivers (Winter *et al*., 1998; Sophocleous, 2002). Hyporheic zones have been recognized as 'hotspots' that influence the overall biogeochemical function of rivers (Naegeli & Uehlinger, 1997; Battin *et al.*, 2003; Kloep & Röske, 2004; Boano *et al*., 2014; Kiel & Bayani Cardenas, 2014; Newcomer *et al.*, 2018) – such as whether a river is a net source or sink of a nutrient element (*e.g.*, carbon, nitrogen, phosphorus).

The value of incorporating an understanding of small-scale biogeochemical processes in hyporheic zones into watershed-scale models to improve accuracy has been recognized (Boano *et al.*, 2014). Some studies have modelled hyporheic zone biogeochemistry at a small scale and discussed the potential implications at larger scales: Newcomer *et al.* (2018) developed a one-dimensional model of hydrological and biological processes controlling carbon and nitrogen cycling in a riverbed and explored how the processing of nutrients would differ under 'gaining river' and 'losing river' conditions. Other studies have used large-scale hydrological models to estimate the cumulative impact of specific riverbed processes: Kiel & Bayani Cardenas (2014) used a numerical model to calculate the residence time of hyporheic exchanges in riverbanks throughout the entire Mississippi River network and estimated the

portion of the riverbanks that could potentially remove nitrogen from the water by denitrification (based on the expected hyporheic residence time required for denitrification to occur).

Since riverbed sediments (especially hyporheic zones) have a large influence on the overall biogeochemical function of river ecosystems, an understanding of small-scale riverbed processes is required for accurate modelling of nutrient cycles at the scale of entire watersheds, which can inform nutrient management strategies for mitigating eutrophication. The transport and retention of POM is a subset of the small-scale riverbed processes that are relevant to biogeochemical cycles. The transport and retention of POM is also directly related to the challenges of eutrophication and harmful algal blooms because algae are an example of POM that can be suspended in water. The settling, transport, and retention of algae in sediments is a possible fate of algae in the water column (Kloep & Röske, 2004). Thus, understanding how algae are transported and retained in sediments is relevant for predicting the ability of aquatic ecosystems to assimilate algal blooms (*e.g.*, in eutrophic river reaches). Combined with an understanding of microbial communities in sediments, this could also be useful for predicting the extent of oxygen depletion driven by decomposition of algae.

1.2: Particle Transport and Retention in Saturated Porous Media

1.2.1: Particle Transport Processes

The transport and retention of POM in riverbed sediments is an example of particle transport through saturated porous media. The foundational processes (which apply to both solutes and suspended particles) for modelling flow through porous media are advection, dispersion, and diffusion. Freeze & Cherry (1979) provided a thorough introduction to these processes, which are explained briefly here to provide a foundation for discussing how particle retention can be added to transport models. Advection is simply transport by the movement of the pore water itself. Solute molecules or suspended particles also undergo random motions that cause them to spread apart from each other. These random motions occur even if the fluid

is not in motion and result in movement from high concentration areas to low concentration areas - this process is called diffusion. Mechanical dispersion refers to other ways in which solute molecules or suspended particles spread apart when the fluid is moving: velocities are faster further away from solid surfaces because of decreased friction, and velocity also varies because of different lengths of the many possible flow paths through a porous medium. These velocity variations cause more spreading to occur in the direction of flow. Diffusion and mechanical dispersion are usually combined into a single term called 'hydrodynamic dispersion' in modelling. These transport processes are all incorporated into what is known as the 'advection-dispersion equation' (ADE), which is a partial differential equation representing how a concentration changes in space and time. Other processes that increase or decrease the concentration (such as chemical reactions) can also be included in the equation. Eq. 1.1 is a simplified version of a one-dimensional ADE (adapted from Freeze & Cherry, 1979):

$$\frac{\partial C}{\partial t} = D\frac{\partial^2 C}{\partial x^2} - v\frac{\partial C}{\partial x} \qquad (1.1)$$

where C is the concentration of the solute or suspended particles of interest (dimensions: mass over volume), t is time, D is the hydrodynamic dispersion coefficient (which depends on properties of the porous medium and the transported solute/particles; dimensions: area/time), x is distance along the direction of flow, and v is the average linear pore water velocity in the direction of flow. v is defined by Eq. 1.2:

$$v = \frac{Q}{A\phi} = \frac{q}{\phi} \qquad (1.2)$$

where Q is the volumetric flow rate (dimensions: volume/time), A is the cross-sectional area perpendicular to flow direction, ϕ is the porosity of the porous medium, and q is the specific discharge: volumetric flow rate per unit area perpendicular to flow (dimensions: volume/area/time, but often written as simplified 'distance/time').

In words, the ADE (Eq. 1.1) expresses that the rate of change in concentration with respect to time is a combination of the rate of change in space due to both hydrodynamic dispersion (the first term on the right side) and advection (the second term on the right side).

If suspended particles are denser than the pore water, then gravitational settling could also be a relevant process influencing transport and retention (Chrysikopoulos & Syngouna, 2014; Jin *et al.*, 2019). During flow directed upwards or horizontally, settling could increase the retention of particles within the porous medium. During downward vertical flow, settling may explain observations of advanced transport of suspended particles relative to the pore water, which has been referred to as 'velocity enhancement' in literature (*e.g.*, Harter *et al.*, 2000).

1.2.2: Particle Retention by Filtration

Filtration is a combination of mechanisms that remove suspended particles from a solution as it flows through a porous 'collector' medium. McDowell-Boyer *et al.* (1986) provided a clear and thorough description of filtration, which is summarized here. Filtration includes surface filtration ('caking'), mechanical filtration ('straining'), and physical-chemical filtration. Surface filtration ('caking') occurs if particles too large to enter the porous medium become deposited as a 'cake' on the surface, which can reduce permeability. Mechanical filtration ('straining') occurs if particles are small enough to enter pore spaces, but too large to pass through. 'Physical-chemical filtration' is removal of particles from solution by attachment to collector surfaces under the influence of both physical and chemical forces. Filtration has also been referred to as 'attachment,' 'deposition,' or 'first-order deposition kinetics' (Bradford *et al.*, 2002). The clogging of pore space and resulting reduction in permeability has also been referred to as 'colmation' (Brunke, 1999): 'external colmation' is like surface filtration ('caking'), while 'internal colmation' is clogging that occurs within pore spaces.

Filtration is a retention process that can be included in the ADE for modelling particle transport in porous media. Filtration is usually modelled as an irreversible process ('permanent

deposition'), while reversible deposition has been referred to as 'sorption' (*e.g.*, Harter *et al.*, 2000). Filtration is usually modelled such that the retention of suspended particles increases with increasing suspended particle concentration (C) and average linear pore water velocity (v). Eq. 1.3 is an ADE with an additional term to model filtration (adapted from Harvey & Garabedian, 1991; Harter *et al.*, 2000).

$$\frac{\partial C}{\partial t} = D\frac{\partial^2 C}{\partial x^2} - v\frac{\partial C}{\partial x} - v\lambda C \qquad (1.3)$$

where λ is the 'filtration coefficient' (dimensions: inverse distance, *e.g.*, cm^{-1}).

1.2.3: Filtration Coefficient

Particle filtration models have defined λ using Eq. 1.4 (Logan *et al.*, 1995; Harter *et al.*, 2000):

$$\lambda = \frac{3(1-\phi)}{2d_m}\alpha\eta \qquad (1.4)$$

where ϕ (dimensionless) and d_m (length units, *e.g.*, cm) are the porosity and median grain size of the collector medium, respectively. Note that λ is also a function of two other dimensionless parameters. η is the 'collector efficiency,' which represents the fraction of particles that collide with collector surfaces (Close *et al.*, 2006). α is the 'collision efficiency:' an empirical constant that represents the fraction of particle-collector collisions that result in attachment (Close *et al.*, 2006).

Harvey & Garabedian (1991) presented an equation for calculating α, but it was specifically derived for a pulsed input of suspended particles (*i.e.*, all mass entering collector medium at one time). Harter *et al.* (2000) and Close *et al.* (2006) estimated λ by other means, then solved Eq. 1.4 for α. An equation for calculating η of a single collector grain is shown in Eq. 1.5, in which η is the sum of collector efficiencies related to diffusion (η_D), interception (η_I), and sedimentation (η_G) defined by Eq. 1.6, 1.7, 1.8 (Yao *et al.*, 1971):

$$\eta = \eta_D + \eta_I + \eta_G \quad (1.5)$$

$$\eta_D = 0.9\left(\frac{k_B T}{\mu d_p d_m \mathrm{v}\phi}\right)^{2/3} \quad (1.6)$$

$$\eta_I = \frac{3}{2}\left(\frac{d_p}{d_m}\right)^2 \quad (1.7)$$

$$\eta_G = \frac{(\rho_p - \rho_w) g {d_p}^2}{18\mu \mathrm{v}\phi} \quad (1.8)$$

where k_B is the Boltzmann constant (1.38×10^{-23} kg m^2 s^{-2} K^{-1} = 1.38×10^{-16} g cm^2 s^{-2} K^{-1}), T is the absolute temperature (*e.g.*, 25°C = 298.15 K), μ and ρ_w are the dynamic viscosity and density of water (*e.g.*, 8.9×10^{-3} g cm^{-1} s^{-1} and 1.0 g cm^{-3} at 298.15 K (Kestin *et al.*, 1978)), d_p and ρ_p are the diameter (cm) and particle density (g cm^{-3}) of suspended particles, and g is the constant for gravitational acceleration (980 cm s^{-2}). A porosity-dependent correction factor has been used to convert η of a single collector grain to η of a porous collector medium, and the equations for η have been further developed to include the role of London-van der Waals forces in particle removal. Logan *et al.* (1995) provided a summary of these developments, and highlighted corrections to the equations that were overlooked elsewhere (*e.g.*, explaining that Eq. 1.6 and Eq. 1.8 should use $q = v\phi$ rather than v to be consistent with how the equations were derived). The equations for the single-collector efficiency are sufficient for the purpose of the present discussion, which is to assess whether λ is theoretically expected to vary with flow rate.

The diffusion component (η_D) of the collector efficiency (η) represents the fraction of particles that collide with collector grains due to random 'Brownian' motions of the particles (Yao *et al.*, 1971). η_I represents the fraction of particles that collide with collector grains because their flow paths are 'intercepted' by collector grains (Yao *et al.*, 1971), which depends on the ratio of particle size to collector grain size ($\frac{d_p}{d_m}$, Eq. 1.7). η_G represents the fraction of

particles that collide with collector grains due to the influence of gravity on their flow paths (Yao *et al.*, 1971) - note that Eq. 1.8 contains Stokes' law for the settling rate of a sphere in a fluid. η_D (Eq. 1.6) and η_G (Eq. 1.8) are inversely related to v: as v increases, the fraction of particles colliding with collector surfaces due to diffusive and gravitational effects on their flow paths decreases. η_I is not related to v. Thus, η decreases as v increases (*i.e.*, as v increases, a smaller fraction of particles collide with collector grains). Unless the decrease in η is cancelled by a greater increase in α, λ would also decrease as v increases, and the mass of suspended particles retained by filtration (per unit volume of flux) would decrease as v increases. For the mass retained (per unit volume of flux) to increase with v, α would have to increase with v. Increased α would mean that a greater fraction of particle-collector collisions result in attachment. In Harter *et al.* (2000), experiments at greater v led to greater estimated α, and this was also the case for most (but not all) experiments in Close *et al.* (2006).

An expression simpler than Eq. 1.4 has been developed to estimate λ using results of laboratory column experiments (discussed in 1.4). Since filtration is modelled as a velocity-dependent process, this thesis chapter explores whether laboratory column experiments that studied particle transport in porous media used flow rates that are representative of the flow of water into riverbeds.

1.3: Review of Riverbed Exchange Fluxes

There are many types of hydrologic exchanges through riverbeds. Cranswick & Cook (2015) provided a summary of the definitions of three categories of exchanges between river water and subsurface water: 'river-aquifer,' 'bank storage,' and 'hyporheic' exchange. It is difficult to distinguish between these categories of exchanges because they all vary in both space and time and can be superimposed on one another. This is not an issue for the present discussion, because all three categories of exchanges can deliver OM into riverbeds.

1.3.1: Literature Search for Riverbed Exchange Fluxes

A literature search was performed to select a sample of scientific articles that reported water fluxes measured in riverbeds. The Ontario Council of University Libraries (OCUL) 'Omni' academic search tool (accessed through the University of Waterloo library website) was used for the search. The desired criterion for selection of articles was that they include measurements of hydrologic flux in riverbeds. To narrow the search further, it was decided that all selected articles should use similar methodology to measure the fluxes, and the 'seepage meter' was chosen for its simplicity. The search terms were that any field contain 'river' OR 'stream' OR 'creek' AND 'seepage meter' AND 'flux,' with the intent of selecting the first six papers that included the desired information and were accessible through the University of Waterloo library.

The desired format of fluxes for comparison between lab experiments and field measurements was specific discharge (q): volumetric discharge per unit area perpendicular to flow (dimensions: volume/area/time, but often written as simplified 'distance/time'). It could be argued that the proper format to compare fluxes would be to use the average linear pore water velocity (v, specific discharge divided by porosity) to account for some of the differences in sediment properties (*e.g.*, porosity and permeability) between the various riverbeds studied and porous media used in column experiments. This was not possible because porosity was not reported in all studies. Seepage meter measurements from the selected papers are presented in Table 1.1. This includes an additional article (Rosenberry & Pitlick, 2009) that was cited in the selected studies.

For Table 1.1, all fluxes were converted to specific discharge in units of m d^{-1}. Fluxes from stream into streambed are written as negative (-), and all other fluxes are positive (from streambed into stream). Differences in methods are summarized in the *'Notes'* column.

Table 1.1: Selected studies that used seepage meters to measure riverbed exchange fluxes.

Seepage Meter Measurements from Literature [positive (+) fluxes = from streambed into stream, negative (-) fluxes = from stream into streambed]					
Lead Author(s)	**Year**	**Location**	**Calculated Seepage Flux (Specific Discharge), [m/d]**		**Notes**
Alexander & Caissie	2003	Catamaran Brook, New Brunswick, Canada (sand and gravel streambed)	1.5E-05	(min)	Installed at 3 locations in 4.5km reach for 6-7 weeks, measured seepage flux weekly (12-24h measurement time).
			0.22	(max)	
Kennedy *et al*.	2010	West Bear Creek, North Carolina, USA (mostly sand streambed)	0.14	(min)	Seepage meters covered by PVC sheet to minimize turbulence. Installed at 53 locations in 62.5m reach, 4-6 repeat measurements (avg. 18min measurement time) at each site.
			0.66	(mean)	
			1.6	(max)	
Moore et al.	2020	Minnehaha Creek, Minnesota, USA (mostly sand and gravel streambed)	-0.043	(min)	Installed at 9 locations in 35km reach, 2-5 one week deployments (24h measurment time) at each site.
			0.007	(mean)	
			0.13	(max)	
Rosenberry *et al*.	2016	Quashnet River, Massachusetts, USA (sand and fine gravel streambed)	-0.14	(one site)	Installed at 28 locations (identified as potential groundwater discharge, by temperature sensing) along 2.3 km reach. Multiple measurements at each site.
			-0.55	(one site)	
			0.05	(min +)	
			0.42	(median +)	
			3.00	(max +)	
Rosenberry & Pitlick	2009	South Platte River, Colorado, USA (medium sand to fine gravel streambed)	-3.40	(min)	Used 'low-profile' seepage meters (designed for use in flowing water), installed in shelters at 24 locations in 300m reach. Repeated at least 3 measurements at each site (measurement time adapted to seepage rate). Used median measurement from each site.
			0.24	(median)	
			2.37	(max)	
Solomon et al.	2020	Middle Loup River, Nebraska, USA (sand streambed)	-0.001	(min)	Used a unique automated seepage meter design. Installed 9 seepage meters in 3x3 grid along 3m reach. Repeated measurements (~35min measurement time) over 20h period.
			0.069	(mean)	
			0.165	(max)	
Wang *et al*.	2014	Manasi River, Xinjiang, China (varied streambed sediment)	-288	(min)	Study of a river disconnected from groundwater. Used modified seepage meter design and procedure.
			-7.63E+03	(max)	

1.3.2: Riverbed Exchange Fluxes

As summarized in Table 1.1, the selected studies were performed in similar sediments (sand and gravel streambeds) and all measured exchange fluxes (specific discharge) ≤3.4 m d^{-1}, except for Wang *et al.* (2014). Wang *et al.* (2014) studied sediments with varied properties throughout a river that was disconnected from underlying groundwater: the unsaturated conditions of the sediments beneath the river explain why the exchange fluxes are negative and very large compared to the other studies. In the other studies, positive fluxes were more common than negative fluxes. The largest positive flux reported in this sample of literature is 3.00 m d^{-1} (Rosenberry *et al.*, 2016) while the largest negative flux is -3.40 m d^{-1} (Rosenberry & Pitlick, 2009). Even if flux into riverbeds is less common, this does not negate the importance of transport and retention of POM in riverbeds. POM delivered into riverbeds during short infiltration events could be retained, degraded, used in microbial reactions, and influence the biogeochemistry of water that enters rivers during the (potentially) more common

hydrologic conditions of upward flux into rivers. Also note that seepage meters measure net exchange: even if net exchange is positive, there may be hyporheic flow of water into riverbed sediments (potentially delivering POM) and back into the river.

1.3.3: Riverbed Exchange Fluxes in Regulated Rivers

It has also been demonstrated in literature that in rivers regulated by dams, large and frequent river stage fluctuations increase the magnitude of riverbed exchange fluxes and the frequency of reversals in exchange flux direction (Arntzen *et al.*, 2006; Fritz & Arntzen, 2007; Shuai *et al.*, 2019; Ferencz *et al.*, 2021). The Hanford Reach of the Columbia River (near Richland, Washington State) is an example of an environment in which frequent riverbed exchange fluxes are driven by river stage fluctuations associated with dam operations. There are many dams along the Columbia River, but no dams interrupt the ~80 km long Hanford Reach, which is connected to an unconfined aquifer (Shuai *et al.*, 2019). Upstream dam operations cause daily river stage fluctuations of up to 2 m, and associated reversals in riverbed exchange flux direction (Arntzen *et al.*, 2006; Fritz & Arntzen, 2007).

Fritz and Arntzen (2007) used hydraulic head measurements and hydraulic conductivity tests to calculate the flux (specific discharge) between the Hanford Reach and the underlying aquifer, and the maximum reported flux into the aquifer was 0.53 m d^{-1}. Shuai *et al.* (2019) used Hanford Reach river stage data from 2011-2015 in a three-dimensional model to predict fluxes between the river and aquifer, and the maximum predicted flux into the aquifer was 0.617 m d^{-1}. Shuai *et al.* (2019) also converted the hourly data to a 'weekly-smoothed case' to estimate the fluxes that would occur in the absence of dam operations. In that case, the maximum flux was reduced to 0.245 m d^{-1}.

Riverbed exchange fluxes driven by anthropogenic (dam-induced) river stage fluctuations could potentially be considered as a unique type of hydrologic exchange flux, because it could be argued that they do (or do not) fit the definitions of any of the three categories of 'river-

aquifer,' 'bank storage,' and 'hyporheic' exchange (as described by Cranswick & Cook, 2015). Fluxes driven by river stage fluctuations might usually be considered 'bank storage' fluxes, but a high frequency of flow reversals could also be argued to fit the definition of 'hyporheic zones'. However, 'bank storage' and 'hyporheic' terms for exchange both imply river water flowing in and out of riverbeds, while 'river-aquifer' exchange implies an interaction of compositionally (and/or hydrologically) distinct river water and groundwater interacting. In river reaches where the operation of dams increases the magnitude and frequency of river stage fluctuations (and by extension, riverbed exchange fluxes), the distinction between 'river water' and 'groundwater' could become less clearly defined. Riverbed exchange fluxes driven by anthropogenic river stage fluctuations may also have a dominantly vertical orientation (while 'bank storage' and 'hyporheic' imply lateral and multi-directional flow paths, respectively).

1.4: Laboratory Column Experiments to Study Particle Transport in Porous Media

Laboratory column experiments are often used to estimate values of parameters such as λ to use in models of particle transport and retention in porous media. This involves introducing the particles of interest into a column packed with the porous material of interest with a solution flowing through. To study the transport and retention of the particles in this simplified one-dimensional flow system, the quantity of particles that reaches the outflow over time and the quantity that remains trapped in the column after the experiment are measured.

The decrease in concentration of particles in suspension that occurs as a fluid flows through a 'clean bed' (a porous medium that contains no previously filtered particles) has been described by a first-order filtration equation, as shown in Eq. 1.9 (Iwasaki, 1937; McDowell-Boyer *et al.*, 1986):

$$\frac{dC}{dx} = -\lambda C \qquad (1.9)$$

where C is the concentration of suspended particles, and x is the distance from the source (in the direction of flow through the porous collector medium). Integrating Eq. 1.9 over the length (L) of a column of porous media (*i.e.*, from a source at $x = 0$ with an initial concentration $C(0) = C_0$ to a column outlet at $x = L$) leads to Eq. 1.10:

$$\frac{dC}{dx} = -\lambda C \rightarrow \frac{1}{C} dC = -\lambda dx \rightarrow \int_0^L \frac{1}{C} dC = -\lambda \int_0^L dx \rightarrow ln\, C(L) - ln\, C(0) = -\lambda(L - 0)$$

$$\rightarrow ln\left(\frac{C(L)}{C(0)}\right) = -\lambda L \rightarrow \frac{C(L)}{C(0)} = e^{-\lambda L} \rightarrow C(L) = C(0)e^{-\lambda L} \rightarrow C_{max} = C_0 e^{-\lambda L}$$

$$\rightarrow \lambda = \frac{ln\left(\frac{C_0}{C_{max}}\right)}{L} \qquad (1.10)$$

where C_{max} is the breakthrough concentration of suspended particles at the column outlet. Eq. 1.10 relates the relative breakthrough of suspended particles through the porous medium to the distance from the source (*i.e.*, relating C_{max} to the length of the column, L), and has been used to estimate the value of the filtration coefficient (*e.g.*, Harter *et al.*, 2000). Note that since this expression was derived by integrating a first-order filtration equation for 'clean-bed filtration', it represents an initial 'clean-bed' value of λ, which may become less reliable as more particles are retained (Iwasaki, 1937; McDowell-Boyer *et al.*, 1986).

Ten previous studies that used column experiments to study transport and retention of suspended particles in porous media were selected as a sample of available literature (Table 1.2). The selected studies used a variety of materials and methods, but all studied particles on the scale of micrometres – the scale of algae cells (Kloep & Röske, 2004; Ru *et al.*, 2020). Fluxes reported as volumetric discharge were divided by the cross-sectional area of the column (calculated from reported radius or diameter) to convert to specific discharge. Fluxes reported as average linear pore water velocities were multiplied by the reported porosity to

convert to specific discharge. Some fluxes were already reported as specific discharge. All units were converted to m d^{-1}.

1.4.1: Fluxes in Laboratory Column Experiments

Some of the selected studies performed column experiments using multiple different fluxes, and this is shown in Table 1.2. Some studies reported a range of fluxes used (Benamar *et al.*, 2007; Cherrey *et al.*, 2003). In this case the minimum and maximum were used for Table 1.2, and this was also done for one article that reported flux values from twenty experiments (Bradford *et al.*, 2002). For comparison to measured riverbed fluxes, the fluxes >3.4 m d^{-1} (the max reported in the sample of literature in Table 1.1) are shaded in red in Table 1.2. Five of the selected articles only used fluxes exceeding this threshold. Three articles only used fluxes below this threshold. Two articles used fluxes both above and below this threshold.

The mismatch between measured riverbed fluxes (Table 1.1) and laboratory column experiment fluxes (Table 1.2) presented here does not necessarily indicate a flaw in the column experiments. This comparison is limited because it only includes one method for measuring riverbed fluxes, and only includes a small number of field and lab studies. This was an exploration of a larger comparison that could potentially be made. Furthermore, only two of the laboratory column studies were focused on studying riverbed environments (Jin *et al.*, 2019; Metge *et al.*, 2010), so replicating riverbed fluxes might not have been a consideration for the authors. Most studies did use porous media that could exist in riverbeds though (aquifer sediments, sandy soil, gravel), so the experiments are still relevant here. An exception is the use of glass beads by Chrysikopoulos & Syngouna (2014), but their exploration of the role of gravitational settling by using different orientations of columns is certainly relevant to the variable orientations of flow that occur in riverbeds.

Table 1.2: Selected studies that used column experiments to study particle transport in porous media.

Column Experiments to Study Particle Transport and Retention in Porous Media: Examples from Literature												
				=	>3.4m/d	Terminology Used for Processes Studied						
Lead Author(s)	**Year**	**Porous Media (diameter)**	**Transported Particles (diameter)**	**Flow Direction**	**Flux (Specific Discharge), [m/d]**	**Settling as a Transport Process**	**Filtration**	**Sorption**	**Other**	**Filtration Modelled as Velocity-Dependent?**	**Study of Riverbed Environment?**
Benamar *et al.*	2007	silica gravel (2.15-3.15 mm), glass beads (2 mm)	quartz silt (2-40 µm range, 14 µm mode)	horizontal	11 3.8E+02	No	Partially	No	Mechanical component of filtration neglected based on ratio between grain size of porous medium and suspended particles. Used irreversible first-order deposition kinetics to model particle retention.	Flow velocity affected first-order kinetic particle-deposition rate coefficient.	Not specifically (silica gravel).
Bradford *et al.*	2002	Ottawa sands (median 0.15-0.71 mm) , glass beads (median 0.26 mm)	carboxylated fluorescent latex colloids (0.45, 1, 2, 3.2 µm)	vertical, upward	1.4 2.4	No	Yes	Yes	First-order deposition kinetics. Included both attachment and detachment.	Yes	Not specifically (sands).
Cherrey *et al.*	2003	coarse Hanford (200 East Area) sediment, colloids and >2mm particles removed	colloids isolated from sediment (~0.35 µm mean)	vertical, upward (unsaturated)	1.5 66	No	No	No	Mobile-immobile model with first-order deposition.	Deposition coefficient is velocity-dependent.	Not specifically (Hanford sediments).
Chrysikopoulos & Syngouna	2014	glass beads	kaolinite colloids (hydrodynamic diameter: 0.843 µm), montmorillonite colloids (hydrodynamic diameter: 1.187 µm)	horizontal, diagonal, vertical (upward and downward)	4.4	Yes	Yes	No	Includes both attachment (filtration) and detachment.	No	No, but study of different directions of flow is relevant to hyporheic zones.
Close *et al.*	2006	homogeneous pea-gravel (well-rounded, 5-7 mm diameter)	microspheres (1, 5, and 10 µm)	30 degree incline, upward flow	4.6 10 19	No	Yes	No	Filtration of colloids has components due to Brownian diffusion, interception, and settling. Includes both attachment and detachment. Discusses velocity enhancement.	Yes	Not specifically (homogeneous gravel).
DeFlaun *et al.*	1999	quartz sand (~0.16 mm), two sandy aquifer sediments	two strains of soil pseudonomad bacteria *Burkholderia cepacia*	vertical, upward	0.076	No	Yes	No	Plotted breakthrough curves and assessed portion of bacteria adhered to medium, but did not model transport.	No modelling.	Not specifically (aquifer sediments).
Harter *et al.*	2000	three sands (effective grain size 0.18, 0.42, 1.4 mm)	*Cryptosporidium parvum* oocysts (4.5-5.5 µm)	not specified	0.70 7.1	No*	Yes (permanent)	Yes (reversible)	Includes both attachment (filtration) and detachment. *Discusses 'velocity enhancement' of colloids..	Yes	Not specifically ('sandy soils and aquifer sediments').
Jin *et al.*	2019	sand (0.25-0.60 mm, median 0.39 mm)	kaolinite colloids (dominant size ~2 µm)	vertical, updward	9.1 19.8 35.2	Yes	Yes	No	Detachment removed from model because it was negligible relative to attachment.	Yes	Yes, focused on hyporheic zones.
McCaulou *et al.*	1995	aquifer sediment: medium sand from Ringold formation at Hanford site (average 0.224 mm)	A0500 flagellated rod bacteria (average 1.7 by 0.8 µm), carboxylated polystyrene microspheres (1.54 µm)	vertical, upward	5.8	No	Yes	No (discussed)	Collection/attachment/filtration of colloids has components due to Brownian diffusion, interception, and settling. Included both attachment and detachment.	Yes	Not specifically (aquifer sediments).
Metge *et al.*	2010	poorly-sorted Fe- and Al-rich sediment from below a riverbank filtration site	formaldehyde-killed oocysts, oocyst-sized microspheres (3 µm)	not specified	2.9	No	Yes	Yes	Measured degree of colloid removal, but did not model transport. Concluded that results suggest immobilization is mainly caused by 'sorptive filtration' rather than 'physical straining.'	No modelling.	Yes, used sediment from a riverbank filtration site.

1.4.2: Retention Processes

Most of the selected studies discussed filtration as a particle retention process, and in most cases, filtration was modelled as a velocity-dependent process. Table 1.2 includes brief notes on the processes discussed in each of the selected column experiment studies. Two studies measured transported and retained particles, but did not include modelling (DeFlaun *et al.*, 1999; Metge *et al.*, 2010). Cherrey *et al.* (2003) is notably different from the other studies in terms of both experimental and modelling methods because it studied unsaturated flow (the deposition of transported particles was still governed by a velocity-dependent coefficient).

The filtration term in particle transport models (*i.e.*, the '$-v\lambda C$' term in Eq. 1.3) is sometimes written with a single rate coefficient (dimensions: inverse time) in place of the pore water velocity (v) and λ (*e.g.*, McCaulou *et al.*, 1995; Bradford *et al.*, 2002; Close *et al.*, 2006; Benamar *et al.*, 2007; Chrysikopoulos & Syngouna, 2014; Jin *et al.*, 2019). v is usually still included in the equations presented to express the rate coefficient, but some studies do not present expressions for the rate coefficient (*e.g.*, Benamar *et al.*, 2007; Chrysikopoulos & Syngouna, 2014). Although Benamar *et al.* (2007) stated intentionally excluding the mechanical (straining) component of filtration (based on the relative size of the transported particles and porous media grains), velocity was still found to affect the 'first-order kinetic particle deposition coefficient' in that study.

Some studies used alternative terminology for filtration (*e.g.*, 'attachment' in Bradford *et al.*, 2002), but used the same equations to model the process. In Chrysikopoulos & Syngouna (2014), it was implied that 'filtration' and 'attachment' are synonymous, but attachment did not seem to be modelled as a velocity-dependent process. The inconsistent terminology used for particle retention processes in the literature could lead to confusion. For example, Bradford *et al.* (2002) suggested that attachment, deposition, filtration, and sorption were equivalent terms in the literature, while Harter *et al.* (2000) defined filtration as irreversible attachment and sorption as reversible attachment.

Although some studies (*e.g.*, McCaulou *et al.*, 1995; Close *et al.*, 2006) acknowledged that gravitational settling is a component included in equations for the collector efficiency η (*i.e.*, gravity is a relevant force influencing attachment when particles are close to collector surfaces), gravitational settling was only clearly included as a transport process in two studies (Chrysikopoulos & Syngouna, 2014; Jin *et al.*, 2019).

1.4.3: Estimating Filtration Coefficients

Generally, literature does not provide detail when describing methods for estimating filtration coefficients. Most of the studies included in Table 1.2 state that models were calibrated or fit to experimental data. Harter *et al.* (2000) provided the most detail and mentioned three methods for estimating the filtration coefficient: from model calibration, from Eq. 1.10, and from the depth distribution of retained particles in the column at the end of the experiment. The values reported in the paper were calculated from Eq. 1.10, using $\frac{C_{max}}{C_0}$ from breakthrough curves (BTCs) fitted to the experimental data. The authors then used Eq. 1.4 with an estimated λ and a calculated η to solve for α. McCaulou *et al.* (1995) used a similar approach, but the explanation is difficult to follow. Eq. 1.10 is likely the most feasible way to obtain an estimated value of λ because it only requires the length of the column, the suspended particle input concentration (C_0), and the suspended particle breakthrough concentration (C_{max}). Estimates can then potentially be adjusted to fit models to experimental data (*i.e.*, breakthrough curves (BTCs) of suspended particles in column outflow, and retention profiles (RPs) of retained particles in column media).

1.5: Thesis Objectives

The objective of this thesis was to identify and quantify vertical transport and retention processes for POM in riverbeds under different flow rates using lab experiments and modelling, and investigate how the magnitude of vertical hydrologic fluxes into riverbeds influence the vertical transport and retention of POM. The hypothesis was that in addition to the POM mass retained per unit time increasing with flow rate (since mass is introduced at a faster rate), the mass retained per unit volume of flux would also increase. For this thesis, a series of lab experiments were designed and conducted to represent downward vertical infiltration of POM into riverbeds. A numerical model of the experiments was constructed to demonstrate what combination of transport and retention processes could explain the results.

1.6 : Thesis Outline

This thesis consists of four chapters. Chapter 1 is an introduction to POM transport and retention in riverbeds. This includes establishing the importance of POM processes in riverbeds, introducing conceptual processes and mathematical equations used in literature to model particle transport through porous media, reviewing a selection of literature for measured hydrologic fluxes into riverbeds, and reviewing a selection of literature on laboratory column experiments that studied particle transport through porous media. Chapter 1 also includes a comparison of fluxes used in column experiment literature and measured in field study literature. Chapter 2 describes experimental methods and numerical modelling methods used for this thesis project. Chapter 3 presents results of lab experiments and explains how the data were used to estimate model parameters. Chapter 4 states conclusions and recommendations regarding the study of POM transport and retention in riverbeds.

Chapter 2: Materials and Methods

2.1: Laboratory Transport Experiments

2.1.1: Sand Samples and Properties

Unground Silica Sand (US Silica QROK #3, expected to consist mostly of quartz) was used for flow-through reactor (FTR) experiments to study POM transport in riverbed sediments. Prior to use in experiments, the sand was sieved to remove particles <200 µm with a Gilson 200 µm Test Sieve (to prevent interference with detection of suspended POM in experiments), rinsed once with 0.001 M hydrochloric acid, rinsed three times with Milli-Q water, and oven-dried (Thermo Scientific Heratherm oven) at 95°C for 24(±0.5) hours. This preparation was done in two 'batches' of sand: the first batch ('Batch A') was used for the 30 mL h^{-1} and 15 mL h^{-1} transport experiments, and the second batch ('Batch B') was prepared for the 10 mL h^{-1} transport experiment. Particle size analysis was completed for both batches of sand using a Fritsch Analysette 22 Microtec Plus laser diffraction particle size analyzer with a Wet Dispersion Unit (using a built-in 'Wet Measurement Full Range' SOP in the MAS Control instrument software). This analysis required removing all particles >2 mm from the sand (Gilson 2 mm Test Sieve). The >2 mm fraction was <0.2% of the sand mass. From each of the two batches of sand, three samples were introduced to the instrument (and each analyzed three times) to confirm the reproducibility of the results. Data from the final measurement of each batch was exported and plotted (Appendix Figure 1, 2). The mode, median, arithmetic mean, and D[4,3] (volume moment mean) diameter reported by MAS Control were all within 75 µm of 1 mm for both batches of sand (Appendix Table 1).

2.1.2: Chlorella Powder

An algae (*Chlorella vulgaris*) powder product (Green Foods Organic *Chlorella* Powder, Lot 080920, Figure 2.1) was used as a simple homogeneous representation of POM in transport experiments. This *Chlorella* powder was a dry 'broken cell wall' product that is

marketed as a nutritional supplement. The ‘broken cell wall’ product might be a better representation of suspended POM transferred from rivers to riverbeds than a live and intact culture of algae cells would be.

Figure 2.1: Green Foods Organic *Chlorella* Powder (LOT 080920).

Chlorella vulgaris is a species of microalgae with a particle size in the range of 2-10 µm (Ru *et al.*, 2020), and the mean particle diameter has been reported in literature to be about 4 µm (*e.g.,* Fung Shek, 2015; Patyna *et al.*, 2018). The laser diffraction particle size analysis method used for the sand was deemed unreliable for the *Chlorella* powder because a ‘blank test’ of the instrument (running the analysis without adding any particles to the dispersion unit) reported a particle size distribution (background signal) in the same size range expected for *Chlorella* (<15 µm). Instead, fluid imaging microscopy was used to confirm the size of the *Chlorella* powder particles. A suspension of the same *Chlorella* powder used in the transport experiments was prepared with a concentration of 0.2 g L^{-1} *Chlorella* (the approximate maximum concentration detected in outflow from the transport experiments) in 50 mg L^{-1} Bromide (Br^-, the tracer solution used in the experiments). This suspension was analyzed

using a Benchtop B3 Series FLOWCAM instrument (Yokogawa Fluid Imaging Technologies, Inc.) with a C70 syringe (1.00 mL), FC50 flow cell (50 µm depth), and 20x objective lens, in 'auto image' mode. The analysis used a flow rate of 0.24 mL min^{-1} and image rate of 20 frames per second (this combination was found to reduce multi-imaging of particles), 'distance to nearest neighbour' set to zero, and a 1-1,000 µm (area-based diameter, 'ABD') size filter (without a size filter, a large portion of detected 'particles' reported were <1 µm, which was assumed to be background noise). Sample volume was set to 1 mL, but analysis was set to stop after detection of 25,000 particles. For this *Chlorella* suspension, detection of 25,000 particles was achieved in about 1 minute. From three repeat analyses (each detecting 25,000 particles) the mean D[4,3] ABD of the *Chlorella* particles was 4 µm, which agrees with the size reported in previous studies (Fung Shek, 2015; Patyna *et al.*, 2018). The maximum particle size (ABD) detected for this sample was 14.15 µm. Figure 2.2 is a sample of the images of *Chlorella* particles in the 0.2 g L^{-1} suspension captured by the FLOWCAM instrument. The variable and irregular shape of the *Chlorella* particles is not surprising, since the powder is labelled as a 'broken cell wall' product.

To verify the settings used for FLOWCAM analysis, a suspension of microparticles with a known mean particle size range close to that of *Chlorella* was analyzed. A suspension of polytetrafluoroethylene (PTFE) microparticles (Goodfellow 500-253-38: PTFE powder, mean particle size 6-9 µm) was prepared in a cetyltrimethylammonium bromide (CTAB) surfactant solution (61.5 mg L^{-1} PTFE and 70 mg L^{-1} CTAB in Milli-Q water). This was more diluted than the *Chlorella* suspension, so fewer particles were detected: with sample volume set to 1 mL, only 770 particles were detected. With sample volume increased to 4 mL (analysis time increase to >16 minutes), still only 6,000-7,000 particles were detected. From the three trial analyses of the PTFE suspension (total 13,508 particles counted), the mean D[4,3] ABD was 7 µm (average of the value reported from each of the three trials, weighted by the number of particles counted in each trial). This is within the expected mean size of the PTFE powder,

which suggests that the D[4,3] ABD value reported by the same analysis methods for the *Chlorella* suspension was reliable.

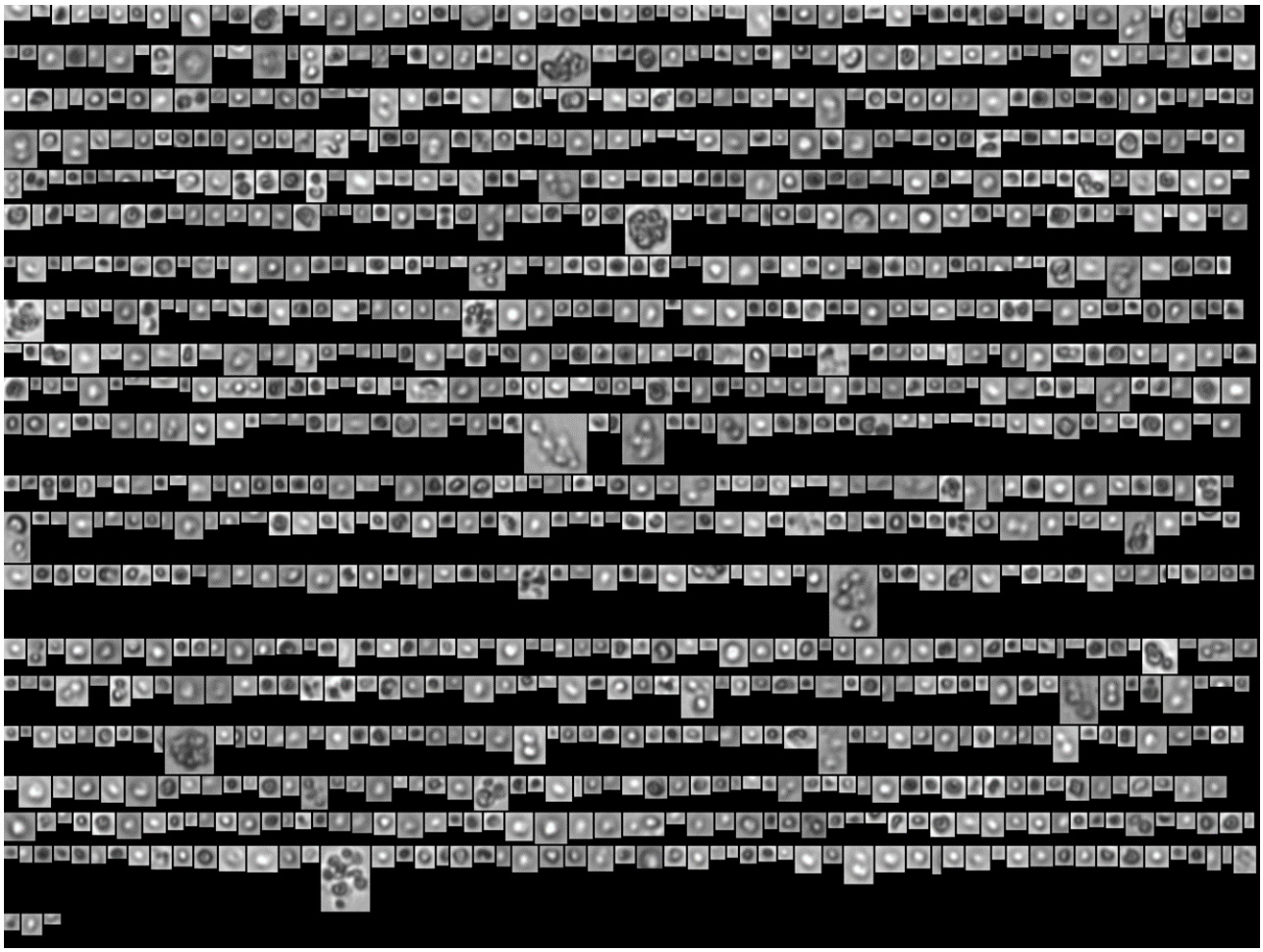

Figure 2.2: A sample of the images (captured by the FLOWCAM instrument) of *Chlorella* particles in a 0.2 g L^{-1} suspension.

The carbon content of the *Chlorella* powder was determined using an Elementar Vario EL Cube CHNS Analyzer. To confirm that the powder does not contain inorganic carbon, 1 M hydrochloric acid was dropped onto a sample of the powder, and no reaction was observed. Thus, the carbon content determined by CHNS analysis was interpreted as organic carbon (OC) content. For CHNS analysis, three samples of ~20 mg *Chlorella* powder were weighed into tin cups (folded to contain sample). The instrument's combustion tube was purged with Argon carrier gas prior to the combustion of each sample. Each sample was combusted at 600°C in oxygen for 150 s. The gaseous combustion products were reduced over hot copper in the instrument's reduction tube to convert carbon to CO_2 gas detected by a thermal

conductivity detector, and the calibrated instrument software converted thermal conductivity peaks to a mass of carbon and then to a percentage of the known sample mass (Callum McCusker, Senior Field Service Engineer for Elementar Americas (personal communication, 2020)). The *Chlorella* powder was 44(±2) % OC (mean from triplicate samples ± standard deviation).

2.1.3: Flow-Through Reactors: Construction and Packing with Sand

Flow-Through Reactors (FTRs) are small-scale (usually <10 cm) columns that have been used for studies of solute transport and reaction kinetics in porous materials including undisturbed sediment (Pallud *et al*., 2007), sediment slurries (Pallud & Van Cappellen, 2006), and intact cores of peat (McCarter *et al.*, 2019). FTRs are typically used for solute transport experiments oriented vertically with upward flow at a rate controlled by a peristaltic pump, but were adapted for the purposes of studying the transport of POM under downward vertical flow conditions.

The FTRs constructed and used for this project (Figure 2.3, 2.4) consisted of an open-ended cylinder (clear acrylic, 5.08 cm outer diameter, 3.8 cm inner diameter, 10 cm length) with two square plates (white HDPE, 6.4 × 6.4 × 1.3 cm) that fit securely onto each end. The top FTR plates had a circular opening for accessing the interior of the FTRs, and a separate circular cap that could be used to cover the opening (with a smaller central hole for input tubing, about 3 mm diameter). The bottom FTR plates had a circular depression, with a small hole (about 3 mm diameter) in the centre leading to the outflow channel that exited one side of the plate. Before assembling each FTR, a 185 µm nylon mesh filter disc (Component Supply CMND-185-055, 55 mm diameter, trimmed with scissors to fit) and a rubber o-ring were placed in the circular depression of the bottom plates. The mesh size was chosen to keep the sand grains (>200 µm) within the FTRs while allowing *Chlorella* particles (<15 µm) through.

Threaded rods connected the FTR end plates at each corner, and the assembly was held together tightly by nuts threaded onto the rods (washers and wing nuts on top plate, hex nuts under bottom plate). The threaded rods extended below the bottom plate to serve as four ‘legs’ that added extra height to the FTRs. The bottom ends of the rods inserted into a stable base that can support up to six FTRs: a platform (white HDPE, 45.5 × 8.6 × 2.5 cm) resting on a metal frame (37 cm height, 45.5 × 25.3 cm footprint). Due to the combined height of the base platform and rods, the outflow port at the base of the FTRs was about 50 cm from the benchtop. This added height allowed the FTRs to be in view of a camera resting on a tripod on the lab bench to record the *Chlorella* transport experiments, and provided a convenient space below the FTRs for collecting outflow samples without entering the camera’s field of view. Additional wing nuts on the threaded bolts at the surface of the platform were adjusted to level the FTRs (using a bubble level to check all four sides).

The bottom FTR plates were connected to tubing (Fisherbrand Catalog No. 14-169-7A: Saint Gobain AGL00007 clear polyvinyl chloride tubing, 1/8” inner diameter, 1/16” wall, ¼” outer diameter) by a threaded fitting (Nordson Medical M5220-1: M5x.8 Thread, ¼” Hex to 200 Series Barb, White Nylon) that was tightly wrapped with pipe joint tape (Masters Orange T-Tape) around the thread and covering the exterior interface between the fitting and tubing. A 16 cm segment of tubing connected the outflow fitting to a two-way stopcock valve (Masterflex Fitting 30600-05: Polycarbonate One-Way Stopcock, Male Luer Lock; connected by Nordson Medical FTLL230-9: Female Luer Thread Style to 200 Series Barb for 1/8” Tubing, Clear Polycarbonate). The other side of the valve was connected (Male Luer Integral Lock Ring to 200 Series Barb for 1/8” Tubing, Clear Polycarbonate) to a 23 cm segment of tubing, from which outflow samples were collected during experiments. The outflow tubing assembly was kept as vertical as possible to prevent suspended *Chlorella* particles from settling in the tubing

before reaching the end. A plastic test tube rack was turned on its side and taped to the benchtop to provide a supporting frame for the outflow tubing (secured to rack with tape).

The sand and nylon mesh discs were permeable enough that the draining rate of the FTRs could not be controlled in the desired range of flow rates using a peristaltic pump. Experiments were instead conducted discontinuously: the stopcock valve on the outflow tubing was manually opened and closed to collect each sample, and the overall flow rate was determined by the volume of sample collected and the duration between the start of each sample collection and the next. A Roller clamp (QOSINA Roller Clamp: white acetal, body #140221 with wheel # 140222) was used on the final segment of outflow tubing to slow down the draining during each sample collection. The actual draining time to collect each sample was recorded (to the nearest second) with a stopwatch. A peristaltic pump (Gilson Minipuls 3 with Gilson Polyvinyl Chloride Pump Tubes, 3.18 mm (1/8”) inner diameter) was used to control the rate of input at the top of the FTRs (speed set to match the overall flow rate of sample collection). During POM transport experiments, the tracer solution reservoir bottle was kept well-mixed by a stir plate (Fisher Scientific Thermix Stirrer Model 120S, speed set to 1-2). The pump and stir plate were each placed on plastic step stools (Canadian Tire Type A Alpha Folding Step Stool, 13” (32 cm) height) on the lab bench to keep the input reservoir above the outflow tubing. Figure 2.3 is a schematic diagram of the experimental setup (see Figure 2.4 for photos).

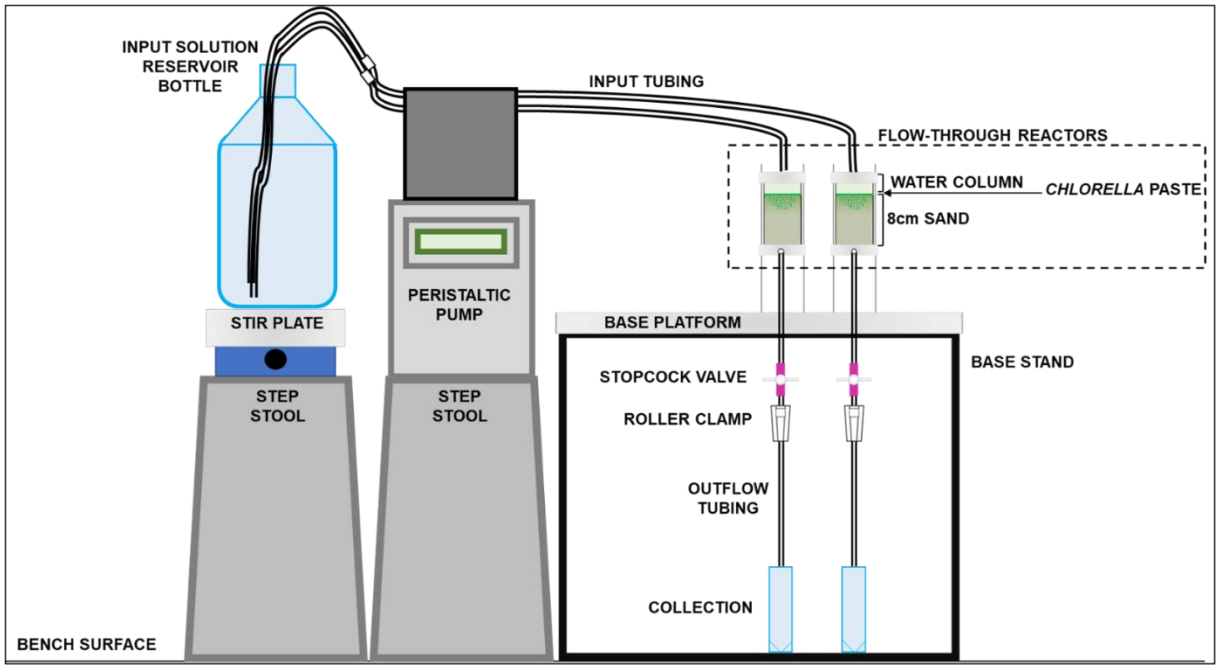

Figure 2.3: Schematic diagram of the setup for *Chlorella* transport experiments in FTRs (scale is not exact).

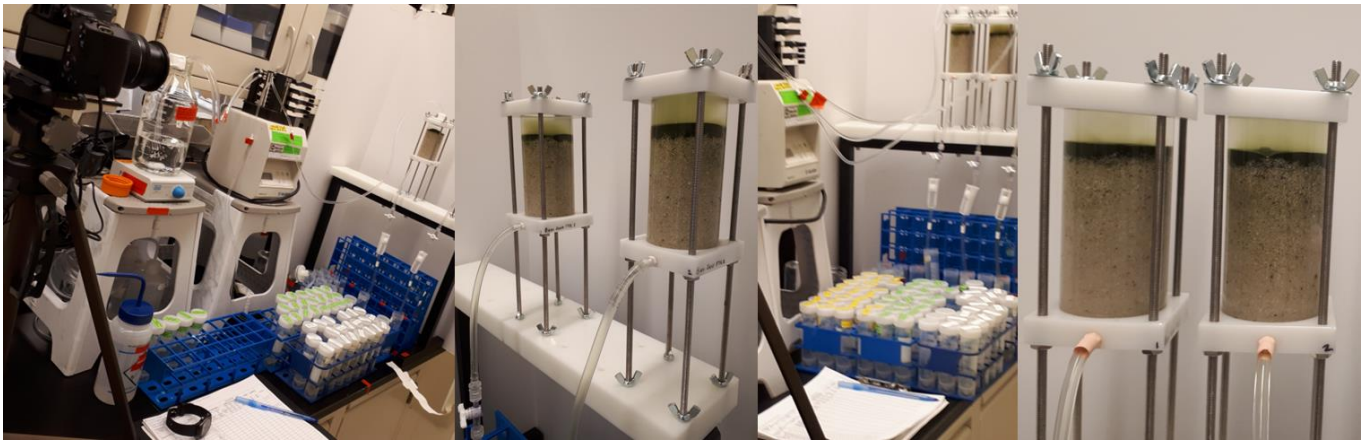

Figure 2.4: Different views of setup for *Chlorella* transport experiments in FTRs. Photos captured (from left to right): during testing of design, end of 30 mL h^{-1} experiment, during 15 mL h^{-1} experiment, end of 10 mL h^{-1} experiment.

To ensure homogeneous and fully saturated packing of sand in the FTRs, Milli-Q water was first pumped in from below, then sand was scooped into the standing water from above, and stirred to homogenize after each layer of about 1 cm. This method was adapted based on best practices recommended in literature on sediment column experiments (Oliveira *et al.*, 1996; Lewis & Sjostrom, 2010). Previous studies of sediment column experiments have also suggested that a length-to-radius ratio ≥ 3:1 is required for a column to include a region of uniform flow, and that a highly permeable 'baffle region' (length ≥ column radius) at the

entrance and exit may help to ensure uniform flow (Barry, 2009; Lewis & Sjostrom, 2010; Gibert *et al.*, 2014). The 10 cm FTRs (1.9 cm radius) were packed with 8 cm of saturated sand with an overlying water column of 2 cm height. This results in a length-to-radius ratio of > 5:1 for the FTR and > 4:1 for the sand-filled portion, while the overlying water column may function as a highly permeable 'baffle region' to uniformly distribute water entering the top of the FTR (from the pump and tubing) before it reaches the sand. Although a 'baffle region' was not present at the bottom of the FTR, the coarse nylon mesh may have helped maintain uniform flow conditions while water flowed through the sand and mesh to the FTR outflow channel.

In case any sand particles <200 µm were not removed by sieving, FTRs were flushed with at least 3× the expected pore volume of the 8 cm sand column using Milli-Q water (vertical downward flow) to remove any particles fine enough to pass the 185 µm filter, so that the only particles reaching the outflow during experiments were *Chlorella*. The expected pore volume was calculated by multiplying the volume of the sand-filled portion of the FTR by the porosity (0.54) estimated from Br^- BTCs in separate test experiments with the sand. After flushing, the FTR was drained such that there was no overlying water column, but sand was fully saturated. To start a transport experiment, the water column was filled from above with 50 mg L^{-1} Br^- tracer solution (initially introduced using a squirt bottle aimed at/down the inner wall of the upper empty FTR cylinder, then kept full during the experiment using tubing from the pump).

For extruding slices of sand from the FTRs at the end of each transport experiment, a custom-made plunger was used. The plunger consisted of a metal rod (handle) with a flat plastic disc (plunger head) that fit snugly inside the FTR cylinder to push sand through (Figure 2.8). The flat plunger head had a rubber ring around its edge to ease movement along the cylinder walls.

2.1.4: Preparation and Application of Chlorella Paste

To conduct *Chlorella* transport experiments, *Chlorella* was applied as a paste to the top surface of the sand in FTRs. Paste was prepared by weighing 2 g of *Chlorella* powder into a zip bag (VWR Reclosable Clear Bags, 2mm Thickness, 76 × 101 mm), adding 6 mL of 50 mg L^{-1} Br^- tracer solution (transferred using 10 mL Eppendorf Research pipet set to 6.00 mL), sealing the bag, and kneading it to form a homogeneous paste. The mass of *Chlorella* powder and tracer solution added to the bag were recorded using an analytical balance (Mettler Toledo XS205). A twist tie was then wrapped around the bag to separate the empty excess portion of the bag from the paste-filled portion. One corner was then cut off the bag using scissors to create an opening with ~1 cm diameter. Like icing from a baker's piping bag (Figure 2.5), the *Chlorella* paste was extruded from the hole in the bag to cover the entire upper surface of saturated sand in the FTR, and the time of application was recorded. The total mass of the bag (plus a supporting weighing boat to capture spilled paste) was recorded before and after transferring paste to the FTR. The difference in masses represented the mass of paste used, from which the mass of *Chlorella* applied to the FTR was calculated using the known mass ratio of *Chlorella* to tracer solution in the paste. It should be noted that some of the change in mass was due to evaporation of water from the paste, so does not truly represent paste added to the FTR, and thus the calculated mass of *Chlorella* applied is not exact. To start a transport experiment, the water column was filled from above with tracer solution (as described in *2.1.3*) immediately after applying the *Chlorella* paste.

Figure 2.5: 'Piping bag' for applying *Chlorella* powder as a paste to the sand surface.

2.1.5: Selection of Flow Rates for Transport Experiments

POM transport experiments were repeated at three overall flow rates (vertical, downward) representative of fluxes into riverbeds. POM could be more common in regulated river reaches (as discussed in *1.1.1*), and the Hanford Reach of the Columbia River is an example of a regulated reach in which frequent riverbed exchange fluxes are driven by river stage fluctuations associated with dam operations (as discussed in *1.3.3*). Based on Hanford Reach literature, transport experiments were repeated with downward vertical fluxes (specific discharge) of 0.2-, 0.3-, and 0.6- m d^{-1} (overall flow rates of 10-, 15-, and 30- mL h^{-1} in the FTRs). 0.6 m d^{-1} approximates the maximum modelled exchange fluxes reported for the Hanford Reach under the influence of dams (Fritz & Arntzen, 2007; Shuai *et al.*, 2019), while 0.2 m d^{-1} approximates what has been modelled to occur without the influence of dams (Shuai *et al.*, 2019), and 0.3 m d^{-1} is an intermediate value within the range of fluxes calculated from field measurements (Fritz & Arntzen, 2007). All three fluxes are within the range measured by seepage meters in literature, as discussed in *1.3*.

2.1.6: Collection of Outflow Samples During Transport Experiments

For each of the three selected flow rates, one experiment (including two replicate FTRs) was completed. Each experiment continued long enough for two pore volumes (about 90 mL) to be eluted from the FTRs, so every experiment involved collecting 18 × 5 mL outflow samples (identified by timepoints 't_1' to 't_{18}') from each FTR. During the transport experiments, flow only occurred during sample collection times. The only intended difference between experiments was the duration of time between sample collections and the total duration of the experiment. The time interval for sampling was defined as the start of one sample collection to the start of the next. To achieve the desired flow rates, the sampling intervals were 10 minutes for 30 mL h^{-1}, 20 minutes for 15 mL h^{-1}, and 30 minutes for 10 mL h^{-1}. The resulting durations

of the experiments (from the start of t_1 to the end of t_{18}) were 3h for 30 mL h^{-1}, 6h for 15 mL h^{-1}, and 9h for 10 mL h^{-1}.

To collect each sample, the outflow valve was opened to release a 5 mL sample into a 50 mL plastic centrifuge tube. The volume of each sample was determined by weighing the collection tube (with cap and label) on an analytical balance (Mettler Toledo XS205), subtracting the pre-recorded mass of the empty tube (including cap and label), and assuming equating 1 g of outflow sample to 1 mL of outflow sample was a reasonable approximation. Before collecting the 18 × 5 mL outflow samples, an initial 3.5 mL sample (the approximate volume of the outflow tubing, identified as 't_0') was collected so that the first 5 mL sample was truly eluted from the FTR. 't_0' was included in volume and flow calculations, but was not shown as a datapoint on BTCs. The duration between the start of 't_0' and 't_1' was reduced by a factor of $\frac{3.5}{5}$ to maintain the desired overall flow rate when collecting this smaller sample (*i.e.*, 7 minutes for 30 mL h^{-1}, 14 minutes for 15 mL h^{-1}, and 21 minutes for 10 mL h^{-1}).

To keep the overlying water column filled during experiments, tracer solution was dripped into the FTR from above (through tubing in the cap) from the peristaltic pump (set to match the overall flow rate of the experiment). The roller clamp on the outflow tubing was intended to maintain a consistent draining rate during each sample collection time. The draining rate still varied but was tracked by recording the duration of each sample collection to the nearest second with a stopwatch.

For each FTR, the entire sampling procedure was completed once without adding any *Chlorella* to the FTRs (to obtain a complete Br^- BTC without any influence of *Chlorella* particles), then the flushing process was repeated before introducing *Chlorella* (with tracer solution filling the overlying water column) for the *Chlorella* transport experiment. After collecting the final outflow sample ('t_{18}') in *Chlorella* transport experiments, the FTRs were

drained before disassembly and extrusion of 1 cm sand slices. The same time interval used between sample collections during the experiment was applied between the start of 't_{18}' and the start of draining. The draining procedure was planned with the intention to collect the contents of the overlying water column, outflow tubing, and pore space separately. The water column was collected from above using an Eppendorf Research pipet, while trying to minimize the disturbance of the remaining *Chlorella* paste layer. To drain the FTRs, a sample with a target volume of 3.5 mL (the approximate volume of the outflow tubing) was collected in the same manner as the other outflow samples. The pore water was then collected separately by fully opening the roller clamps, draining the FTRs as quickly as possible to minimize the opportunity for the final distribution of retained *Chlorella* to be disturbed. Sometimes, attaching a syringe to the outflow tubing was required to completely drain the FTRs.

The downward vertical transport of *Chlorella* particles through the sand in the FTRs was visually observable as a green 'front' of *Chlorella* advancing into the sand, so a visual record of each transport experiment was captured using the timelapse feature of a Canon Rebel SL3 camera. A white tri-fold display board was set up behind the FTRs to provide a blank backdrop for the timelapse recordings (Figure 2.4). The timelapse feature of the camera operates by capturing a set number of images at a set time interval, and automatically combines all images into a single video file. Further details regarding the camera are provided in Appendix Tables 2 and 3.

2.1.7: Subsampling and Analysis of Outflow Samples from Experiments

All subsampling of outflow samples was completed within 48h of the end each experiment, and samples were refrigerated when not in use. The centrifuge tubes in which the samples were collected were inverted at least 12× and shaken by hand before collecting each subsample using Eppendorf Research pipets. As an additional mixing step, pipet tips were filled/emptied of sample 3× before completing each transfer, and a new pipet tip was used for

each sample. First, 2× 0.8 mL (1,000 µL pipet set to 800 µL) subsamples were transferred into 2 mL amber vials (one for absorbance measurements, one for potential FLOWCAM analysis). The remaining sample was filtered through a 3.1 µm glass microfibre syringe filter, to remove most of the algae before filtering through a 0.45 µm nylon syringe filter (new filters used for each sample).

To determine Br^- concentrations, a subsample of at least 0.5 mL was filtered through a 0.2 µm polyether sulfone syringe filter into 1.5 mL polypropylene vials with septa caps and stored frozen until ion chromatography analysis (Thermo Fisher Scientific Dionex ICS-5000 instrument with AS11-HC column, potassium hydroxide eluent (45 minute gradient from 1.0mM to 60mM), suppressed conductivity detector, method detection limit 0.075 mg L^{-1} Br^-).

If adequate sample remained, a 0.5 mL subsample was transferred into a glass test tube, diluted with 5 mL Milli-Q water, acidified with 3 drops of 1M HCl, and refrigerated until analysis for dissolved organic carbon (DOC). If adequate sample remained, then another 0.5 mL subsample was prepared in the same manner (but without acidification) to be analyzed for dissolved inorganic carbon (DIC). These analyses were completed within 10 days using a Shimadzu TOC-LCPH/CPN analyzer.

Absorbance measurements of outflow samples for determination of suspended *Chlorella* concentrations were completed the next day after the transport experiments (or on the same day). A new batch of suspended *Chlorella* calibration standards (Figure 2.6) was prepared the day before each transport experiment (refrigerated until use), so that the standards were of similar age to the samples when measured. Suspensions of 2 g L^{-1} and 1 g L^{-1} were prepared by weighing *Chlorella* powder (by difference) onto weighing paper using an analytical balance (Mettler Toledo XS205), transferring into a glass volumetric flask, and bringing to mark with 50 mg L^{-1} Br^- solution (0.5 g in 250 mL for 2 g L^{-1}, 1 g in 1,000 mL for 1 g L^{-1}, exact masses recorded). The flasks were fully inverted 12× to mix, sonicated (VWR B1500-MT, ‘HI’ Sonics

Power) for 20 minutes to reduce flocculation of particles, inverted 12× to mix again, transferred to glass bottles, and sonicated for another 20 minutes. The 1 g L^{-1} suspension was used to prepare a 0.1 g L^{-1} suspension (10 mL diluted to 100 mL in volumetric flask, then same sonication procedure as described previously). These suspensions were diluted to make suspensions of 1.1-1.9 g L^{-1} (from 2 g L^{-1}), 0.1-0.9 g L^{-1} (from 1 g L^{-1}), and 0.01-0.09 g L^{-1} (from 0.1 g L^{-1}) *Chlorella* in 50 mg L^{-1} Br^-. The diluted suspensions were prepared in 20 mL glass vials (Figure 2.6), using Eppendorf Research pipets for the transfers. Stocks were inverted 12× before each transfer, pipet tips were filled/emptied 3× before each transfer, and a separate tip was used for each stock.

Figure 2.6: Suspensions of *Chlorella* prepared at a range of concentrations, used as standards to calibrate absorbance measurements for determining suspended *Chlorella* concentrations in outflow samples from FTRs.

The wavelength used for absorbance measurements was selected based on an absorbance scan of a 1 g L^{-1} *Chlorella* suspension using a Thermo Evolution 260 UV-Vis Spectrophotometer, which indicated maximum absorbance at about 660 nm. Absorbance was measured at the 660 nm wavelength using a Molecular Devices Flexstation Multimode Microplate Reader and Corning 3370 Clear Costar Polystyrene Flat-Bottom 96-Well Microplates. One plate was used for analyzing the calibration standards, and an additional plate was used for samples from each FTR (plates were not reused). For each standard and sample, three wells were filled with 200 µL aliquots. Extra wells were filled with 'blanks' of Milli-Q water or 50 mg L^{-1} Br^- solution. Before loading the microplates, the standards (20 mL glass vials) were sonicated for 5 minutes, and each FTR outflow sample (2 mL amber vials) was mixed on a VWR Digital Vortex Mixer (30s with speed set to 1500). Each standard and sample were inverted 12× immediately before use, pipet tips were filled/emptied 3× before each transfer, and a separate tip was used for each standard/sample. Absorbance measurements were performed using the 'well scan' mode (30s auto-mix before scan, 9 measurement points in each well, 'well-scan-editor-pattern' set to 'fill', 'density' = 3).

For each standard and sample, the mean absorbance value from the three replicate wells was calculated. If the relative standard deviation of the three wells exceeded 10%, then the least consistent replicate was excluded. The mean absorbance of all blank wells (including wells of Milli-Q water and of 50 mg L^{-1} Br^- solution) in each plate was subtracted from all the other samples in the same plate. The blank-subtracted mean absorbance value of each standard was plotted against the known concentrations (g L^{-1} *Chlorella*) to generate a calibration curve in Microsoft Excel, and the equation of the line (linear regression, intercept not set) was used to convert the mean blank-subtracted absorbance of each FTR outflow sample to a concentration of *Chlorella* in g L^{-1}. The calibration curve included standards from 0.01 to 1.3 g L^{-1} *Chlorella*. Standards >1.4 g L^{-1} *Chlorella* were excluded because their

absorbance exceeded the limit of 1. In some calibrations, the 1.4 g L^{-1} standard could have been included, but for consistency all calibration curves only included up to 1.3 g L^{-1} (which was well above the concentrations determined in outflow samples). The determination of suspended *Chlorella* concentrations in each experiment sample was performed using a calibration curve generated the same day (using standards prepared the day before the experiment). The standard deviation from triplicate well plates was used as the uncertainty of each sample for plotting error bars. Each calibration curve had $R^2 \geq 0.93$. The calibration curves are shown in Figure 2.7.

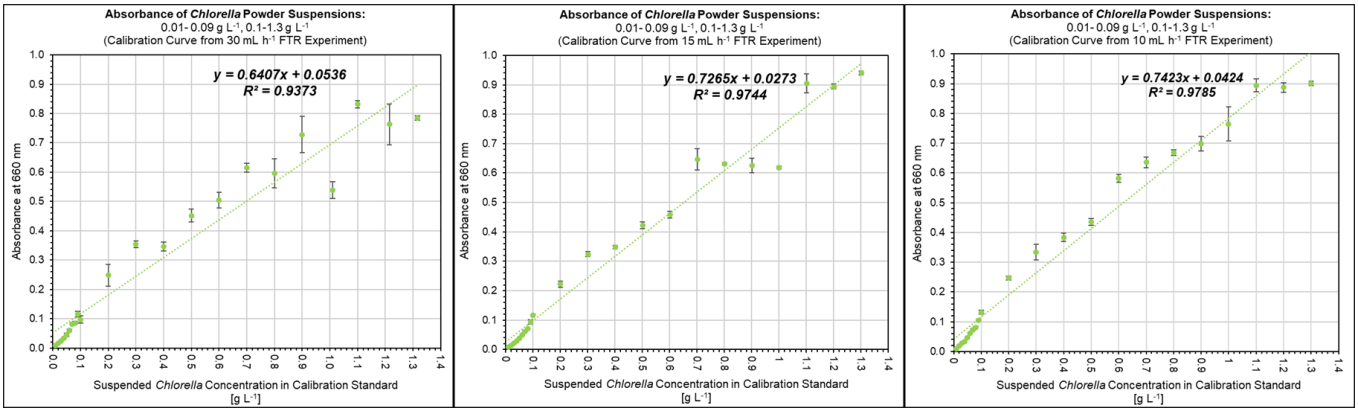

Figure 2.7: Calibration curves for determining suspended *Chlorella* concentrations from absorbance measurements.

2.1.8: Determination of Chlorella Retained on Sand

The mass of *Chlorella* retained on sand during transport experiments was determined by the loss on ignition (LOI) method (adapted from Dean, 1974; Heiri *et al.*, 2001; Olsen & Townsend, 2005; Wall *et al.*, 2005) and was completed after each of the three transport experiments (both FTRs from the experiment were included in one round of the procedure). After draining FTRs at the end of transport experiments, each FTR was moved off the base platform. The custom-built plunger was then inserted through the top opening of the FTR and held firmly in place (with the face of the plunger head against the top surface of the *Chlorella* paste layer) while the FTR was inverted. The plunger and inverted FTR cylinder were held in one hand while removing the nuts, threaded rods, end plates, nylon mesh, and o-ring. The

plunger was then gently twisted and pushed upward to extrude a 1 cm slice from the FTR cylinder (Figure 2.8). A metal scoopula was then used to scrape the slice into a plastic weighing boat (already labelled with the FTR identifier and depth interval), which was elevated by a footstool on the benchtop for easier transfer from the FTR. With the FTR inverted, the bottom slice (7-8 cm depth interval) was extruded first, and the top slice (0-1 cm depth interval) was extruded last (Figure 2.8). Measured markings were drawn on the FTR cylinders during setup of the experiments to guide the extrusion process, accounting for the offset between the visible edge of the plunger head and the actual location of its face (Figure 2.8). The top slice could not be separated from the remaining excess paste layer (which could not be fully transferred from the plunger). Thus, the concentration of *Chlorella* determined in the 0-1 cm slices was not an accurate representation of the mass retained on the first 1 cm of sand, nor did it fully capture the excess mass that did not enter the sand medium. Only the results from 1-8 cm depth were used for plotting retention profiles ('RPs', plots of concentration vs. depth).

Figure 2.8: Extruding the last slice of sand (top 0-1 cm) from a FTR after the 30 mL h^{-1} experiment.

Each slice of sand was transferred from the plastic weighing boat to a 100 mL glass bottle (Corning PYREX or VWR) and covered with a plastic screw cap (already labelled with FTR identifier and depth interval). The empty mass of each bottle (with cap and label) was recorded in advance using an analytical balance (Mettler Toledo XS205). To obtain the initial oven-dry mass of each sample, the sample bottles were oven-dried (Thermo Scientific Heratherm oven) for 24h at 60(±1)°C (temperature selected following Wall *et al.*, 2005; Van Wychen & Laurens, 2015), with the plastic caps replaced by ribbed watch glass covers (Corning PYREX, 75 mm diameter). Since the labels were on the caps and not the bottles, the layout in the oven was carefully tracked. After oven-drying, the sample bottles were transferred to a desiccator cabinet to keep dry while cooling to room temperature (capped during transport, uncapped while in desiccator). The sample bottles were removed from the desiccator, capped, and weighed on the analytical balance three times (on three separate days, when possible) to measure the initial oven-dry masses.

After determining the initial oven-dry masses, the samples were transferred to a muffle furnace (Fisher Scientific Isotemp), with caps replaced by the ribbed watch glass covers (layout carefully tracked). The furnace was heated to 550(±1)°C, held for 4h. 550°C is the temperature commonly used for igniting organic matter (Dean, 1974; Heiri *et al.*, 2001; Wall *et al.*, 2005), and Heiri *et al.* (2001) suggested that the common duration of 1h or 2h (Dean, 1974) may be insufficient for samples with a high content of organic matter. Extending the duration to 4h still allowed loading, heating, cooling, and unloading of samples in the muffle furnace to be completed in a single day. When samples were cool enough for safe removal from the muffle furnace, the process for determination of dry mass was repeated (including oven-drying, in case any moisture accumulated during cooling).

For each of the three transport experiments, the LOI procedure described above also included triplicate ‘sand blanks’ (10 g of sand, with no *Chlorella*) and ‘process blanks’ (glass

bottle with no sample) to check and correct for 'background' LOI signal. Triplicate '*Chlorella* blanks' (1 g of *Chlorella*, with no sand) were also included to determine the ash content of *Chlorella* and convert the mass loss (organic matter content) in samples to a total *Chlorella* mass. To verify the accuracy of the LOI procedure for the range of *Chlorella*/sand ratios determined in experimental samples, an additional round of the procedure was completed for mixtures of sand and *Chlorella* in known *Chlorella*/sand mass ratios (1-, 2-, 3-, 4-, and 5- mg g^{-1}; each in triplicate). This additional round also included triplicates of sand blanks, *Chlorella* blanks, and process blanks. The results of this verification are provided in Table 2.1 (after an explanation of how retained *Chlorella* concentrations were calculated from results).

The initial (and post-ignition) oven-dry masses of the samples were calculated by subtracting the masses of the empty bottles from each mass measurement and calculating the mean of the three measurements. The standard deviation of the three measurements was calculated as the 'uncertainty' on the dry mass, which was less than ≤0.001 g. This uncertainty was carried throughout subsequent calculations, following standard rules for error propagation (Harris, 2016). The ash content of *Chlorella* blanks was calculated using Eq. 2.1:

$$R_{Chl} = (M_{D_a}/M_{D_i}) \qquad (2.1)$$

where M_{D_i} is the initial oven-dry sample mass, M_{D_a} is the oven-dry mass of the ash (material remaining post-ignition), and R_{Chl} (the ash content) is the fraction of M_{D_i} recovered as M_{D_a}. For every sample, mass combusted (M_c) was calculated by Eq. 2.2:

$$M_c = M_{D_i} - M_{D_a} \qquad (2.2)$$

For the process blanks, the calculated M_c was ±0.001 g, which is less than or equal to the uncertainty assigned to the combusted mass of each sample by error propagation methods, so mass loss associated with the glass bottles was not considered to be significant, and no

'process blank correction' was performed. For the sand blanks, the mass combusted was converted to a fraction by Eq. 2.3:

$$M_{c_{fraction}} = M_c / M_{D_i} \quad (2.3)$$

where $M_{c_{fraction}}$ is the fraction of the initial mass of sand that was lost during ignition. For samples with unknown *Chlorella*/sand ratios (slices from FTRs), M_{D_i} was multiplied by the mean $M_{c_{fraction}}$ value from the triplicate sand blanks (the mean fraction of mass combusted in sand blanks) to determine the expected mass loss associated with sand (not *Chlorella*), $M_{c_{sand}}$. The mass of *Chlorella* combusted in the FTR samples ($M_{c_{Chl}}$) was then calculated using Eq. 2.4:

$$M_{c_{Chl}} = M_c - M_{c_{sand}} \quad (2.4)$$

where $M_{c_{Chl}}$ represents the mass of *Chlorella* combusted. This was converted to the total mass of *Chlorella* present in the sample (M_{Chl}) using Eq. 2.5:

$$M_{Chl} = M_{c_{Chl}} / (1 - R_{Chl_{avg}}) \quad (2.5)$$

where $R_{Chl_{avg}}$ is the mean ash content (R_{Chl}) from the three *Chlorella* blanks. M_{Chl} of each sample was subtracted from M_{D_i} to calculate the mass of sand in the sample (M_{sand}, g), as shown in Eq. 2.6:

$$M_{sand} = M_{D_i} - M_{Chl} \quad (2.6)$$

M_{Chl} was then converted from g to mg, and the concentration of *Chlorella* in each FTR sample ($C_{Chl/sand}$, expressed as a mass ratio, mg *Chlorella* per g sand) was calculated using Eq. 2.7:

$$C_{Chl/sand} = M_{Chl} / M_{sand} \quad (2.7)$$

Table 2.1 presents the results of applying the procedure and calculations described above to samples of sand with a known *Chlorella* content. The error in the determination of M_{Chl} is <0.01 g, and the error in the determination of $C_{Chl/sand}$ is <0.4 mg g^{-1}. To plot retention profiles, the $C_{Chl/sand}$ for each sample from 1-8 cm depth was plotted at the midpoint of the depth interval, and the propagated uncertainty in $C_{Chl/sand}$ was used for plotting error bars.

Table 2.1: Verification of the loss-on-ignition method for determining the concentration of *Chlorella* in sand.

Replicate	Initial *Chlorella* Mass	Calculated *Chlorella* Mass	Error	Mean Error	Initial *Chlorella* Concentration	Calculated *Chlorella* Concentration	Error	Mean Error
[#]	[g]	[g]	[g]	[g]	[mg]·[g sand]$^{-1}$	[mg]·[g sand]$^{-1}$	[mg]·[g sand]$^{-1}$	[mg]·[g sand]$^{-1}$
1	0.0194	0.018	0.00	0.00	0.9878	0.91	-0.08	-0.10
2	0.0236	0.021	0.00		1.1696	1.06	-0.11	
3	0.0236	0.022	0.00		1.1784	1.08	-0.10	
1	0.0439	0.039	0.00	0.00	2.1823	1.96	-0.22	-0.20
2	0.0403	0.037	0.00		2.0137	1.84	-0.18	
3	0.0402	0.036	0.00		2.0067	1.82	-0.19	
1	0.0640	0.058	-0.01	-0.01	3.1759	2.88	-0.30	-0.26
2	0.0681	0.064	0.00		3.3879	3.16	-0.22	
3	0.0748	0.068	-0.01		2.9438	2.68	-0.27	
1	0.0968	0.091	-0.01	-0.01	3.9254	3.68	-0.24	-0.24
2	0.0893	0.084	0.00		3.9594	3.74	-0.22	
3	0.0810	0.075	-0.01		3.7842	3.52	-0.26	
1	0.1100	0.103	-0.01	-0.01	5.2323	4.91	-0.32	-0.35
2	0.1050	0.099	-0.01		4.9901	4.69	-0.30	
3	0.1145	0.106	-0.01		4.9974	4.61	-0.39	
4	0.1006	0.092	-0.01		4.9337	4.53	-0.41	

Table 2.2 compiles the ash content (% of total mass that remained after ignition) determined for *Chlorella* blanks in four rounds of the LOI procedure (one round associated with each of the three FTR experiments, and one round for method verification). The reproducibility of the resulting ash contents suggests that the supply of *Chlorella* powder used for the experiments was homogeneous in terms of organic matter content and that the muffle furnace performed consistently.

Table 2.2: Ash content of *Chlorella* powder used in experiments, determined by loss-on-ignition (4h at 550°C).

Ash Content of Green Foods Organic *Chlorella* Powder (Lot 080920)				
Replicate	**Ash Content**	**Uncertainty**	**Mean Ash Content**	**Mean Uncertainty**
[#]	[%]	[%]	[%]	[%]
1	6.9%	0.2%	6.9%	0.1%
2	5.5%	0.2%		
3	7.0%	0.3%		
1	6.8%	0.1%		
2	6.9%	0.1%		
3	6.8%	0.1%		
1	7.2%	0.1%		
2	7.2%	0.1%		
3	7.2%	0.1%		
1	6.96%	0.03%		
2	6.95%	0.04%		
3	6.87%	0.05%		

$C_{Chl/sand}$ can be converted to a concentration of particulate organic carbon (POC, $C_{POC/sand}$), based on the OC content of the *Chlorella* powder (44% OC, as determined using a CHNS Analyzer, described in *2.1.2*), using Eq. 2.8:

$$C_{POC/sand} = 0.44 \times C_{Chl/sand} \quad (2.8)$$

where $C_{POC/sand}$ is the concentration of POC in each sand slice from the FTRs (expressed as a mass ratio, mg POC per g sand).

2.1.9: Settling Experiments

Settling experiments were conducted to estimate the rate at which *Chlorella* particles are transported downwards through the sand medium in the absence of water flow. The settling experiments used a customized FTR that had a plastic ring inside the cylinder to support a coarse metal mesh disc and a nylon mesh disc that separated the column of saturated sand from a water-filled space underneath (Figure 2.9). Sand was packed into the FTR using the same methods described for the transport experiments. Settling experiments were conducted by applying *Chlorella* paste to the surface of the sand (prepared and applied by the same methods described for the transport experiments) and monitoring how long it took for the *Chlorella* to reach the underlying water chamber (as indicated by the appearance of a green

colour) under the influence of gravity alone, without causing any downward water flow by collecting outflow samples. A timelapse video of each settling experiment was recorded (details in Appendix Tables 2 and 3). The time at which the *Chlorella* paste was applied (noting the time of both the beginning and end of the application process, which took about 1 minute) and the time at which the camera recording started were tracked. The timelapse feature of the camera operates by capturing a set number of images at a set time interval, and automatically combining all images into a single video file. After each settling experiment, the timelapse video was reviewed to identify the time (in the video) at which a green colour first appeared in the underlying water chamber of the customized FTR. This was then converted to a 'real time' duration since the start of the video recording using the ratio of the total real time duration to the total video duration. Any delay between the start of *Chlorella* application and the start of recording was added to the real duration to determine the total real duration between when the *Chlorella* was first introduced to the saturated sand and when it began to become visible in the underlying water chamber. The height of sand in the FTR (*e.g.,* 8 cm) was then divided by this time to estimate the gravitational settling rate for transport of *Chlorella* particles through the sand. Throughout these experiments, the observed depth that the visible green front of *Chlorella* particles reached in the sand was variable throughout the FTR (which suggests that the connectivity of flow paths through the sand was heterogeneous in space). Thus, the estimated rates from these experiments are considered to indicate the upper limit of a range of rates at which the particles move through the sand by settling. It should also be noted, however, that due to the microscopic size of individual *Chlorella* particles, there could be a delay between when the first *Chlorella* arrives in the underlying water chamber and when the green colour becomes visible.

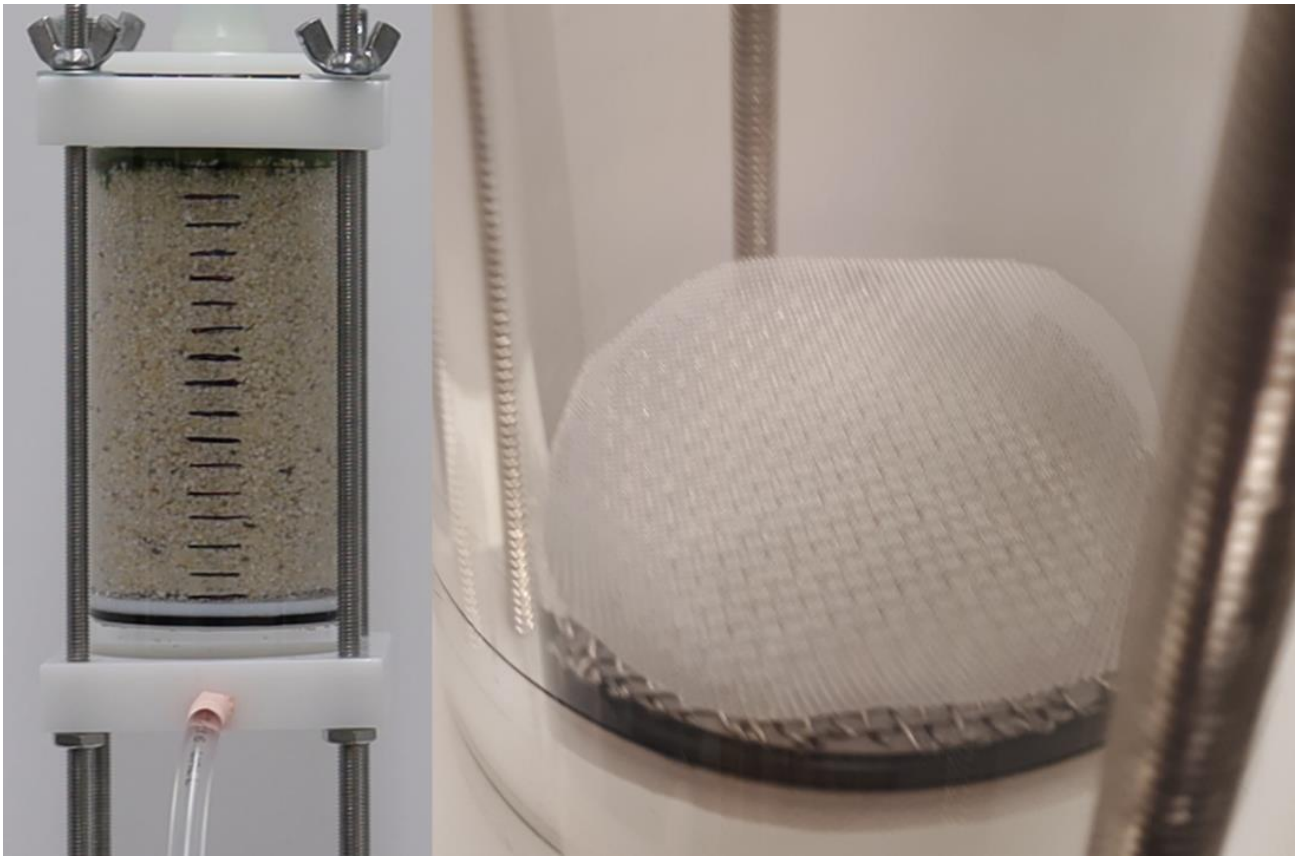

Figure 2.9: Setup of settling experiments. **Left:** FTR packed with saturated sand, with *Chlorella* paste on the surface and an underlying water chamber (stopcock valve on outflow tubing kept closed to prevent draining). **Right:** close-up of the plastic ring, steel mesh, and nylon mesh separating the sand from the underlying water chamber.

2.2: Numerical Modelling of Transport Experiments

2.2.1: Modelling Transport of Non-Reactive Bromide Tracer

To simulate the transport experiments, a one-dimensional numerical model was constructed in MATLAB (R2022a). Transport of the non-reactive Br^- tracer through a sand-filled FTR is modelled by the advection-dispersion equation (ADE), as shown in Eq. 2.9 (adapted from Freeze & Cherry, 1979):

$$\frac{\partial C_i}{\partial t} = D\frac{\partial^2 C_i}{\partial x^2} - v\frac{\partial C_i}{\partial x} \qquad (2.9)$$

where the subscript i is a spatial index, C_i is the concentration of Br^- (mmol cm^{-3}) in spatial cell i, t is time (s) since start of simulation (introduction of tracer), x is depth (cm) from the upper boundary of the sand, D is the hydrodynamic dispersion coefficient (cm^2 s^{-1}) for Br^-, and v is

the average linear pore water velocity (cm s^{-1}). The model also included code for retardation in the ADE, but it was assumed that no retardation occurred, so the retardation coefficient is set to '1' (no effect on the ADE) in the model. D is calculated from Eq. 2.10 (Freeze & Cherry, 1979):

$$D = \alpha_L v + D^* \qquad (2.10)$$

where α_L is the dispersivity of the sand (cm^{-1}), and D^* is the effective molecular diffusion coefficient ($cm^2\ s^{-1}$) for Br^-, which is calculated from Eq. 2.11:

$$D^* = 0.75 D_m \qquad (2.11)$$

where D_m is the molecular diffusion coefficient for Br^- ($cm^2\ s^{-1}$). Eq. 2.11 is a relationship determined for the transport of Chloride (Cl^-) in a quartz sand (Sorbie & Tomlinson, 1993), and is used here as an approximation for D^* of Br^- in silica sand. The conversion of D_m to D^* was not found to have a notable impact on the shape of modelled Br^- BTCs. The model uses the D_m value from the PHREEQC database for Br^- in water at 298K (25°C). The model also includes a temperature correction using equations and coefficients from Appelo (2017) with water viscosity values from Kestin *et al.* (1978). However, the experiments in the present study were conducted at room temperature (23(±3)°C), so the temperature in the model was kept at 25°C.

The average linear pore water velocity is defined by Eq. 2.12 (Freeze & Cherry, 1979):

$$v = \frac{q}{\phi} \qquad (2.12)$$

where ϕ is the porosity of the sand and q is specific discharge (cm s^{-1}). q was calculated by dividing the volumetric flow rate of the simulated experiment ($cm^3\ s^{-1}$) by the cross-sectional area of the FTR cylinder. Applying forward differencing to the time-dependent term in the ADE

(Eq. 2.9), and applying central spatial weighting and Crank-Nicolson (central) temporal weighting to the other terms leads to the form of the ADE shown in Eq. 2.13:

$$\frac{C_i^{n+1}-C_i^n}{\Delta t} = \frac{D}{2}\left[\left(\frac{C_{i-1}^{n+1}-2C_i^{n+1}+C_{i+1}^{n+1}}{\Delta x^2}\right)+\left(\frac{C_{i-1}^{n}-2C_i^{n}+C_{i+1}^{n}}{\Delta x^2}\right)\right]-\frac{v}{2}\left[\left(\frac{C_{i+1}^{n+1}-C_{i-1}^{n+1}}{2\Delta x}\right)+\left(\frac{C_{i+1}^{n}-C_{i-1}^{n}}{2\Delta x}\right)\right] \quad (2.13)$$

where Δt is the timestep size for the model simulation and Δx is the spatial cell size for the one-dimensional sand medium. The superscripts are temporal indices where n represents the current timestep (with known concentrations C^n) and $n+1$ represents the next timestep (with unknown concentrations C^{n+1}). The subscripts are spatial indices where i represents the current spatial cell, $i+1$ represents the next spatial cell (in direction of flow), and $i-1$ represents the previous spatial cell. Collecting terms into groups for spatial cells $i-1$, i, and $i+1$; then multiplying both sides of the equation by Δt and grouping constants leads to Eq. 2.14:

$$\left(\frac{-s}{2}-p\right)C_{i-1}^{n+1}+(s)C_i^{n+1}+\left(\frac{-s}{2}+p\right)C_{i+1}^{n+1}=\left(\frac{s}{2}+p\right)C_{i-1}^{n}+(-s)C_i^{n}+(\frac{s}{2}-p)C_{i+1}^{n} \quad (2.14)$$

where s and p are dimensionless grouped constants defined by Eq. 2.15 and 2.16, respectively:

$$s=\frac{D\Delta t}{\Delta x^2} \quad (2.15)$$

$$p=\frac{v\Delta t}{4\Delta x} \quad (2.16)$$

The model uses initial conditions of zero Br^- concentration at all depths. The upper boundary condition is a constant ('Dirichlet type') boundary condition: input concentration C_o is a constant value (6.26×10^{-4} mmol cm^{-3} KBr = 50 mg L^{-1} Br^-, the concentration of tracer in the experiments) for the entire simulation. The lower boundary condition is a zero-flux ('Neumann-type') boundary condition. It is understood that these boundary conditions are not completely correct, but are commonly used (Van Genuchten & Parker, 1984). However, to avoid problems

with lower boundary conditions, the FTR is modelled as 10× the actual length, and concentrations at the depth corresponding to the actual length (8 cm) were used to plot BTCs. The model uses a total of 2500 spatial cells (250 within the actual length of the FTR). This was found to be sufficient to prevent irregularities in the modelled retention profile near the upper boundary, while further increasing the spatial resolution significantly increased run-time without providing any apparent benefit. The number of timesteps used in the model differs slightly for each flow rate (because the code was written to allow the option of a time-varying flow rate, and the way this was implemented required an integer number of timesteps within each minute) but is within the range of 2000 to 3000 timesteps.

Eq. 2.14 is represented by arrays in the MATLAB scripts. Constants in the C^{n+1} terms are represented by matrix 'A,' the C^n terms (known concentrations at current timestep, n) are represented by column vector 'B,' and the C^{n+1} values (unknown concentrations at next timestep, $n+1$) are represented by column vector 'C.' More detail is available in the MATLAB live scripts. The concentrations at the next timestep are determined by setting vector 'C' equal to the result of performing matrix division of matrix A over vector B.

2.2.2: Modelling Transport and Retention of Chlorella Particles

The transport of *Chlorella* particles through a sand-filled FTR is modelled using a modified version of the ADE in which a gravitational settling term is included to model the early arrival of suspended *Chlorella* in the outflow (relative to Br^-) and a filtration term is included to model the removal of suspended *Chlorella* from solution (as shown in Eq. 2.17, with subscript c used to distinguish *Chlorella* symbols from Br^- symbols):

$$\frac{\partial C_{c_i}}{\partial t} = D_c \frac{\partial^2 C_{c_i}}{\partial x^2} - (v + v_s)\frac{\partial C_{c_i}}{\partial x} - (v + v_s)\lambda C_{c_i} \qquad (2.17)$$

where C_{c_i} is the concentration of suspended *Chlorella* (mg cm^{-3}) in spatial cell i, D_c is a hydrodynamic dispersion coefficient (cm^2 s^{-1}) for suspended *Chlorella* particles, v_s is the

gravitational settling rate of suspended *Chlorella* particles in the sand medium (cm s^{-1}), and λ is a filtration coefficient (cm^{-1}). The model also includes code for reversible sorption (two additional terms in Eq. 2.17: one for sorption, one for detachment), but the retention process of filtration was found to be sufficient for modelling the experiments, so coefficients in the reversible sorption terms are set equal to 'zero' (no affect on Eq. 2.17). D_c is calculated from Eq. 2.18:

$$D_c = \alpha_L(v + v_s) + D_c^* \qquad (2.18)$$

where D_c^* is an effective diffusion coefficient for *Chlorella* particles, which was set to a value used in existing literature (Jin *et al.*, 2019) for kaolinite colloids of similar size (dominant grain size ~2 μm) as *Chlorella* particles. For each model simulation of a FTR experiment, λ was estimated by Eq. 2.19:

$$\lambda = \frac{ln\left(\frac{C_{c_0}}{C_{c_{max}}}\right)}{l} \qquad (2.19)$$

where C_{c_0} is the input concentration of suspended *Chlorella* used in the model simulation, $C_{c_{max}}$ is the breakthrough concentration of suspended *Chlorella* detected in the outflow of the experiment (set to the average concentration in outflow samples after one pore volume has been eluted, to the nearest 0.01 mg cm^{-3}), and l is the depth of the FTR outflow below the upper boundary of the sand (8 cm).

The same process described for arranging the Br^- transport ADE (Eq. 2.9, 2.13, 2.14) into a system of equations represented by arrays in MATLAB and solving for unknown concentrations at the next timestep was used for the *Chlorella* transport ADE (Eq. 2.17). Crank-Nicolson (central) temporal weighting was applied to C_{c_i} in the filtration term. The rearranged form of Eq. 2.17 is shown in Eq. 2.20, with dimensionless grouped constants defined by Eq. 2.21, 2.22, 2.23:

$$\left(\frac{-s_c}{2} - p_c\right) C_{c_{i-1}}^{n+1} + (s_c + w_c) C_{c_i}^{n+1} + \left(\frac{-s_c}{2} + p_c\right) C_{c_{i+1}}^{n+1}$$

$$= \left(\frac{s_c}{2} + p_c\right) C_{c_{i-1}}^{n} + (-s_c - w_c) C_{c_i}^{n} + \left(\frac{s}{2} - p_c\right) C_{c_{i+1}}^{n} \qquad (2.20)$$

$$s_c = \frac{D_c \Delta t}{\Delta x^2} \qquad (2.21)$$

$$p_c = \frac{(v+v_s)\Delta t}{4\Delta x} \qquad (2.22)$$

$$w_c = \frac{(v+v_s)\lambda \Delta t}{2} \qquad (2.23)$$

The model tracks the *Chlorella* flux entering each spatial cell in the sand medium ($F_{c_{in}}$, mg cm^{-2} s^{-1}) during each timestep using Eq. 2.24 (with central spatial weighting of diffusive flux term):

$$F_{c_{in}} = -D_c \frac{\partial C_c^{\,n}}{\partial x} + (v + v_s) C_c^{\,n} = -D_c \left[\frac{\left(C_{c_i}^{\,n} - C_{c_{i-1}}^{\,n}\right)}{2\Delta x}\right] + (v + v_s) C_{c_{i-1}}^{\,n} \qquad (2.24)$$

For the upper boundary of the first cell, $C_{c_i}^{\,n} = C_{c_1}^{\,n}$ and $C_{c_{i-1}}^{\,n} = C_{c_0}$. The model also tracks the *Chlorella* flux exiting the lower boundary of each spatial cell in the sand medium ($F_{c_{out}}$, mg cm^{-2} s^{-1}) during each timestep using Eq. 2.25:

$$F_{c_{out}} = -D_c \frac{\partial C_c^{\,n}}{\partial x} + (v + v_s) C_c^{\,n} = -D_c \left[\frac{\left(C_{c_{i+1}}^{\,n} - C_{c_i}^{\,n}\right)}{2\Delta x}\right] + (v + v_s) C_{c_i}^{\,n} \qquad (2.25)$$

The mass of *Chlorella* filtered ($M_{c_{filtered}}$, mg) in each spatial cell of the sand medium during each timestep is calculated using Eq. 2.26:

$$M_{c_{filtered}} = (v + v_s)\lambda \left[\frac{\left(C_{c_i}^{\,n} - C_{c_i}^{\,n+1}\right)}{2}\right] PV_{cell} \Delta t \qquad (2.26)$$

where PV_{cell} is the pore volume of a single spatial cell, calculated by Eq. 2.27:

$$PV_{cell} = V_{cell}\phi = A\Delta x \phi \qquad (2.27)$$

where V_{cell} is the total volume of a single spatial cell (cm^3), A is the cross-sectional area of the FTR (cm^2), spatial cell size Δx is the thickness of each cell (cm), and ϕ is the porosity of the sand.

The mass retained (filtered) at each timestep is added to the previously retained mass in each cell. The cumulative retained mass is divided by PV_{cell} to calculate the retained concentration in the next timestep ($C_{cr_i}^{n+1}$, mg *Chlorella* per cm^3 of pore space).

For each spatial cell at each timestep, a mass balance calculation is performed. 'Sources' of *Chlorella* available to each cell in each timestep are the mass that entered ($F_{c_{in_i}}^{n} A\phi\Delta t$ to convert flux to mass in mg) and the mass initially suspended ($C_{c_i}^{n} PV_{cell}$ to convert concentration to mass in mg). 'Sinks' of *Chlorella* in each cell during each timestep are the mass that exited ($F_{c_{out_i}}^{n} A\phi\Delta t$), the mass filtered during the timestep (non-cumulative $M_{c_{filtered}}$), and the mass remaining suspended after the timestep ($C_{c_i}^{n+1} PV_{cell}$). A 'mass balance error' is then calculated as the difference between the 'sources' and 'sinks'. To express the error as a percentage, it is divided by the sum of 'sources'. The mass balance error was also calculated for the entire FTR (error in each timestep as well as the cumulative error from all timesteps).

The model plots Br^- and suspended *Chlorella* concentrations against the number of pore volumes eluted (breakthrough curves, 'BTCs'), and retained *Chlorella* concentrations against depth below the upper boundary (a retention profile, 'RP'), and a summary of the mass balance error.

Chapter 3: Results and Discussion

3.1: Data Package for Experimental Results

Data summaries were prepared as comma-separated values (CSV) files for each transport experiment, following CSV formatting guidelines (Velliquette *et al.*, 2021) for the United States Department of Energy's (DOE) 'Environmental System Science Data Infrastructure for a Virtual Ecosystem' (ESS-DIVE). The data summaries and MATLAB modelling scripts will be made available for open public access. For each experiment, there are up to three CSV files for each of the two replicate FTRs: one file for outflow samples from the preliminary Br^- breakthrough test, one file for outflow samples from the *Chlorella* transport experiment, and one file for sand slices. The exception is the 30 mL h^{-1} experiment, for which there were no preliminary Br^- breakthrough tests. CSV files for outflow samples include columns for sample identifiers ('t_0' to 't_{18}'), date, time of sample collection, duration of sample collection, sample volume, Br^- concentration (as determined by IC analysis), and (where applicable) the concentrations of *Chlorella* (as determined from absorbance measurements) and DOC (as determined using the TOC analyzer). CSV files for sand slices include columns for sample identifiers (*e.g.*, '1-2 cm'), date of experiment, depth to top of slice, depth to bottom of slice, calculated mass of retained *Chlorella*, calculated mass of sand, calculated concentration of retained *Chlorella*, and calculated uncertainty for the concentration. The calculations are described in *2.1.8*. All columns of the CSV data files are clearly defined in the 'data dictionary' (an additional CSV file). The data package also includes the timelapse recording and MATLAB live script (as both a '.mlx' file and as a '.pdf' for readers who do not have MATLAB access) for each transport experiment. The 'file-level metadata' (FLMD) is an additional CSV file that provides an inventory of all other files in the data package.

3.2: Processing Data for Model

A MATLAB 'live script' was prepared for each of the three FTR transport experiments (*i.e.*, each flow rate: 30-, 15-, and 10- mL h^{-1}). The scripts read experimental results from the summary CSV files (described in *3.1*). The scripts used this data to perform several initial calculations, as described below.

The sample collection times were converted to a duration since the start of the experiment. For preliminary Br^- breakthrough tests, the start time was defined as the 't_0' time. For *Chlorella* transport experiments, the start time was defined as the time at which *Chlorella* paste was applied (entered manually into modelling scripts), to account for any potential 'head start' of *Chlorella* between paste application and the start of sample collection. The sample volumes were converted into cumulative volume eluted. The 'overall' flow rate for each sample collection was calculated as the sample volume divided by the duration between the start time of the sample collection and the start time of the next sample collection (intended to be 10, 20, and 30 minutes for experiments at 30-, 15-, and 10- mL h^{-1}, respectively). The 'true' flow rate of each sample collection was calculated as the sample volume divided by the duration of the sample collection (*i.e.*, the time the outflow valve was open to collect the sample). The mean 'true' and 'overall' flow rates were both calculated for each dataset (each set of 't_0' to 't_{18}' outflow samples). The mean 'true' and 'overall' flow rates from *Chlorella* transport datasets for both FTRs were also calculated. For each experiment, 'overall' and 'true' flow rates from all datasets were plotted versus time (Figure 3.1). The cumulative volumes eluted were also plotted versus time (along with a line representing the target flow rate) in Figure 3.1, demonstrating that the overall flow rates were close to the targets.

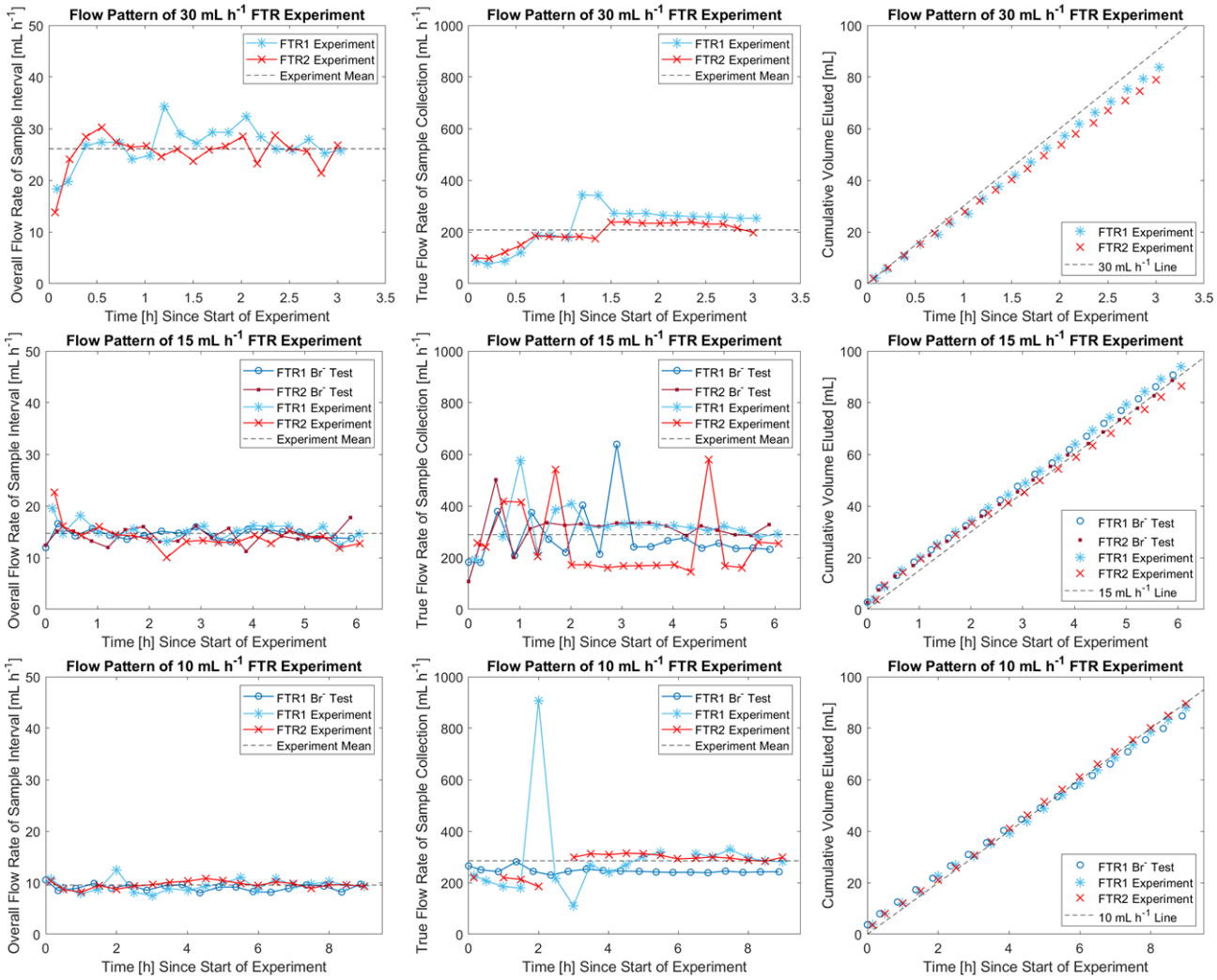

Figure 3.1: The measured flow patterns for all Br^- breakthrough tests and *Chlorella* transport experiments.

3.3: Estimating Sand Properties for Model

The preliminary Br^- breakthrough test data (Br^- concentrations and cumulative volumes eluted) were used to estimate the pore volume of the sand-filled portion of the FTRs. The pore volume was estimated by interpolating the volume eluted at which the outflow Br^- concentration reached half of the input concentration (which was 50 mg L^{-1} Br^- = 6.26×10^{-4} mmol cm^{-3} KBr for all experiments). The 30 mL h^{-1} experiment did not include a preliminary Br^- breakthrough test, and the IC subsamples for FTR2 in the 10 mL h^{-1} experiment were lost, so there were three preliminary Br^- breakthrough datasets: FTR1 and FTR2 from the 15 mL h^{-1} experiment, and FTR1 from the 10 mL h^{-1} experiment. The mean estimated pore volume estimated from these

three Br^- breakthrough datasets was 49(±1) mL (standard deviation of the three estimates assigned as uncertainty), and this value was used for all modelling.

The mean estimated pore volume was divided by the total volume of the sand column (calculated from known dimensions: 1.9 cm radius, 8 cm length) to define the porosity in the model, leading to an estimated porosity of 0.54. Cumulative volumes eluted were normalized by converting to the number of pore volumes eluted (when plotting BTCs on the same axes as model simulations). Br^- concentrations were normalized to the input concentration (C/C_0, ranging from 0 to 1). Concentrations of suspended *Chlorella* (g L^{-1} = mg cm^{-3}) were plotted on the same axes without normalizing concentration (all concentrations were <1 g L^{-1}), because the input concentration (C_{c_0}) was not necessarily the same for all experiments. The Br^- and *Chlorella* BTCs from experiments at all three flow rates are presented in Figure 3.2. The associated *Chlorella* RPs are presented in Figure 3.3.

The dispersivity (α_L) of the sand influences the shape of the modelled BTCs. According to Freeze & Cherry (1979), typical values of α_L reported for 'column tests with unconsolidated material' are in the range of 0.01 to 2 cm. Values in this range were tested in the model, and an α_L value of 0.2 cm was found to generate modelled Br^- BTCs that matched the shape of the experimental Br^- BTCs (Figure 3.4).

The particle density (ρ_s) of the sand was assumed to be that of quartz: 2.65 g cm^{-3} (Rumble, 2023). ρ_s and porosity (ϕ) were used to calculate the bulk density (ρ_b) of the sand from Eq. 3.1, and the mass of sand in each spatial cell in the model from Eq. 3.2:

$$\rho_b = (1 - \phi)\rho_s \qquad (3.1)$$

$$M_{cell} = \rho_b V_{cell} = \rho_b A \Delta x \qquad (3.2)$$

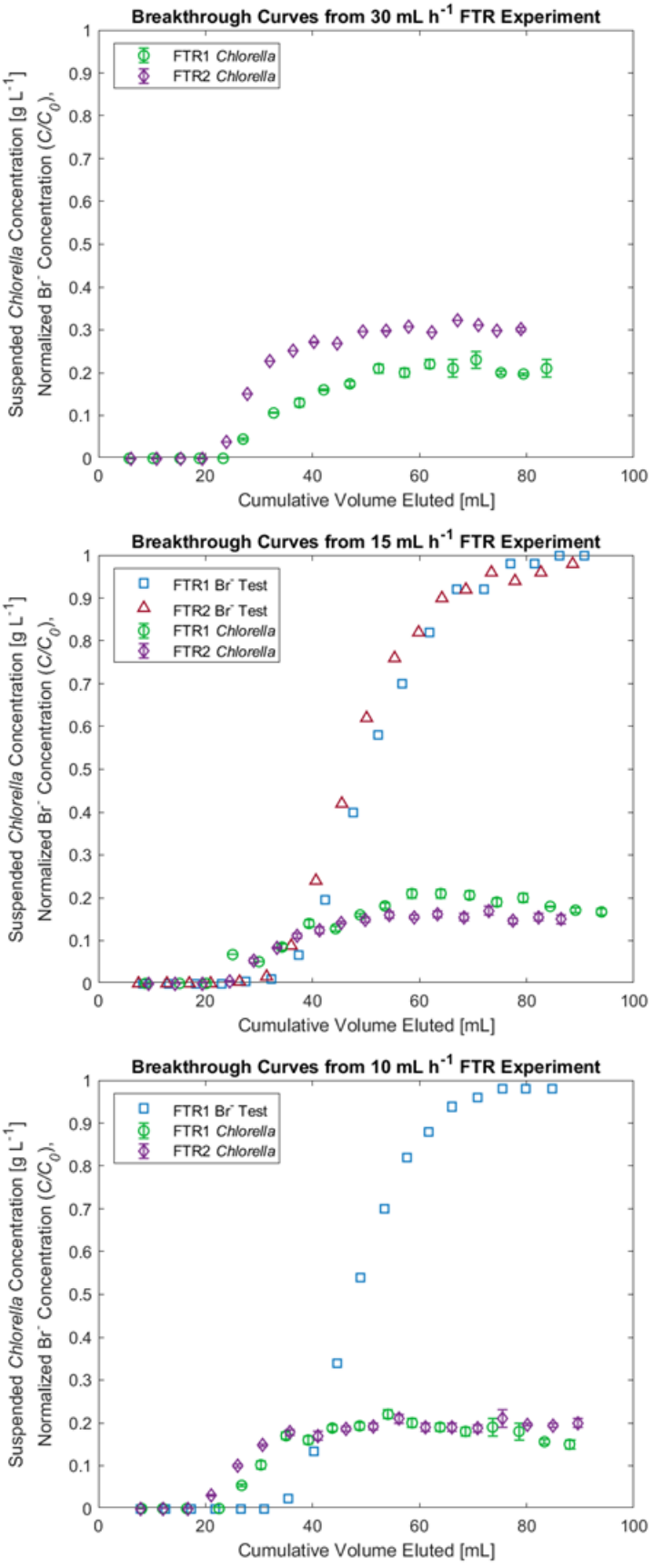

Figure 3.2: *Chlorella* breakthrough curves for each experiment, plotted with associated Br^- breakthrough tests, if applicable.

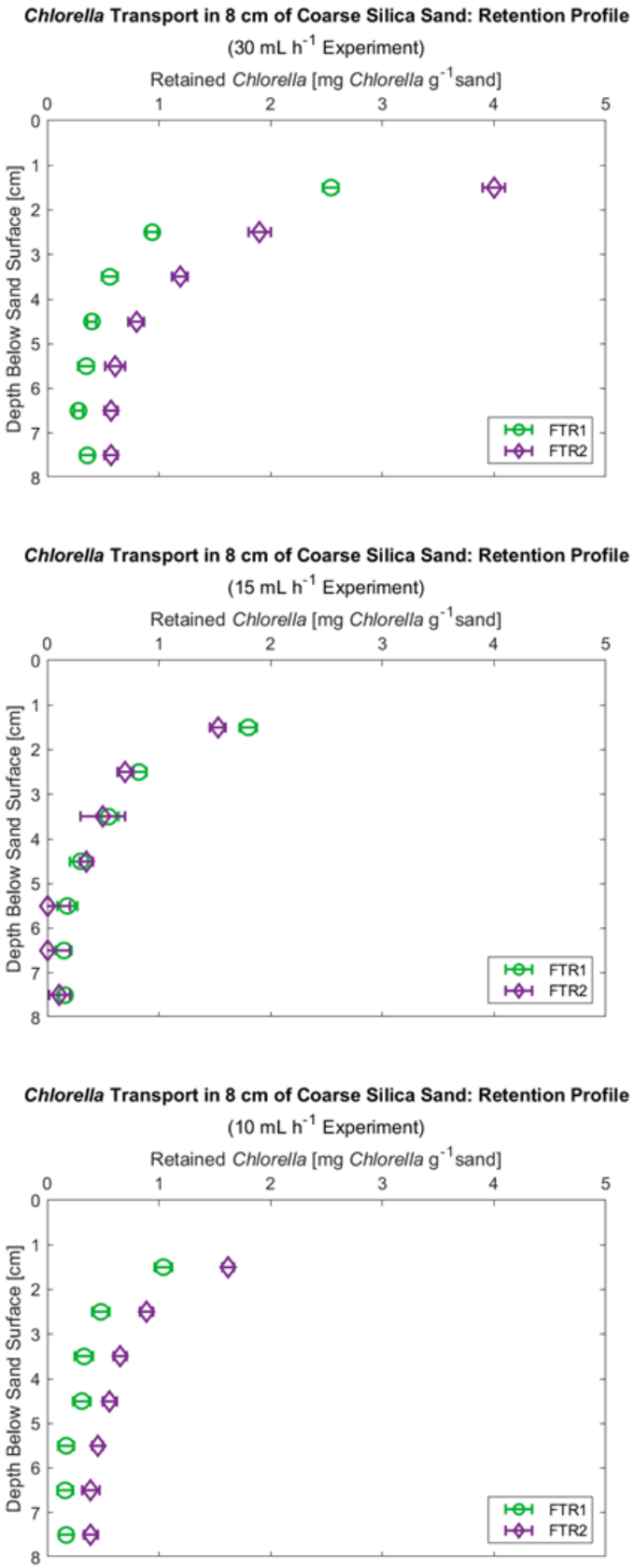

Figure 3.3: Retention profiles from each *Chlorella* transport experiment, as determined by loss-on-ignition.

3.4: Estimating Model Parameters for *Chlorella* Transport and Retention

The disadvantage of the numerical approach to solving the partial differential equations for modelling Br^- and *Chlorella* transport was that this approach did not produce a 'function' to enter into MATLAB's built-in curve-fitting tools for parameter estimation. As explained in *2.2*, the partial differential equations were arranged into systems of equations represented by matrices and solved in each timestep to model transport. Parameters were estimated using data from laboratory experiments.

The settling rate (v_s) of suspended *Chlorella* particles was adjusted to fit the experimental data through trial and error (and validated using additional laboratory settling tests, described in *2.1.9*), and the filtration coefficient (λ) was estimated from calculations using experimental data. The process of estimating these parameters is described in detail in sections *3.4.1*, *3.4.2*, and *3.4.3*.

3.4.1: Settling Rate of Suspended Chlorella Particles

BTCs (Figures 3.2, 3.4) indicated that suspended *Chlorella* particles arrived in the FTR outflow early (relative to the preliminary Br^- BTC). The early arrival of *Chlorella* particles was interpreted as 'velocity enhancement' caused by gravitational settling. This was modelled by including a gravitational settling rate (v_s, cm s^{-1}) in the *Chlorella* transport equation (Eq. 2.17). v_s is added to the linear pore water velocity and determines how early *Chlorella* arrives relative to Br^- in model simulations. A settling velocity used in literature for kaolinite colloids in sand was used as an initial estimate: Jin *et al.* (2019) used a settling velocity of 2×10^{-3} cm s^{-1} for modelling the transport of kaolinite colloids (dominant grain size ~2 µm) in sand (porosity 0.457), which is a similar scenario to the transport of *Chlorella* particles (dominant particle size ~4 µm, see *2.1.2*) in sand (porosity 0.54, see *3.3*) studied here. This initial estimate was tested in the model and adjusted so that the initial 'rising limb' of the modelled *Chlorella* BTC aligned

with the experimental BTC (Figure 3.4). A rate of 2.5×10^{-4} cm s^{-1} provided a good fit for experiments at all three flow rates (except for FTR2 in the 30 mL h^{-1} experiment).

A series of additional lab experiments were performed to validate the estimated settling rate (see *2.1.9*). These experiments led to estimated settling rates on the order of $1\text{-}2\times10^{-3}$ cm s^{-1} (calculations summarized in Table 3.1). As explained in *2.1.9*, the estimated rates from lab experiments represent the higher end of a range of settling rates. In consideration of the upper limit of settling rates estimated from lab experiments, the rate fit to the model is realistic because it is below that limit.

Table 3.1: Summary of settling rate estimate calculations using timelapse recordings of final settling experiments.

Sand Thickness	**Ratio of Real Time to Time in Video File**	**Time of Earliest Visible *Chlorella* Arrival in Video**	**Equivalent in Real Time**	**Equivalent in Real Time (adjusted for lag between paste application and start of recording)**	**Settling Rate**
[cm]	[-]	[s]	[s]	[s]	[cm s^{-1}]
8	89.98	75	6748.5	6808.5	1.2E-03
8	89.98	58	5218.84	5278.84	1.5E-03

3.4.2: Filtration Coefficient for Chlorella Particles in the Sand Medium

In the transport experiments, *Chlorella* was applied to the upper surface of the sand as a thick paste layer (procedure described in *2.1.4*), most of which remained at the surface after the experiments, so the actual concentration carried in suspension to enter the upper boundary of the sand was not known. The model used experimental data to perform mass balance calculations for estimating this concentration, as described below.

First, the concentration of *Chlorella* in each outflow sample (as determined by absorbance measurements) was multiplied by the sample volume to calculate the mass in each sample. For each FTR, the *Chlorella* masses in all outflow samples were summed to calculate the total mass eluted during the experiment. The *Chlorella* mass suspended in the

pore water of each FTR at the end of each experiment was estimated by multiplying the concentration of the final outflow sample ('t_{18}') by the pore volume.

The masses of *Chlorella* retained in 1 cm sand slices (as determined by loss-on-ignition) were summed to calculate the total mass retained on sand (from 1-8 cm depth). The 0-1 cm sand slices could not be separated from the remaining excess paste layer, which prevented an accurate determination of the mass retained in that interval. The mass retained in 0-1 cm was instead estimated for each FTR by fitting an exponential curve to the *Chlorella* RP (Figure 3.5) using the built-in 'non-linear regression model' ('fitnlm') in MATLAB. Eq. 3.3 models the exponential relationship between concentration and depth:

$$C_{Chl/sand} = ae^{-bx} \qquad (3.3)$$

where $C_{Chl/sand}$ is the concentration of retained *Chlorella* (mg *Chlorella* g^{-1} sand), and x is depth (cm) below the upper boundary of sand (for samples from experiments, the depth of the midpoint of the slice was used). a (mg *Chlorella* g^{-1} sand) and b (cm^{-1}) are the coefficients estimated by 'fitnlm'. This function for representing how retained particle concentration decreases with depth is of the same exponential form as the function (obtained from Eq. 1.9) for representing how suspended particle concentration decreases with depth. a is the retained particle concentration at x = 0, and b is analogous to the 'filtration coefficient' (see Eqs. 1.9, 1.10). The initial coefficient values entered in 'fitnlm' were a = 1 and b = 1. For each FTR, the estimated coefficients (and associated statistics) from 'fitnlm' are provided in Table 3.2. The exponential curves are plotted with the experimental data in Figure 3.5.

The exponential curve coefficients estimated by 'fitnlm' were used in Eq. 3.3 to predict the concentration of *Chlorella* retained in the 0-1 cm sand slices by setting x = 0.5 cm. The mass of sand in the 0-1 cm slices was assumed to be equal to the mean sand mass calculated for the other slices from the same experiment, and the predicted concentration was multiplied by

this mean sand mass to convert to a mass of *Chlorella*. This provided an estimate of the mass retained in the 0-1 cm sand slices.

Table 3.2: Coefficients for exponential curves (Eq. 3.3) fit to *Chlorella* retention profiles, estimated by MATLAB non-linear regression model 'fitnlm' using initial values a = 1 and b = 1.

Experiment	FTR	Coefficient a [mg g^{-1}]	'p-value' for a	Coefficient b [cm^{-1}]	'p-value' for b	Coefficient of Determination, R^2
30 mL h^{-1}	1	7.0532	1E-02	0.70649	3E-03	0.928
	2	8.4332	2E-03	0.52938	7E-04	0.952
15 mL h^{-1}	1	4.3637	3E-04	0.60925	1E-04	0.982
	2	3.8659	2E-03	0.62931	5E-04	0.968
10 mL h^{-1}	1	1.9079	3E-03	0.45482	2E-03	0.922
	2	2.3577	1E-03	0.31574	2E-03	0.905

For each FTR: the cumulative *Chlorella* mass eluted, final mass suspended in pore water, mass retained in 1-8 cm depth, and estimated mass retained in 0-1 cm depth calculated from experimental data were summed to obtain an estimate of the total mass of *Chlorella* that entered the sand during the experiment. This estimated 'total mass entered' was divided by the cumulative volume eluted (multiplied by $\frac{v+v_s}{v}$, because the *Chlorella* model effectively introduces that much more volume to model the early arrival) to calculate the input concentration of suspended *Chlorella* particles that would be required to introduce the estimated 'total mass entered' within the duration of the experiment. This approach assumes that the input concentration remained constant over time. For each modelling script (each flow rate), the mean estimated input concentration from both FTRs (to two significant figures) was used as the input concentration for the model simulation (C_{c_0}, mg cm^{-3}), which was used to estimate the filtration coefficient (λ, cm^{-1}, to two significant figures) using Eq. 2.19. The mean concentration of suspended *Chlorella* in outflow after the elution of one pore volume (mean from both FTRs, to two significant figures) was used as $C_{c_{max}}$ in Eq. 2.19, so λ then caused that to be the approximate modelled breakthrough concentration. The mass balance calculations, estimated C_{c_0}, and estimated λ for each FTR are provided in Table 3.3. Figures

3.4, 3.5, and 3.6 show the modelled BTCs, RPs, and resulting mass balance error plots. To plot the modelled RP, the concentration of retained *Chlorella* (C_{cr}) in each spatial cell was converted from mg cm^{-3} of pore space to mg g^{-1} sand ($C_{Chl/sand}$) by Eq. 3.4:

$$C_{Chl/sand} = (C_{cr} P V_{cell})/M_{cell} = C_{cr}(V_{cell}\phi)/(\rho_b V_{cell}) = C_{cr}\frac{\phi}{\rho_b} \qquad (3.4)$$

Table 3.3: Summary of calculations performed using experimental data to estimate input concentrations and filtration coefficients for the *Chlorella* model.

Total Depth of Sand [cm]:	**8**					
Target Flow Rate of Experiment [mL h^{-1}]:	**30**		**15**		**10**	
Flow-Through Reactor ('FTR'):	**1**	**2**	**1**	**2**	**1**	**2**
Approximate Mass of *Chlorella* Applied to Upper Boundary [g]:	1.14	1.42	1.11	1.05	1.12	1.30
Total *Chlorella* Mass Eluted [mg]:	10.7	15.5	11.6	8.50	11.0	12.6
***Chlorella* Mass Suspended in Pore Water at End of Experiment [mg]:**	10.3	14.7	8.20	7.40	7.40	9.80
***Chlorella* Mass Retained in 1-8 cm depth [mg]:**	92.0	161	64	53.0	46.0	82.8
Predicted *Chlorella* Mass Retained in 0-1 cm depth [mg]:	81.4	107	53.2	46.7	25.6	33.9
Total *Chlorella* Mass Entered [mg]:	194	298	137	116	90.0	139
Total Volume Eluted [cm^3]:	83.7	78.9	94.0	86.4	88.0	89.6
Mean Pore Volume from (three) Br$^-$ Breakthrough Tests [cm^3]:	**49**					
± Uncertainty (Standard Deviation) of Estimated Pore Volume [cm^3]:	**1**					
Pore Volumes Eluted [-]:	1.71	1.61	1.92	1.76	1.80	1.83
Estimated Input Concentration of Suspended *Chlorella*, Cc_0 ((Total *Chlorella* Mass Entered) / ((Total Volume Eluted)×((v+v_s)/v))) [mg cm^{-3} = g L^{-1}]:	1.92	3.11	1.06	0.97	0.648	0.985
Mean Cc_0 Estimate from Two FTRs [g L^{-1}]:	**2.5**		**1.0**		**0.82**	
Breakthrough Concentration of Suspended *Chlorella*, Cc_{max} (mean outflow concentration after 1 Pore Volume eluted) [g L^{-1}]:	0.206	0.304	0.188	0.156	0.184	0.197
Mean Cc_{max} from Two FTRs [cm^{-1}]:	**0.25**		**0.17**		**0.19**	
Estimated Filtration Coefficient, λ [cm^{-1}]:	0.279	0.291	0.217	0.229	0.157	0.201
λ (using mean Cc_0 and Cc_{max} from Two FTRs) [cm^{-1}]:	**0.29**		**0.22**		**0.18**	

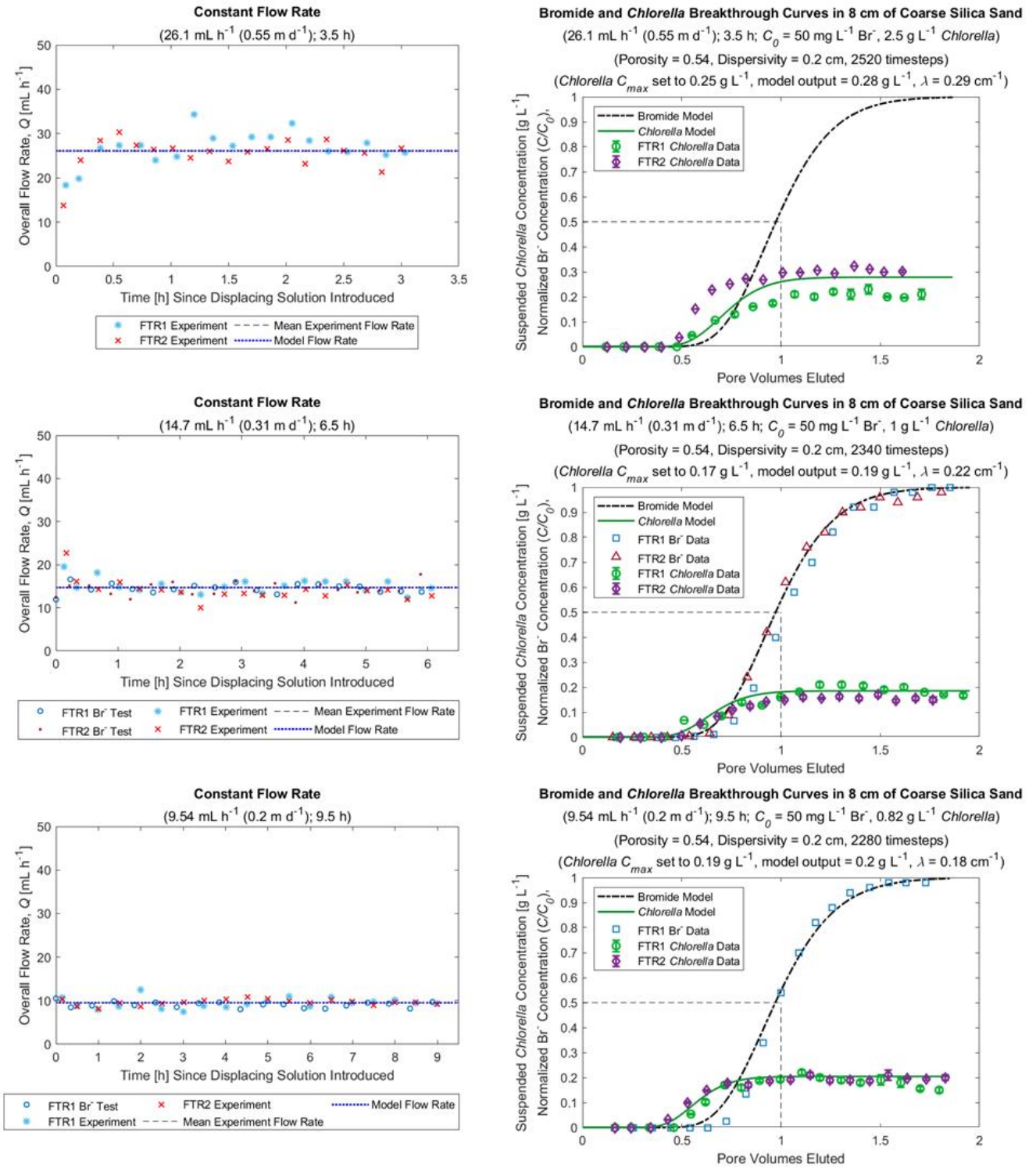

Figure 3.4: Results from *Chlorella* transport experiments at three flow rates. **Left:** plots of the overall flow rate of each sample collection, and the mean overall flow rate (which was used in the model simulation). **Right:** *Chlorella* breakthrough curves for each experiment, plotted with associated Br^- breakthrough tests (if applicable) and breakthrough curves from the associated model simulations.

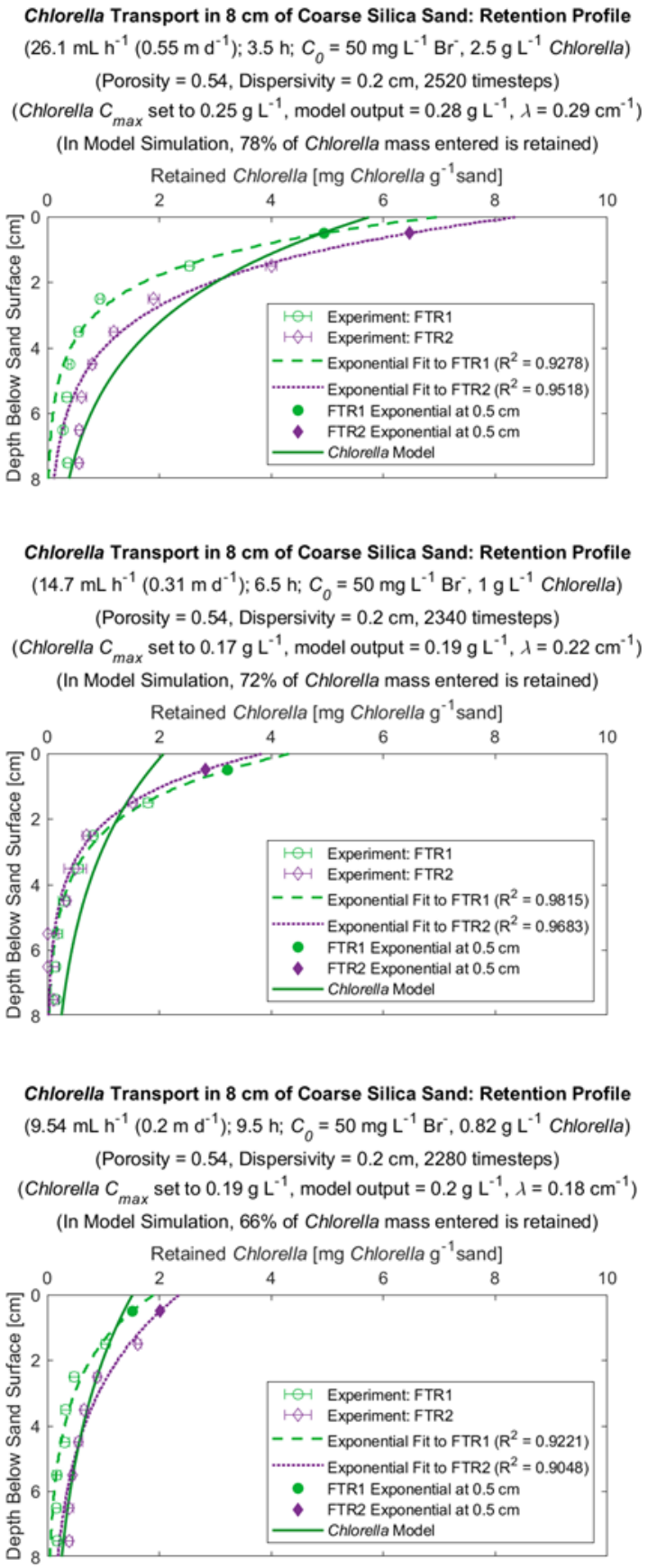

Figure 3.5: Retention profiles from each *Chlorella* transport experiment (as determined by loss-on-ignition), plotted with fitted exponential curves, predicted concentrations at 0.5 cm depth, and the retention profiles from the associated model simulations.

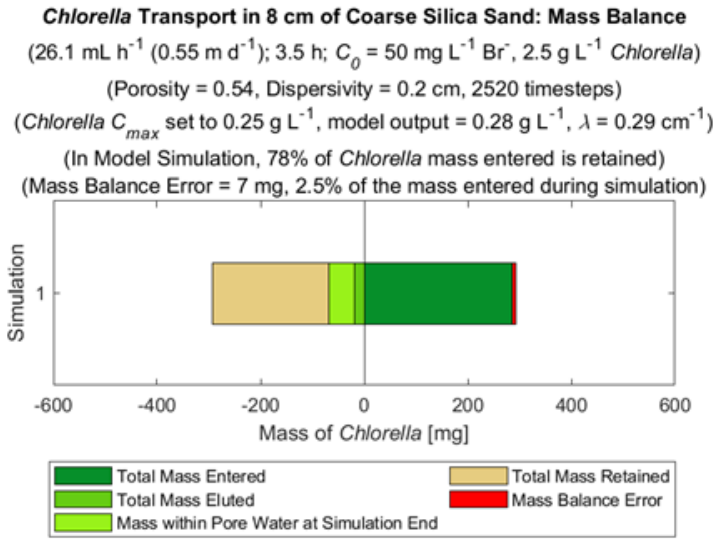

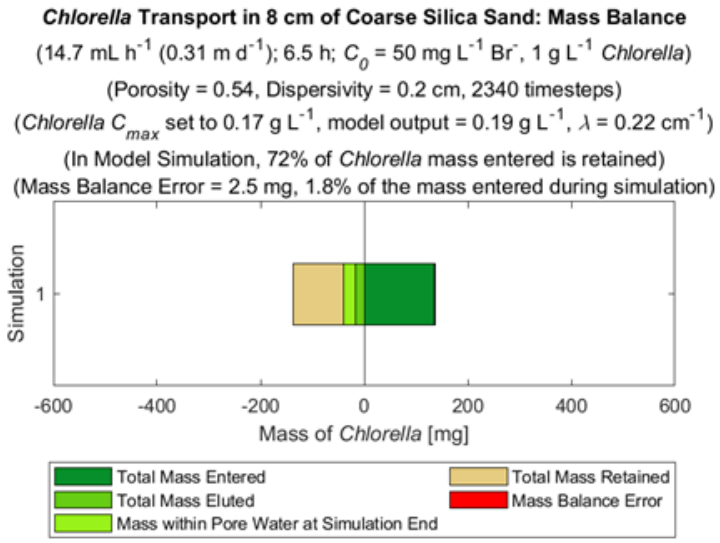

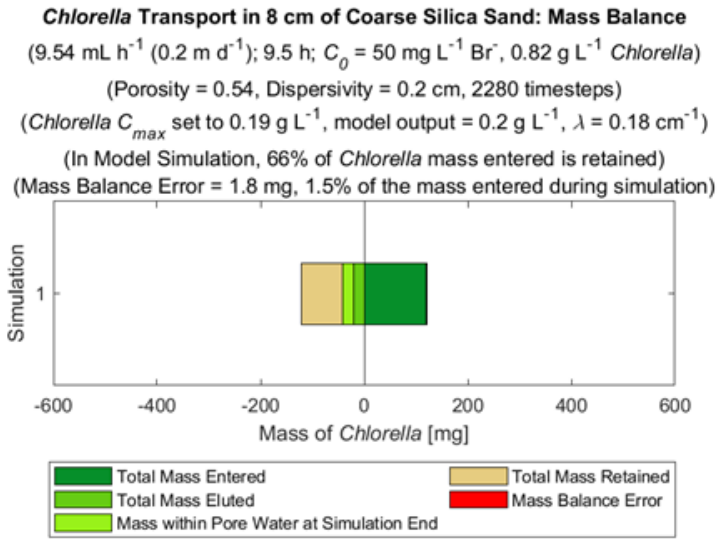

Figure 3.6: Plots summarizing the *Chlorella* mass balance in the model simulation of each transport experiment.

Table 3.4 provides a summary of each transport experiment and the associated model simulation, including estimated parameters.

Table 3.4: Summary table for *Chlorella* transport experiments and model simulations at three flow rates.

Total Depth of Sand [cm]:	**8**					
Target Flow Rate of Experiment [mL h^{-1}]:	**30**		**15**		**10**	
Sample Collection Interval [minutes]:	10		20		30	
Duration of Experiment (from application of *Chlorella* to final draining) [h]:	3.3		6.4		9.6	
Duration of Model Simulation [h]:	3.5		6.5		9.5	
Mean 'Overall' Flow Rate (as Volumetric Discharge, *Q*) [mL h^{-1}]: (also the flow rate used for the model simulation)	26.1		14.7		9.54	
Mean 'Overall' Flow Rate (as Specific Discharge, *q*) [m d^{-1}]:	0.552		0.311		0.202	
Mean 'Overall' Flow Rate (as Linear Pore Water Velocity, *v*) [m d^{-1}]:	1.02		0.576		0.374	
Mean 'True' Flow Rate During Sample Collection [mL h^{-1}]:	208		289		285	
Flow-Through Reactor ('FTR'):	**1**	**2**	**1**	**2**	**1**	**2**
Approximate Mass of *Chlorella* Applied to Sand for Experiment [g]:	1.14	1.42	1.11	1.05	1.12	1.30
Estimated *Chlorella* Mass Retained [g]: (measured mass for 1-8cm depth, plus predicted mass for 0-1cm depth)	0.173	0.268	0.117	0.100	0.0716	0.117
Estimated Total *Chlorella* Mass Entered [g]:	0.194	0.298	0.137	0.116	0.0900	0.139
Estimated Total *Chlorella* Mass Entered, as % of Approximate Mass Applied [%]:	17.0%	21.0%	12.3%	11.0%	8.04%	10.7%
Estimated *Chlorella* Mass Retained, as % of Approximate Mass Applied [%]:	15.2%	18.8%	10.6%	9.49%	6.39%	8.98%
Estimated *Chlorella* Mass Retained, as % of Estimated Mass Entered [%]:	89.2%	89.9%	85.5%	86.3%	79.5%	83.9%
Total Volume Eluted [cm^3]:	83.7	78.9	94.0	86.4	88.0	89.6
Estimated *Chlorella* Mass Entered per Unit Volume Eluted [mg cm^{-3}]:	2.32	3.77	1.46	1.34	1.02	1.55
Estimated *Chlorella* Mass Retained per Unit Volume Eluted [mg cm^{-3}]:	2.07	3.39	1.25	1.15	0.813	1.30
Estimated *Chlorella* Mass Entered per Unit Volume Eluted, as % of Approximate Mass Applied [%]:	0.204%	0.266%	0.131%	0.127%	0.091%	0.120%
Estimated *Chlorella* Mass Retained per Unit Volume Eluted, as % of Estimated Mass Entered [%]:	1.07%	1.14%	0.91%	1.00%	0.90%	0.94%
Mean Pore Volume from (three) Br^- Breakthrough Tests [cm^3]:	**49**					
± Uncertainty (Standard Deviation) of Estimated Pore Volume [cm^3]:	**1**					
Pore Volumes Eluted [-]:	1.71	1.61	1.92	1.76	1.80	1.83
Estimated Input Concentration of Suspended *Chlorella*, Cc_0 [mg cm^{-3} = g L^{-1}]:	1.92	3.11	1.06	0.973	0.648	0.985
Mean Cc_0 Estimate from Two FTRs [g L^{-1}]:	**2.5**		**1.0**		**0.82**	
Breakthrough Concentration of Suspended *Chlorella*, Cc_{max} (mean outflow concentration after 1 Pore Volume eluted) **[g L^{-1}]:**	0.206	0.304	0.188	0.156	0.184	0.197
Mean Cc_{max} from Two FTRs [cm^{-1}]:	**0.25**		**0.17**		**0.19**	
Estimated Filtration Coefficient, λ [cm^{-1}]:	0.279	0.291	0.217	0.229	0.157	0.201
λ (using mean Cc_0 and Cc_{max} from Two FTRs) [cm^{-1}]:	**0.29**		**0.22**		**0.18**	
***Chlorella* Mass Balance Error in Model Simulation [%]:**	2.46		1.83		1.47	
***Chlorella* Mass Entered in Model Simulation [mg]:**	286		135		120	
***Chlorella* Mass Retained in first 3h of Model Simulation [mg]:**	188		37.4		17.6	
***Chlorella* Mass Retained in first 6h of Model Simulation [mg]:**	N/A		88.8		46.2	
Total *Chlorella* Mass Retained in Model Simulation [mg]:	224		97.4		74.9	
Total Volume Eluted in Model Simulation [cm^3]:	91.4		95.6		90.6	
Total Pore Volumes Eluted in Model Simulation [-]:	1.86		1.95		1.85	
***Chlorella* Mass Retained per Unit Volume Eluted in Model Simulation [mg cm^{-3}]:**	2.46		1.02		0.88	
***Chlorella* Mass Retained per Unit Volume Eluted in Model Simulation, as % of Total Mass Entered During Simulation:**	0.859%		0.755%		0.733%	

3.4.3: Dissolved Carbon in Outflow from Chlorella Transport Experiments

Analyses of outflow samples for suspended *Chlorella* particles and Br^- tracer were prioritized, so there was not always enough subsample available (after losses during filtering and transfer) for dissolved carbon analyses. DOC analysis was completed for most samples, but DIC analysis was only completed for a subset. The method detection limit (MDL) was 0.15 mg-C L^{-1} DOC and 0.04 mg-C L^{-1} DIC. The mean blank concentrations were above the MDL, at 0.54 mg-C L^{-1} DOC and 0.08 mg-C L^{-1} DIC, so sample values were first blank-corrected (subtracting the mean concentration of blanks from the same instrument run) and then dilution-corrected (dilution and instrumental analysis briefly described in *2.1.7*). The DOC concentrations included in the CSV files for each experiment are the corrected concentrations. The corrected concentrations in 'filter blanks' (samples of Milli-Q water subjected to same filtering and subsampling procedure as outflow samples) were <30 mg-C L^{-1} DOC and <0.7 mg-C L^{-1} DIC. The corrected concentrations in samples ranged from 12 to 1319 mg-C L^{-1} DOC and 0 to 7.80 mg-C L^{-1} DIC. For outflow samples from the 30 mL h^{-1} and 15 mL h^{-1} transport experiments, the maximum DIC concentrations were <1% of the maximum DOC concentrations. DIC concentrations were much higher in the 10 mL h^{-1} experiment, but still <7% of the max DOC concentration. The DOC concentrations (as g-C L^{-1}) in outflow samples are plotted against pore volumes eluted in Figure 3.7, with suspended *Chlorella* concentrations (multiplied by organic carbon fraction 0.44 to convert from g L^{-1} *Chlorella* to g L^{-1} POC, for comparison to DOC concentrations) and modelled BTCs included on the same plots. Since the DIC datasets are incomplete and the DIC concentrations are (compared to DOC) likely insignificant, the DIC results are not presented.

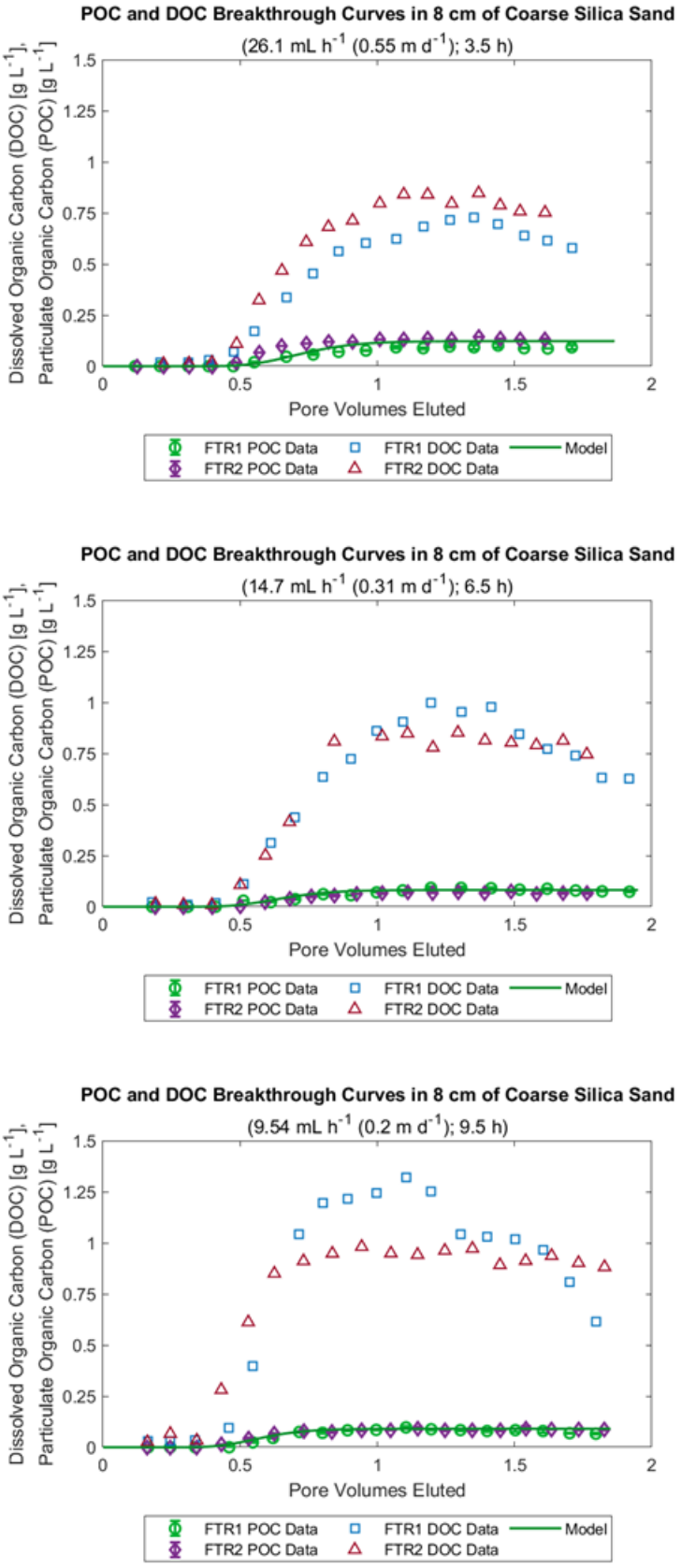

Figure 3.7: Particulate organic carbon (POC) breakthrough curves for each experiment plotted with associated dissolved organic carbon (DOC) data and POC breakthrough curves from the associated model simulations. Measured (and modelled) concentrations of suspended *Chlorella* were converted to POC concentrations using the % organic carbon content of *Chlorella*.

3.4.4: Discontinuous Modelling

The model simulations presented so far used continuous flow at the average 'overall' flow rate of the experiments. As explained in *2.1.6*, the experiments were performed discontinuously, with flow only occurring for a short time (typically about 1 minute) when the outflow valve was opened to collect each sample (~5 mL). To verify that the continuous model simulations were a valid representation of the discontinuous experiments, discontinuous versions of the model simulations were also prepared. In the discontinuous versions, flow only occurred at the specified sampling interval (10 minutes for 30 mL h^{-1}, 20 minutes for 15 mL h^{-1}, and 30 minutes for 10 mL h^{-1}) at the mean 'true' flow rate of sample collection (calculated using data from the experiment), for 1 minute each time. In the 30 mL h^{-1} experiment, the mean collection rate was lower (and mean collection duration was longer), so the 30 mL h^{-1} simulation used a duration of 1.5 minutes for each collection. Figure 3.8 shows plots of the modelled flow rate (with the collection rates from the experiments) and resulting BTCs (with concentrations from the experiments). This test of the discontinuous model demonstrated that both the discontinuous and continuous models can produce BTCs (plotted in terms of pore volumes) that represent the experimental data, so discontinuous modelling was not pursued further.

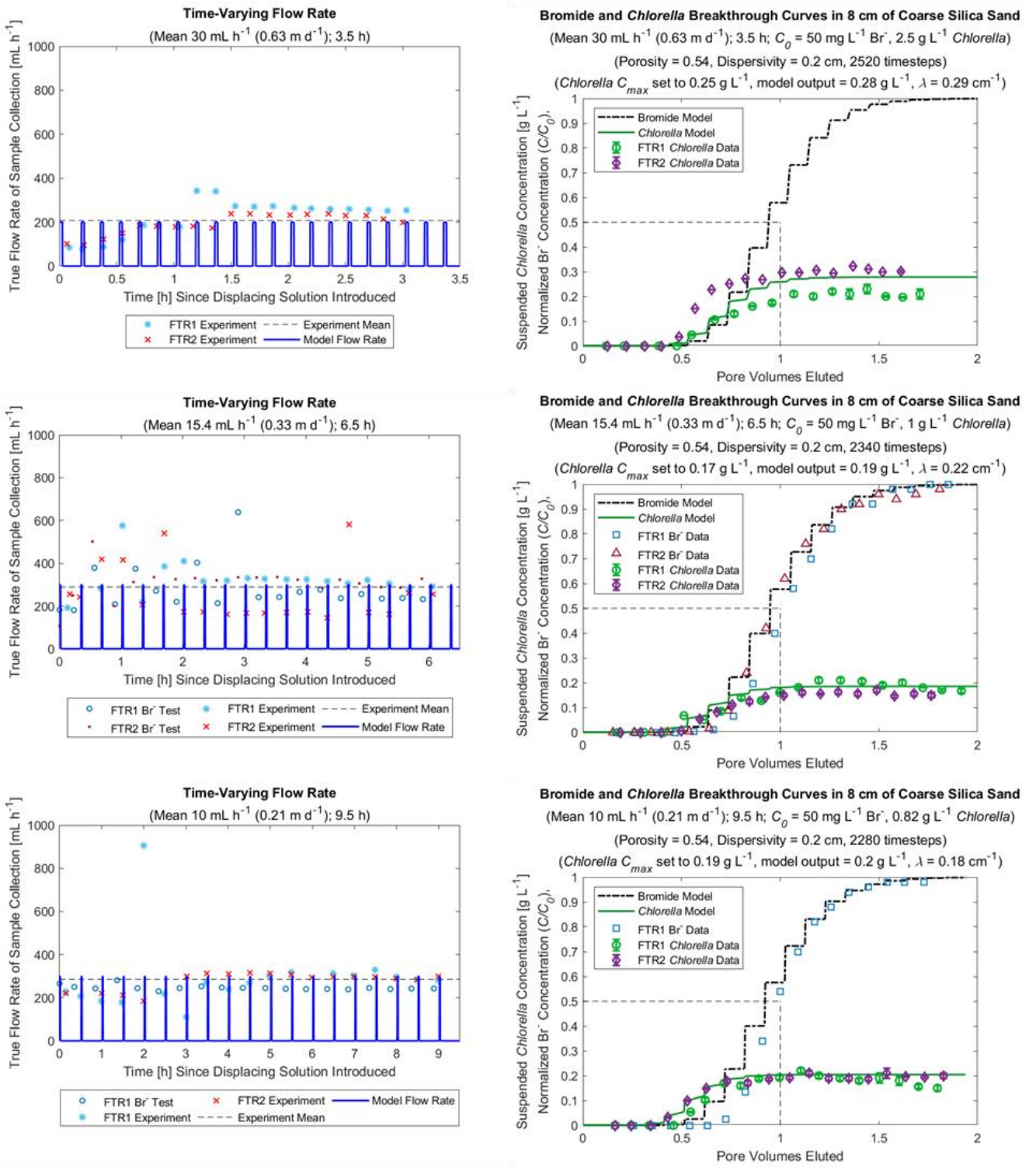

Figure 3.8: Left: plots of the modelled discontinuous flow pattern with the measured rate of each sample collection. **Right:** *Chlorella* breakthrough curves for each experiment, plotted with associated Br^- breakthrough tests (if applicable) and breakthrough curves from the associated discontinuous model simulations.

3.5: Discussion

Within each transport experiment (*i.e.*, at each of the three flow rates), the consistency of the resulting BTCs and RPs between the two FTRs suggests that the results are reproducible (Figures 3.4, 3.5, 3.6). The only exception is the BTC for FTR2 in the 30 mL h^{-1} experiment, which has a greater breakthrough concentration and earlier arrival of suspended *Chlorella* (compared to FTR1 in the same experiment). The higher concentration might be due to the larger mass of *Chlorella* that was applied to FTR2 in that experiment. As noted in *2.1.9*, the settling rate can vary throughout the sand, which could be the reason for the earlier arrival of *Chlorella* in FTR2 in that experiment.

The velocity enhancement (early arrival) of *Chlorella* was interpreted as being caused solely by gravitational settling of the suspended particles. It is noted that gravitational settling is not the only possible explanation for velocity enhancement. Close *et al.* (2006) observed velocity enhancement of microspheres (1-, 5-, and 10- µm) in gravel (5-7 mm) relative to Br^- tracer during column experiments with upward flow at a 30° incline (Table 1.2). Harter *et al.* (2000) observed velocity enhancement of oocysts (4.5-5.5 µm) relative to Chloride tracer in sands (Table 1.2), but flow direction was not specified. Harter *et al.* (2000) discussed that colloids can have higher transport velocities than water because of 'excluded pore volume' (exclusion of colloids from 'margins' of pores) and 'inaccessible pore volume' (pores completely inaccessible to colloids). However, even if velocity enhancement of *Chlorella* was not due to gravitational settling, modelling the early arrival could still be achieved the same way (by increasing pore water velocity in the *Chlorella* model). Another interpretation of the early arrival of *Chlorella* would be that the timing of arrival is the net result of retardation (delaying arrival) and gravitational settling (advancing arrival). Here, the simplest explanation was chosen: it was assumed that retardation did not occur, and that the early arrival of *Chlorella* was directly determined by gravitational settling. Experiments conducted in a

horizontal orientation could help to test this hypothesis: gravitational settling would have a less direct influence on transport, but if there were other causes of velocity enhancement, they would presumably still occur (as would any delay caused by retardation). Bulur (2021) conducted POM transport experiments in horizontally oriented columns using POM and sandy sediments (both from the riverbed of the Hanford Reach) and did not observe any indication of either early or delayed arrival of POM relative to a nonreactive Br^- tracer. This supports the hypothesis that gravitational settling was the key determinant of the early arrival of *Chlorella*. This hypothesis is also strongly supported by the settling experiments described in 2.1.9, in which *Chlorella* travelled downwards through 8 cm of saturated sand without any water flow.

From a visual comparison of the measured *Chlorella* BTCs from the 15- and 10- mL h^{-1} experiments, the early arrival of *Chlorella* seems to become more pronounced when the flow rate is decreased (Figure 3.4). This is what would be expected since the velocity enhancement of suspended particles by gravitational settling should become less relevant as pore water velocity is increased. For the 30 mL h^{-1} experiment, the arrival of *Chlorella* is closer to that of the nonreactive Br^- tracer for both FTR1 and the model simulation, but this is contradicted by FTR2 (as previously discussed), so further research might be required for a complete understanding of the role of settling (or other velocity enhancement) in vertical POM transport. Table 3.5 compares the flow rate (converted to average linear pore water velocity, v, cm s^{-1}) to the settling rate estimated and used for model simulations (considered to approximate the mean rate of *Chlorella* settling through the sand) and the settling rate estimated using settling experiments (considered to represent the upper limit of the rate of *Chlorella* settling through the sand), and calculates the distance that *Chlorella* could be transported by the settling rates during each of the transport experiments. Note that the rate estimated from settling experiments is faster than v of each experiment, and the results of transport experiments do not suggest a significant amount of *Chlorella* settled at that rate. Even at the lower settling rate

estimated and used for the model, some *Chlorella* could potentially travel through the full depth of the sand by only gravitational settling within the duration of the 10 mL h^{-1} experiment.

Table 3.5: Comparison of estimated settling rates for suspended *Chlorella* particles in saturated sand to flow rates used for *Chlorella* transport experiments in FTRs, and calculated distances that *Chlorella* particles could be transported by settling during the time frame of each experiment.

Total Depth of Sand [cm]:	8		
***Chlorella* Settling Rate Estimated (and used) for Model Simulations, v_s [cm s^{-1}]:**	2.5E-04		
Calculated Time for *Chlorella* to Settle through 8 cm Saturated Sand (No Flow) at v_s [h]:	8.9		
Maximum *Chlorella* Settling Rate (Estimated from Settling Experiments), v_{s_max} [cm s^{-1}]:	1.5E-03		
Calculated Time for *Chlorella* to Settle through 8 cm Saturated Sand (No Flow) at v_s [h]:	1.5		
Target Flow Rate of Experiment [mL h^{-1}]:	30	15	10
Target Flow Rate (as Linear Pore Water Velocity, v) [cm s^{-1}]:	1.4E-03	6.8E-04	4.5E-04
Mean 'Overall' Flow Rate (as Volumetric Discharge, Q) [mL h^{-1}]: (also the flow rate used for the model simulation)	26.1	14.7	9.54
Mean 'Overall' Flow Rate (as Linear Pore Water Velocity, v) [m d^{-1}]:	1.023	0.576	0.374
Mean 'Overall' Flow Rate (as Linear Pore Water Velocity, v) [cm s^{-1}]:	1.2E-03	6.7E-04	4.3E-04
v/v_s Ratio [-]:	4.7	2.7	1.7
Sample Collection Interval [minutes]:	10	20	30
Predicted Settling Distance Between Each Sample Collection, at v_s [cm]:	0.15	0.30	0.45
Predicted Settling Distance Between Sample Collections, at v_{s_max} [cm]:	0.90	1.8	2.7
Duration of Experiment (from application of *Chlorella* to final draining) [h]:	3.3	6.4	9.6
Predicted Settling Distance During Experiment, at v_s [cm]:	3.0	5.8	8.6
Predicted Settling Distance During Experiment, at v_{s_max} [cm]:	18	35	52

The estimated input concentration of suspended *Chlorella* particles (C_{c_0}) increased with flow rate but is also related to the mass of *Chlorella* used for each experiment (Table 3.4). The estimated C_{c_0} was most consistent between FTRs in the 15 mL h^{-1} experiment, in which the mass applied was most consistent between FTRs. In the 30- and 10-mL h^{-1} experiments, the mass applied to each FTR differed more, leading to a greater difference in estimated input concentrations between the two FTRs. In both the 30- and 10-mL h^{-1} experiments, the FTR with more mass applied had a higher estimated input concentration.

Breakthrough concentrations ($C_{c_{max}}$, defined here as mean concentration after one pore volume eluted) of suspended *Chlorella* were similar between all FTRs, but higher in FTRs with more mass applied. $C_{c_{max}}$ was within 0.16-0.21 g L^{-1} for all FTRs except for 30mL h^{-1} FTR2 (0.30 g L^{-1}), which had the largest mass of *Chlorella* applied.

Despite $C_{c_{max}}$ being similar at all three flow rates (as shown by BTCs, Figure 3.4), RPs (Figure 3.5) suggest that more *Chlorella* mass was retained at higher flow rates (but it should be noted that the RPs do not account for differences in the mass entered). Since the estimated C_{c_0} increased with increased flow rate while the measured $C_{c_{max}}$ was similar at all three flow rates, this led to a slight increase in the estimated λ value with increased flow rate. This seems to support the idea that filtration increases with flow rate, but this trend in λ might only be apparent. Since the collector efficiency (η) decreases with increased flow rate, an increase in λ requires an increased collision efficiency (α), as discussed in *1.2.3*.

Table 3.4 reports the mass retained in the first 3 hours of each model simulation (each simulation was at least that long, so this is a basic comparison between the different flow rates), and the mass retained increases with increasing flow rate. This is expected because a higher flow rate introduces a greater volume of water per unit time, and thus (for a given concentration of suspension) a greater mass of suspended particles, but this comparison does not account for the different input concentrations of each model simulation.

For a proper comparison of the experiments (and model simulations), the variation in the amount of *Chlorella* that entered the sand must be accounted for, so Table 3.4 presents the estimated masses of *Chlorella* entered and retained in each FTR as a percentage of the mass applied to the surface of the sand (note that most of the *Chlorella* paste remained on the surface at the end of each experiment). When expressed as a percentage of the mass applied, the estimated masses entered and retained both increased as flow rate was increased (Table 3.4). However, that comparison is not relevant to the model simulations, so Table 3.4 also includes the estimated mass retained as a percentage of the estimated mass that entered the sand medium (to account for the different mass entered for each experiment). This can be compared to the modelled mass retained (expressed as a percentage of the modelled mass entered).

In addition to expressing *Chlorella* mass retained as % of mass entered, comparisons between experiments and between model simulations at different flow rates are further improved by expressing the mass retained per unit volume eluted, to account for the different durations of each experiment. It is evident that increasing the flow rate introduces (and likely retains) more mass per unit time, but comparing the mass retained on a per unit volume basis allows for an investigation of whether the influence of flow rate on retention extends beyond that basic impact. In these experiments and model simulations, the mass retained per unit volume eluted (as a percentage of the total mass entered) did tend to increase as flow rate was increased in both the experimental results and the model simulations. The only exception to this was that the mass retained per unit volume eluted (as a percentage of the total mass entered) was greater for FTR2 in the 10 mL h^{-1} experiment than for FTR1 in the 15 mL h^{-1} experiment, but otherwise the overall trend is that this value increased with flow rate. Figure 3.9 illustrates that when differences in duration and mass entered are accounted for, there is still a strong positive correlation between mass retained and flow rate. This supports the hypothesis that retention of suspended particles in sediments increases with hydrologic flux (not simply due to the increase of mass introduced per unit time, but also per unit volume of flux).

As shown in Figure 3.7, a pulse of DOC was detected during each experiment, coincident with the arrival of suspended *Chlorella* particles. This demonstrates that even in a short time (<10h), POC in sediments can release DOC (which would then be available to microbes). The concentrations of DOC exceeded those of suspended POC (based on the 44% OC content of *Chlorella*). This suggests that much of the detected DOC may have been released from *Chlorella* that was retained in the sand or remained in the excess paste layer at the surface of the sand (rather than being released from suspended *Chlorella*). All of this supports the idea that POM retained in riverbed sediments can provide a source of DOM for microbes. In these experiments, peak DOC concentrations were higher when the flow rate of the experiment was

slower. This may simply be due to the longer duration of the slower experiments (9.5 h for 10 mL h^{-1}, 6.5 h for 15 mL h^{-1}, 3.5 h for 30 mL h^{-1}). The low DIC concentrations relative to DOC concentrations in outflow from experiments suggests that there was minimal mineralization of DOC during the experiments (which makes sense, since no microbes were intentionally added). Higher DIC concentrations in the 10 mL h^{-1} experiment could be due to the longer duration of the experiment.

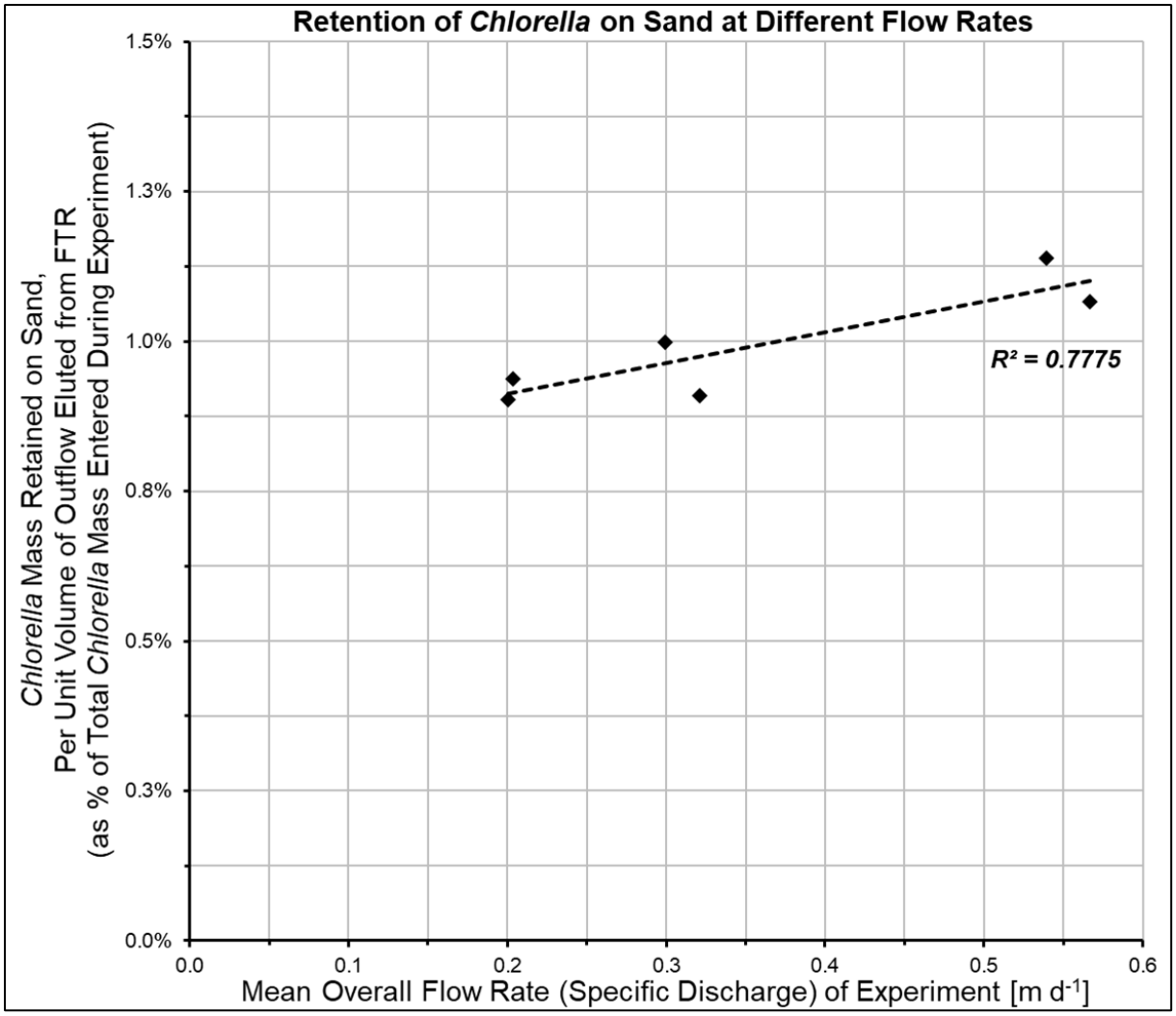

Figure 3.9: The influence of flow rate on the retention of *Chlorella* on sand during FTR experiments (each point represents one FTR). Retained mass is expressed as % of total mass entered (during the total length of an experiment) per unit volume eluted, to account for differences between experiments in mass entered and duration of flow. R^2 value obtained using linear trendline in Microsoft Excel.

Chapter 4: Conclusions and Recommendations

4.1: Conclusions

Flow-through reactor (FTR) experiments were conducted to represent one-dimensional downward vertical transport of particulate organic matter (POM) in riverbeds, using a simple sediment (coarse silica sand, dominant grain size of ~1mm) and a homogeneous POM analog (*Chlorella* powder). A numerical model of the experiments was also developed. The combination of laboratory and modelling methods was used to test a conceptual model of processes for the transport and retention of POM in riverbed sediments. The experiments were repeated at a range of downward vertical flow rates that are representative of hydrologic fluxes entering riverbeds (as reported in a selection of literature). Specifically, flow rates were selected to represent fluxes driven by river stage fluctuations in the Hanford Reach (under the influence of upstream dam operations), and the fluxes expected in the absence of dam operations (reported by Fritz & Arntzen, 2007; Shuai *et al.*, 2019).

In each FTR experiment, 1-1.4 g of *Chlorella* powder (0.44 – 0.62 g POC) was applied to the upper surface of 8 cm of saturated silica sand in two replicate FTRs, and approximately 2 pore volumes of outflow were collected (at an interval that achieved the desired flow rate). The measured concentration of suspended *Chlorella* in outflow reached up to 0.30 g L^{-1} *Chlorella* (0.13 g L^{-1} POC), with an associated pulse of up to 1.3 g L^{-1} of DOC, demonstrating the potential for POM to provide a source of DOM in riverbeds. The percentage of applied *Chlorella* that entered the sand (per unit volume of flux) was found to increase with increased flow rate, which suggests that increasing the vertical hydrologic flux into riverbeds could increase the mass of POM transferred from rivers (or riverbed surfaces) into riverbeds (per unit volume of flux).

By comparing breakthrough curves (BTCs) for suspended *Chlorella* and a nonreactive tracer (Bromide, Br^-), it was concluded that under downward vertical flow conditions,

gravitational settling may cause ‘velocity enhancement’ of POM (as indicated by early arrival of suspended *Chlorella* in FTR experiments, relative to tracer tests). It is expected that during periods of upward flow, the opposite effect would occur (gravitational settling would delay the transport of suspended POM). Thus, under repeated vertical flow reversals in riverbeds, there could be net infiltration and downward transport of POM. In river reaches where dam operations increase the frequency of reversals in flux direction, the mass of POM delivered to microbial communities in riverbeds may also be increased.

In addition to demonstrating that POM can travel through sediment, the FTR experiments also demonstrated that it can be retained on sediment (as evidenced by *Chlorella* retention profiles obtained by the loss-on-ignition method), which would allow POM to accumulate in riverbeds and provide a long-term source of DOM to microbes.

Numerical modelling simulations of the FTR experiments demonstrated that the transport and retention of POM in sediments can be modelled by an advection-dispersion equation with a gravitational settling rate added to the pore water velocity, and an additional term included for filtration. At each selected flow rate, experimental results and model simulations both support the hypothesis that in addition to the mass retained per unit time increasing with flow rate (since mass is introduced at a faster rate), the mass retained (as % of mass entered) per unit volume of flux (to account for differences in mass entered and flux duration) also increases. Therefore, in river reaches where dam operations increase the magnitude of riverbed exchange fluxes, the mass of POM delivered to microbial communities in riverbeds may also be increased.

The direct impact of dams on nutrient cycles by reducing downstream transport of nutrient elements has been established in literature (*e.g.*, Maavara *et al.*, 2017; Maavara *et al.*, 2020). In river reaches downstream from dams, autochthonous OM could become an important source of nutrients (and/or an important source of carbon and electron donors for

microbial redox reactions that transform the limited nutrients available). Studying POM transport and retention processes in the riverbeds of these reaches is therefore an important component of understanding, modelling, and predicting the biogeochemical function of regulated river reaches.

4.2: Recommendations

The methods used in this study could be improved to provide more accurate estimates of parameters for POM transport and retention, which could then potentially be used in more complex models of riverbed biogeochemistry (*e.g.*, two-dimensional models that include multi-directional fluxes and relate concentrations of POM, DOM, and various electron acceptors to microbial redox reactions).

A recommended improvement to pursue is developing an experimental design that allows POM to be introduced as a suspension with a known input concentration (this was attempted in this study, but *Chlorella* concentrations decreased within input tubing). A known (rather than estimated) input concentration would improve the estimation of filtration coefficients.

It is also recommended that when using nonreactive tracer tests to compare the transport of suspended particles to the movement of pore water, the tracer tests should be done prior to the introduction of the suspended particles. The presence of suspended particles may influence the behaviour of the tracer, making it a poor representation of the pore water movement. Attempts were made to obtain Br^- BTCs during the *Chlorella* transport experiments in this study, but Br^- arrived early (*i.e.*, less volume was eluted before detection of Br^-, relative to Br^- tracer tests done without *Chlorella*), as shown in Appendix Figure 3. This cannot be explained by a reduction of porosity caused by particle retention, because the same sand-packed FTRs used for the earlier Br^- tracer tests (without *Chlorella*) were saturated (but flushed of tracer by 3 pore volumes of Milli-Q water) prior to the introduction of *Chlorella* and Br^-, so the same volume needed to be eluted to displace the resident solution.

To further test the hypothesis that the velocity enhancement of *Chlorella* was caused by gravitational settling, experiments could be conducted in other orientations of flow (*e.g.*, horizontal FTRs). Additionally, more sophisticated experiments could potentially be designed to directly measure the settling rate of suspended particles. For example, image analysis has been used to study the infiltration of fluid into initially dry porous media (Rezanezhad *et al.*, 2006), and it might be possible to develop a similar experimental design for quantifying the settling rate of POM in saturated porous media.

Another possibility for future research is that sorption experiments could be conducted separately from transport experiments, to investigate whether modelling of POM transport and retention in sediments should include reversible sorption in addition to filtration. If so, sorption experiments could be used to obtain a direct estimate of a ‘sorption coefficient’.

Finally, once methods are further developed and proven for a given combination of materials (suspended particles and porous media), experiments and modelling could be expanded to other materials to obtain model parameters (*e.g.*, settling rate, filtration coefficient) that are specific to field sites of interest. The effects of more complex flow regimes (*e.g.*, variations in magnitude and direction of hydrologic fluxes) on POM transport and retention could be explored. Literature has also demonstrated that solution chemistry (*e.g.*, pH and ionic strength) influence the transport and retention of suspended particles (Torkzaban *et al.*, 2006; Bradford *et al.*, 2007), so the effect of solution chemistry on POM transport and retention could be investigated as well.

References

Alexander, M.D., and Caissie, D. 2003. Variability and Comparison of Hyporheic Water Temperatures and Seepage Fluxes in a Small Atlantic Salmon Stream. Groundwater, 41: 72–82. doi:10.1111/j.1745-6584.2003.tb02570.x.

Appelo, C.A.J. 2017. Solute transport solved with the Nernst-Planck equation for concrete pores with 'free' water and a double layer. Cement and Concrete Research, 101: 102–113. doi:10.1016/j.cemconres.2017.08.030.

Arntzen, E. V., Geist, D.R., and Dresel, P.E. 2006. Effects of fluctuating river flow on groundwater/surface water mixing in the hyporheic zone of a regulated, large cobble bed river. River Research and Applications, 22: 937–946. doi:10.1002/rra.947.

Barry, D.A. 2009. Effect of nonuniform boundary conditions on steady flow in saturated homogeneous cylindrical soil columns. Advances in Water Resources, 32: 522–531. doi:10.1016/j.advwatres.2009.01.003.

Battin, T.J., Kaplan, L.A., Newbold, J.D., and Hendricks, S.P. 2003. A mixing model analysis of stream solute dynamics and the contribution of a hyporheic zone to ecosystem function. Freshwater Biology, 48: 995–1014. doi:10.1046/j.1365-2427.2003.01062.x.

Benamar, A., Ahfir, N.D., Wang, H.Q., and Alem, A. 2007. Particle transport in a saturated porous medium: Pore structure effects. Comptes Rendus - Geoscience, 339: 674–681. doi:10.1016/j.crte.2007.07.012.

Benner, R. 2002. Molecular Indicators of the Bioavailability of Dissolved Organic Matter. *In* Aquatic Ecosystems: Interactivity of Dissolved Organic Matter. *Edited by* S. Findlay. Elsevier Science & Technology. pp. 121–137. doi:10.1016/b978-012256371-3/50006-8.

Boano, F., Harvey, J.W., Marion, A., Packman, A.I., Revelli, R., Ridolfi, L., and Wörman, A. 2014. Hyporheic flow and transport processes: mechanisms, models, and biogeochemical implications. Reviews of Geophysics, 52: 603–679. doi:10.1002/2012RG000417.

Bradford, S.A., Torkzaban, S., and Walker, S.L. 2007. Coupling of physical and chemical mechanisms of colloid straining in saturated porous media. Water Research, 41: 3012–3024. doi:10.1016/j.watres.2007.03.030.

Bradford, S.A., Yates, S.R., Bettahar, M., and Simunek, J. 2002. Physical factors affecting the transport and fate of colloids in saturated porous media. Water Resources Research, 38: 63-1-63–12. doi:10.1029/2002wr001340.

Brailsford, F.L., Glanville, H.C., Marshall, M.R., Golyshin, P.N., Johnes, P.J., Yates, C.A., Owen, A.T., and Jones, D.L. 2017. Microbial use of low molecular weight DOM in filtered and unfiltered freshwater: Role of ultra-small microorganisms and implications for water quality monitoring. Science of the Total Environment, 598: 377–384. doi:10.1016/j.scitotenv.2017.04.049.

Brunke, M. 1999. Colmation and depth filtration within streambeds: Retention of particles in hyporheic interstices. International Review of Hydrobiology, 84: 99–117. doi:10.1002/iroh.199900014.

Bulur, E. 2021. Particulate Organic Matter Transport in Experimental Riverbed Sand Columns. University of Wisconsin-Madison. Available from http://digital.library.wisc.edu/1793/82378.

Cherrey, K.D., Flury, M., and Harsh, J.B. 2003. Nitrate and colloid transport through coarse Hanford sediments under steady state, variably saturated flow. Water Resources Research, 39: 1–10. doi:10.1029/2002WR001944.

Chrysikopoulos, C. V., and Syngouna, V.I. 2014. Effect of Gravity on Colloid Transport through Water-Saturated Columns Packed with Glass Beads: Modeling and Experiments. Environmental Science & Technology, 48: 6805–6813. doi:dx.doi.org/10.1021/es501295n.

Close, M.E., Pang, L., Flintoft, M.J., and Sinton, L.W. 2006. Distance and Flow Effects on Microsphere Transport in a Large Gravel Column. Journal of Environmental Quality, 35: 1204–1212. doi:10.2134/jeq2005.0286.

Cranswick, R.H., and Cook, P.G. 2015. Scales and magnitude of hyporheic, river-aquifer and bank storage exchange fluxes. Hydrological Processes, 29: 3084–3097. doi:10.1002/hyp.10421.

Dean, W.E. 1974. Determination of Carbonate and Organic Matter in Calcareous Sediments and Sedimentary Rocks by Loss on Ignition: Comparison with Other Methods. Journal of Sedimentary Petrology, 44: 242–248. doi:10.1306/74D729D2-2B21-11D7-8648000102C1865D

DeFlaun, M.F., Oppenheimer, S.R., Streger, S., Condee, C.W., and Fletcher, M. 1999. Alterations in adhesion, transport, and membrane characteristics in an adhesion-deficient pseudomonad. Applied and Environmental Microbiology, 65: 759–765. doi:10.1128/aem.65.2.759-765.1999.

Ferencz, S.B., Bayani Cardenas, M., and Neilson, B.T. 2021. Aerobic respiration in riparian exchange zones of regulated river corridors. Hydrological Processes, 35. doi:10.1002/hyp.14386.

Freeze, A., and Cherry, J.A. 1979. Groundwater. Prentice-Hall, Inc., Englewood Cliffs, New Jersey. Available from http://hydrogeologistswithoutborders.org/wordpress/1979-english/.

Fritz, B.G., and Arntzen, E. V. 2007. Effect of rapidly changing river stage on uranium flux through the hyporheic zone. Ground Water, 45: 753–760. doi:10.1111/j.1745-6584.2007.00365.x.

Fung Shek, C.J. 2015. Dynamic imaging particle analysis for quantitative morphological analysis and cell counting. Johns Hopkins University. Available from http://jhir.library.jhu.edu/handle/1774.2/39422.

Gibert, O., Hernandez, M., Vilanova, E., and Cornella, O. 2014. Guidelining protocol for soil-column experiments assessing fate and transport of trace organics. Available from https://demeau-fp7.eu/sites/files/D123a Guidelines Column experiments.pdf.

Harris, D.C. 2016. Quantitative Chemical Analysis. Ninth Edition. Freeman and Company, New York, NY. p. 57.

Harter, T., Wagner, S., and Atwill, E.R. 2000. Colloid transport and filtration of Cryptosporidium parvum in sandy soils and aquifer sediments. Environmental Science and Technology, 34: 62–70. doi:10.1021/es990132w.

Harvey, R.W., and Garabedian, S. 1991. Use of Colloid Filtration Theory in Modeling Movement of Bacteria through a Contaminated Sandy Aquifer. Environmental Science and Technology, 25: 178–185. doi:10.1021/es00013a021.

Heiri, O., Lotter, A.F., and Lemcke, G. 2001. Loss on Ignition as a Method for Estimating Organic and Carbonate Content in Sediments: Reproducibility and Comparability of Results. Journal of Paleolimnology, 25: 101–110. doi:10.1023/A:1008119611481.

Iwasaki, T. 1937. Some Notes on Sand Filtration. American Water Works Association, 29: 1591–1597. doi:10.1002/j.1551-8833.1937.tb14014.x.

Jin, G., Zhang, Z., Tang, H., Xiaoquan, Y., Li, L., and Barry, D.A. 2019. Colloid transport and distribution in the hyporheic zone. Hydrological Processes, 33: 932–944. doi:10.1002/hyp.13375.

Kennedy, C.D., Murdoch, L.C., Genereux, D.P., Corbett, D.R., Stone, K., Pham, P., and Mitasova, H. 2010. Comparison of Darcian flux calculations and seepage meter measurements in a sandy streambed in North Carolina, United States. Water Resources Research, 46. doi:10.1029/2009WR008342.

Kestin, J., Sokolov, M., and Wakeham, W.A. 1978. Viscosity of liquid water in the range -8 °C to 150 °C. Journal of Physical and Chemical Reference Data, 7: 941-948. doi:10.1063/1.555581.

Kiel, B.A., and Bayani Cardenas, M. 2014. Lateral hyporheic exchange throughout the Mississippi River network. Nature Geoscience, 7: 413–417. doi:10.1038/ngeo2157.

Kloep, F., and Röske, I. 2004. Transport of Algal Cells in Hyporheic Sediments of the River Elbe (Germany). International Review of Hydrobiology, 89: 88–101. doi:10.1002/iroh.200310662.

LaRowe, D.E., and Van Cappellen, P. 2011. Degradation of natural organic matter: A thermodynamic analysis. Geochimica et Cosmochimica Acta, 75: 2030–2042. doi:10.1016/j.gca.2011.01.020.

Lehmann, J., and Kleber, M. 2015. The contentious nature of soil organic matter. Nature, 528: 60–68. doi:10.1038/nature16069.

Lewis, J., and Sjöstrom, J. 2010. Optimizing the experimental design of soil columns in saturated and unsaturated transport experiments. Journal of Contaminant Hydrology, 115: 1–13. Elsevier B.V. doi:10.1016/j.jconhyd.2010.04.001.

Logan, B.E., Jewett, D.G., Arnold, R.G., Bouwer, E.J., and O'Melia, C.R. 1995. Clarification of Clean-Bed Filtration Models. Journal of Environmental Engineering, 121: 869–873. doi:10.1061/(asce)0733-9372(1995)121:12(869).

Maavara, T., Lauerwald, R., Regnier, P., and Van Cappellen, P. 2017. Global perturbation of organic carbon cycling by river damming. Nature Communications, 8: 1–10. doi:10.1038/ncomms15347.

Maavara, T., Chen, Q., Van Meter, K., Brown, L.E., Zhang, J., Ni, J., and Zarfl, C. 2020. River dam impacts on biogeochemical cycling. Nature Reviews: Earth and Environment, 1: 103–116. Springer US. doi:10.1038/s43017-019-0019-0.

McCarter, C.P.R., Rezanezhad, F., Gharedaghloo, B., Price, J.S., and Van Cappellen, P. 2019. Transport of chloride and deuterated water in peat: The role of anion exclusion, diffusion, and anion adsorption in a dual porosity organic media. Journal of Contaminant Hydrology, 225. doi:10.1016/j.jconhyd.2019.103497.

McCaulou, D.R., Bales, R.C., and Arnold, R.G. 1995. Effect of Temperature-Controlled Motility on Transport of Bacteria and Microspheres Through Saturated Sediment. Water Resources Research, 31: 271–280. doi:10.1029/94WR02569.

McDowell-Boyer, L.M., Hunt, J.R., and Sitar, N. 1986. Particle Transport Through Porous Media. Water Resources Research, 22: 1901–1921. doi:10.1029/WR022i013p01901.

Metge, D.W., Harvey, R.W., Aiken, G.R., Anders, R., Lincoln, G., and Jasperse, J. 2010. Influence of organic carbon loading, sediment associated metal oxide content and sediment grain size distributions upon Cryptosporidium parvum removal during riverbank filtration operations, Sonoma County, CA. Water Research, 44: 1126–1137. doi:10.1016/j.watres.2009.11.033.

Moore, T.L., Nieber, J.L., Gulliver, J.S., and Magner, J.A. 2020. Field investigation of the groundwater contribution to baseflow in an urban stream from a Quaternary aquifer with a leaky base. Hydrological Processes, 34: 5512–5527. doi:10.1002/hyp.13959.

Naegeli, M.W., and Uehlinger, U. 1997. Contribution of the Hyporheic Zone to Ecosystem Metabolism in a Prealpine Gravel-Bed-River. Journal of the North American Benthological Society, 16: 794–804. doi:10.2307/1468172.

Newcomer, M.E., Hubbard, S.S., Fleckenstein, J.H., Maier, U., Schmidt, C., Thullner, M., Ulrich, C., Flipo, N., and Rubin, Y. 2018. Influence of Hydrological Perturbations and Riverbed Sediment Characteristics on Hyporheic Zone Respiration of CO2 and N2. Journal of Geophysical Research: Biogeosciences, 123: 902–922. doi:10.1002/2017JG004090.

Nimptsch, J., Woelfl, S., Kronvang, B., Giesecke, R., González, H.E., Caputo, L., Gelbrecht, J., von Tuempling, W., and Graeber, D. 2014. Does filter type and pore size influence spectroscopic analysis of freshwater chromophoric DOM composition? Limnologica, 48: 57–64. doi:10.1016/j.limno.2014.06.003.

Oliveira, I.B., Demond, A.H., and Salehzadeh, A. 1996. Packing of Sands for the Production of Homogeneous Porous Media. Soil Science Society of America Journal, 60: 49–53. doi:10.2136/sssaj1996.03615995006000010010x

Olsen, D.A., and Townsend, C.R. 2005. Flood effects on invertebrates, sediments and particulate organic matter in the hyporheic zone of a gravel-bed stream. Freshwater Biology, 50: 839–853. doi:10.1111/j.1365-2427.2005.01365.x.

Ortega-Retuerta, E., Frazer, T.K., Duarte, C.M., Ruiz-Halpern, S., Tovar-Sańchez, A., Arrieta, J.M., and Reche, I. 2009. Biogeneration of chromophoric dissolved organic matter by bacteria and krill in the southern ocean. Limnology and Oceanography, 54: 1941–1950. doi:10.4319/lo.2009.54.6.1941

Pallud, C., Meile, C., Laverman, A.M., Abell, J., and Van Cappellen, P. 2007. The use of flow-through sediment reactors in biogeochemical kinetics: Methodology and examples of applications. Marine Chemistry, 106: 256–271. doi:10.1016/j.marchem.2006.12.011.

Pallud, C., and Van Cappellen, P. 2006. Kinetics of microbial sulfate reduction in estuarine sediments. Geochimica et Cosmochimica Acta, 70: 1148–1162. doi:10.1016/j.gca.2005.11.002.

Patyna, A., Płaczek, M., and Witczak, S. 2018. Study of Chlorella vulgaris sedimentation process. MATEC Web of Conferences, 240: 1–5. doi:10.1051/matecconf/201824005023.

Rezanezhad, F., Vogel, H.-J., and Roth, K. 2006. Experimental study of fingered flow through initially dry sand. Hydrology and Earth System Sciences Discussions, European Geosciences Union, 3: 2595–2620. Available from https://hal.archives-ouvertes.fr/hal-00298761.

Rosenberry, D.O., Briggs, M.A., Delin, G., and Hare, D.K. 2016. Combined use of thermal methods and seepage meters to efficiently locate, quantify, and monitor focused groundwater discharge to a sand-bed stream. Water Resources Research, 52: 4486–4503. doi:10.1002/2016WR018808.

Rosenberry, D.O., and Pitlick, J. 2009. Local-scale variability of seepage and hydraulic conductivity in a shallow gravel-bed river. Hydrological Processes, 23: 3306–3318. doi:10.1002/hyp.7433.

Ru, I.T.K., Sung, Y.Y., Jusoh, M., Wahid, M.E.A., and Nagappan, T. 2020. Chlorella vulgaris : a perspective on its potential for combining high biomass with high value bioproducts . Applied Phycology, 1: 2–11. Taylor & Francis. doi:10.1080/26388081.2020.1715256.

Rumble, J.R. (Editor). 2023. Density, Hardness, and Refractive Index of Common Minerals. In CRC Handbook of Chemistry and Physics Online, 103rd edition. CRC Press, Taylor & Francis Group.

Shuai, P., Chen, X., Song, X., Hammond, G.E., Zachara, J., Royer, P., Ren, H., Perkins, W.A., Richmond, M.C., and Huang, M. 2019. Dam Operations and Subsurface Hydrogeology Control Dynamics of Hydrologic Exchange Flows in a Regulated River Reach. Water Resources Research, 55: 2593–2612. doi:10.1029/2018WR024193.

Solomon, D.K., Humphrey, E., Gilmore, T.E., Genereux, D.P., and Zlotnik, V. 2019. An Automated Seepage Meter for Streams and Lakes. Water Resources Research, 56. doi:10.1029/2019WR026983.

Sophocleous, M. 2002. Interactions between groundwater and surface water: The state of the science. Hydrogeology Journal, 10: 52–67. doi:10.1007/s10040-001-0170-8.

Sorbie, K.S., and Tomlinson, C.J. 1993. Analytical Method for Evaluating the Effective Molecular Diffusion Coefficient within Porous Media. Chemical Engineering Science, 48: 1813–1818. doi:10.1016/0009-2509(93)80351-P.

Spencer, R.G.M., Aiken, G.R., Butler, K.D., Dornblaser, M.M., Striegl, R.G., and Hernes, P.J. 2009. Utilizing chromophoric dissolved organic matter measurements to derive export and reactivity of dissolved organic carbon exported to the Arctic Ocean: A case study of the Yukon River, Alaska. Geophysical Research Letters, 36: 1–6. doi:10.1029/2008GL036831.

Swift, R.S. 1996. Chapter 35: Organic Matter Characterization. *In* Methods of Soil Analysis: Part 3: Chemical Methods. *Edited by* D.L. Sparks, A.L. Page, P.A. Helmke, R.H. Loeppert, P.N. Soltanpour, M.A. Tabatabai, C.T. Johnston, and M.E. Sumner. Soil Science Society of America, Inc., Madison, Wisconsin, USA. pp. 1011–1069. doi:10.2136/sssabookser5.3.

Thurman, E.M. 1985. Organic Chemistry of Natural Waters. In 1st edition. Springer Netherlands. doi:10.1007/978-94-009-5095-5.

Torkzaban, S., Hassanizadeh, S.M., Schijven, J.F., de Bruin, H.A.M., and de Roda Husman, A.M. 2006. Virus Transport in Saturated and Unsaturated Sand Columns. Vadose Zone Journal, 5: 877–885. doi:10.2136/vzj2005.0086.

Van Genuchten, M.T., and Parker, J.C. 1984. Boundary Conditions for Displacement Experiments through Short Laboratory Soil Columns. Soil Science Society of America Journal, 48(4): 703–708. doi:10.2136/sssaj1984.03615995004800040002x.

Van Wychen, S., and Laurens, M. 2015. Determination of Total Solids and Ash in Algal Biomass: Laboratory Analytical Procedure. National Renewable Energy Laboratory. Golden, CO. Available from https://www.nrel.gov/docs/fy16osti/60956.pdf.

Velliquette, T., Welch, J., Crow, M., Devarakonda, R., Heinz, S., and Crystal-Ornelas, R. 2021. ESS-DIVE Reporting Format for Comma-separated Values (CSV) File Structure. Environmental Systems Science Data Infrastructure for a Virtual Ecosystem (ESS-DIVE), ESS-DIVE Repository. doi:10.15485/1734841

Wall, L.G., Tank, J.L., Royer, T. V., and Bernot, M.J. 2005. Spatial and temporal variability in sediment denitrification within an agriculturally influenced reservoir. Biogeochemistry, 76: 85–111. doi:10.1007/s10533-005-2199-6.

Wang, W., Li, J., Wang, W., Chen, X., Cheng, D., and Jia, J. 2014. Estimating streambed parameters for a disconnected river. Hydrological Processes, 28: 3267–3641. doi:10.1002/hyp.9904.

Williams, R.J.P., and Frausto da Silva, J.J.R. 2005. Chapter 2: Basic Chemistry of the Ecosystem. *In* The Chemistry of Evolution: The Development of our Ecosystem. p. 57. doi:10.1016/B978-044452115-6/50045-2.

Winter, T.C., Harvey, J.W., Franke, O.L., and Alley, W.M. 1998. Ground Water and Surface Water; A Single Resource - U.S. Geological Survey Circular 1139. doi:10.3133/cir1139.

Yao, K.-M., Habibian, M.T., and O'Melia, C.R. 1971. Water and Waste Water Filtration: Concepts and Applications. Environmental Science and Technology, 5: 1105–1112. doi:10.1021/es60058a005.

Zhang, Y., Liu, M., Qin, B., and Feng, S. 2009. Photochemical degradation of chromophoric dissolved organic matter exposed to simulated UV-B and natural solar radiation. Hydrobiologica: 159–168. doi:10.1007/s10750-009-9722-z.

Appendix

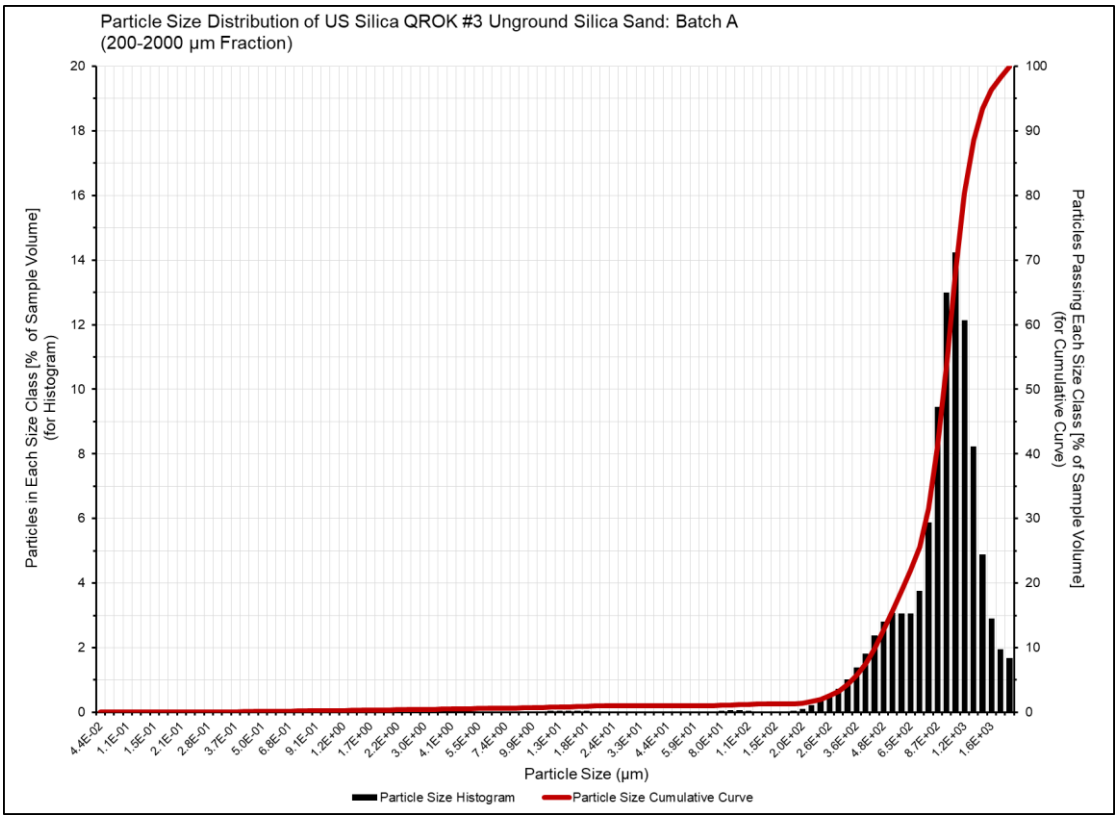

Appendix Figure 1: Particle size distribution of Sand Batch A (methods in *2.1.1*).

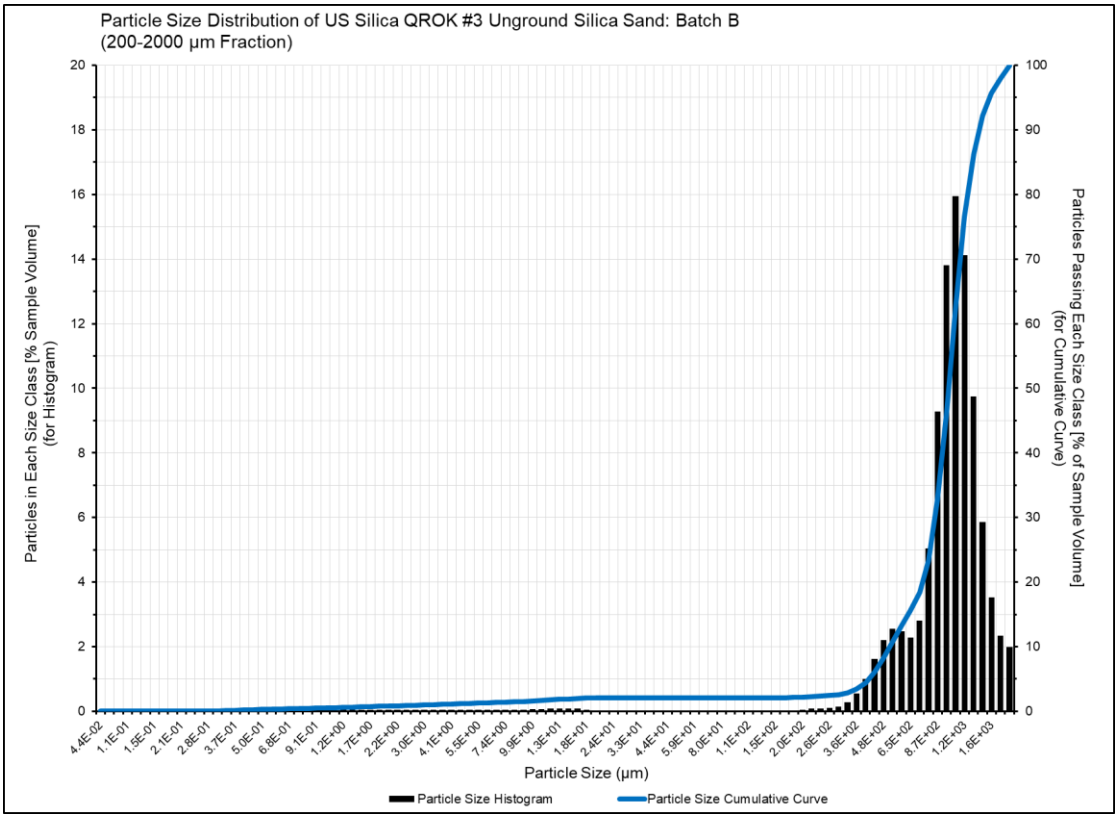

Appendix Figure 2: Particle size distribution of Sand Batch B (methods in *2.1.1*).

Appendix Table 1: Mean particle size statistics of QROK #3 sand (corresponding to data plotted in Appendix Figures 1, 2) reported by MAScontrol instrument software for Fritsch Analysette laser diffraction particle size analyzer.

Statistics Reported by MAScontrol Software				
Sand Batch	Particle Diameter Values [µm]			
	Mode	Median	Arithmetic Mean	Volume Moment Mean, D[4,3]
A	1,038.069	979.349	958.811	958.811
B	1,072.340	1,030.168	1,018.595	1,018.595

Appendix Table 2: Camera settings used for timelapse recordings (these are the exact settings used for settling experiments but may have differed slightly for transport experiments). 'Custom White Balance' set using image of white tri-fold backdrop.

Camera	Lens	Distance from front of Lens to front of FTR [cm]	Mode	Drive Mode	Image Quality	White Balance	Picture Style	Shutter Speed	Aperture	ISO	Movie Recording Size	Timelapse Movie
Canon EOS Rebel SL3	EFS 18-55 mm	94 (± 0.5)	Video, Manual	Single Shooting	Large, Fine	Custom	Fine Detail	1/30	F5.6	200	FHD	Enabled, Custom

Appendix Table 3: Settings used for timelapse recordings during each experiment.

Experiment	Date [YYYY-MM-DD]	Timelapse Details			
		Interval [s]	# Shots	Recording Duration [hh:mm:ss]	Video Duration [mm:ss]
30 mL/h Transport	2022-04-05	5	2160	3:00:00	1:12
15 mL/h Transport	2022-04-20	6	3600	5:59:54	2:00
10 mL/h Transport	2022-05-11	9	3600	8:59:51	2:00
Settling (No Flow)	2022-07-06	3	3600	2:59:57	2:00
Settling (No Flow)	2022-07-13	3	3600	2:59:57	2:00

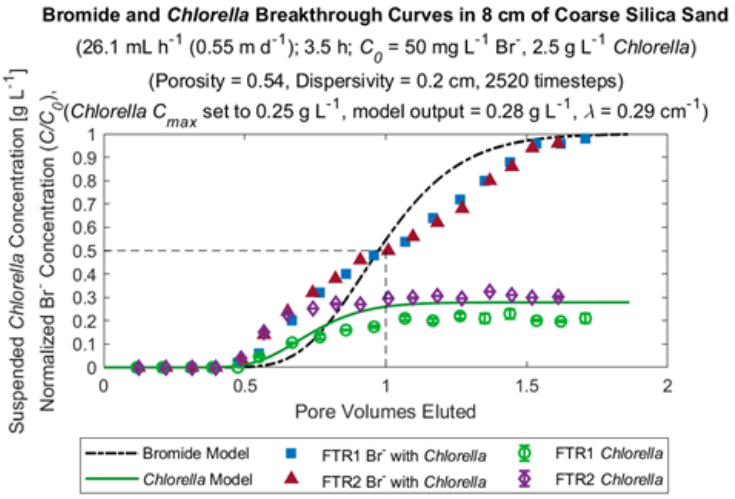

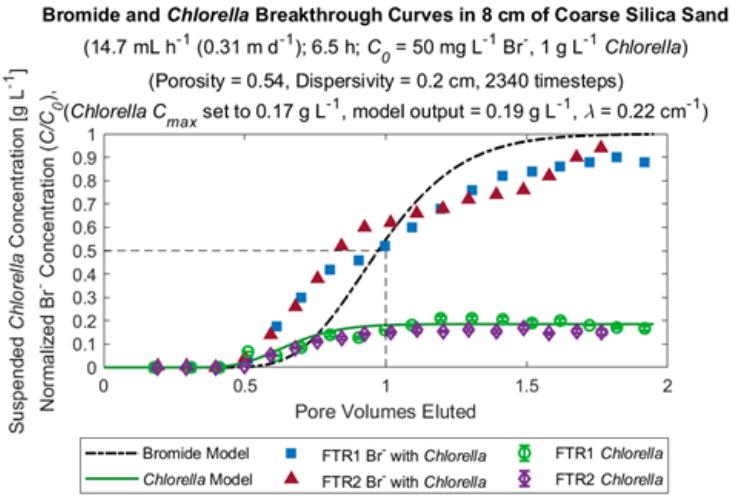

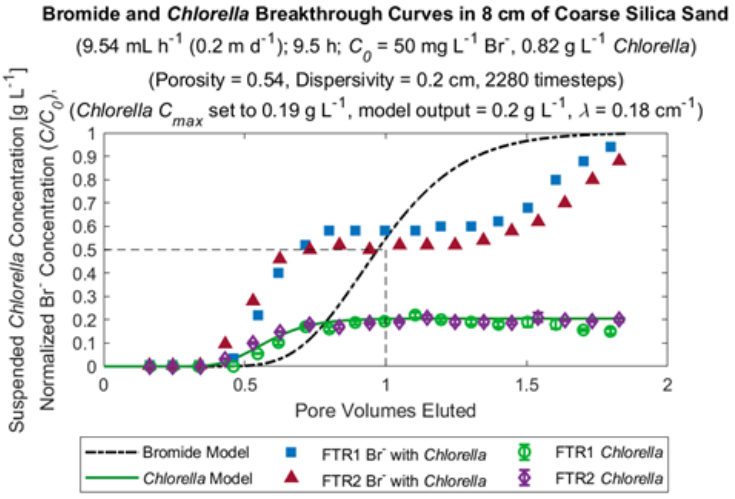

Appendix Figure 3: *Chlorella* breakthrough curves for each experiment, plotted with associated Br^- breakthrough tests obtained during the *Chlorella* experiment, and breakthrough curves from the associated model simulations. The interpretation of these BTCs is that the early arrival (relative to Br^- BTCs obtained without *Chlorella*) is caused by gravitational settling of suspended *Chlorella* particles carrying Br^-.